LONG-TERM DEFORMATION BEHAVIOR OF HYBRID GIRDER WITH HEADED STUD SHEAR CONNECTIONS UNDER SUSTAINED LOADING

（頭付きスタッドを有する鋼コンクリート混合桁の持続荷重下における長期変形挙動）

A Dissertation Submitted to the Department of Civil and Environmental Engineering
in Partial Fulfilment of the Requirements for the degree of
Doctor of Philosophy

埼玉大学

Haque Mohammad Najmol
(17DE052)

Supervisor
Professor Takeshi Maki

Department of Civil and Environmental Engineering
Graduate School of Science and Engineering
Saitama University, Saitama, Japan
September 2020

ACKNOWLEDGEMENT

First and foremost, the author expresses his profound gratitude to the almighty Allah (SWT) for the materialization of the doctoral course research outcome accomplished till date.

The author would like to pay the deepest honor and gratitude to his supervisor **Professor Takeshi Maki**, whose continuous support, guidance, encouragement and supervision from the very first day helped the author a comprehensive understanding of the subject and; without his guidance and mentoring, the author could not have reached at this level of research to materialize the dissertation. Further, all his support in academic and nonacademic matters, deemed a step forward motivation to the author to develop his personal career.

The author would like to express his sincere gratitude to **Professor Emeritus Hiroshi Mutsuyoshi, Associate Professor Shingo Asamoto and Assistant Professor Luan Yao** of Structural Material Laboratory**,** who extended their all-out support, cooperation and constructive suggestion throughout his study period. The author would also like to express his gratefulness to the committee members, **Professor Yoshiaki Okui** and **Professor Yasunao Matsumoto** for their very valuable comments and suggestions that enriched the dissertation contents.

The author would like to acknowledge the support of Saitama University for granting scholarship to provide financial support to carry out his doctoral course. The **Road Transport and highways Division** of Ministry of Road Transport and Bridges and **Roads and Highways Department (RHD)** of Government of Bangladesh is gratefully acknowledged for granting the deputation and supporting him to pursue his doctoral study at Saitama University, Japan.

The author is deeply thankful to Mr. Shota Sekimoto, Mr. Jun Sasaki, Ms. Saki Shiiya, Mr. Takeru Suzuki and Mr. Fawaz for their unconditional and valuable support in experiments. Mr. Sato and Ms. Gunji are also acknowledged for their administrative as well as laboratory support time to time. Moreover, the author offers regards to all the student members of this laboratory for their cordial assistance at different times of his living in Japan.

Finally**,** and most importantly, the author would like to pay innermost indebtedness to his **wife, son, parents and family members** for their undivided love, sacrifice, inspiration, relentless support, prayers and blessings**.** The author is also indebted to all his teachers, colleagues and most lovable well-wishers who inspired him throughout the career**.** It would not be possible to write any line of this dissertation without affection, encouragement and moral support offered by the parents since his childhood.

Mohammad Najmol Haque

Saitama University, September 01, 2020.

ABSTRACT

Steel-concrete composite girders have gained popularity worldwide; as combining them become more effective and beneficial with the properties of both, i.e., can double the flexural strength and stiffness, reduce its span-to-depth ratio with consequent cost savings in real structural construction. In addition, they are lighter, guarantee better quality and have easier and faster erection than concrete structures as well as environmentally friendly. Based on the concept of composite structures, a further innovative idea of hybrid steel–concrete girder system is developed that uses lighter steel girder and inexpensive concrete girder which provides an economical solution for bridge girders. In general, most composite bridge girders are girder composite and box girder composite in nature, which are efficient for longer spans. Considering the longitudinal compositions, prestressed reinforced concrete (PRC) girders instead of concrete girders are preferred because of high stiffness and durability that leads to significant cost savings. For hybrid girder, assessing the performances of the junction or overlapping part with different shear connectors is much important, since this lack determines the limited applications of this structural type. This junction part must be designed to prevent separation between them as well as to ensure resisting the shear forces to the steel-PRC interface. Performance of such girder under any static and dynamic load significantly depends on force transfer mechanism at the junction and headed stud shear connections are most commonly used for this purpose. In Japan, the existing specifications considers very limited nominal shear force for the connector than its actual capacity and assumes almost insignificant deformation. Therefore, effective uses of stud shear strength could be a way forward in perspective of a more rational and economical design for practical applications. To adopt such a design method that allows effective uses of stud strength and incorporates parameters that clarify the influence on its deformation behaviour, and mechanism are very crucial. Due to the local deformation behaviour of stud connections, how they can influence the deformation behaviour of structure as a whole are also an important issue. For hybrid girder, particularly the creep induced long-term deformation behavior of junction under sustained loading is not considered explicitly but using of enhanced stud strength in the junction part will reduce the number of shear connections; for which the time-dependent behaviour of concrete may weaken the strength of the shear connections. It is assumed that under the sustained load the stiffness of junction will be slightly reduced even though the capacity might be same. Therefore, owing to the sustained loading action, there is a possibility that the mechanical behavior of stud connections and concrete will have an influence on the overall deformation of the whole structure; and this particular area was not considered in the previous research. The type of junction that adopted for hybrid girder is designed mainly according to structural details based on the results of experimental works. The junction is

considered to have greater capacity than the other parts but there is no way to verify the capacity. Therefore, to ensure a safety-side design approach; so many shear connectors are provided in junction that usually induce a problem in construction works as it becomes very congested with steel plates, reinforcements, prestressing bars, and studs within a narrow space. Thus, the main concern of this study is to reduce the number of shear connectors in junction part; aiming to improve the constructability with a consequent savings of cost.

For practical applicability, before reducing the number of shear connectors, it needs to investigate its impact on the structural performance of junction considering serviceability and ultimate limits. For serviceability approach, it may influence on deflection, vibration, fatigue, etc and for ultimate limit, capacity will be a major concern. Since, the junction part is a composite section with a same sized concrete cross section with steel girder section, thus, even though the number of shear connectors are reduced capacity will not be a major issue. Therefore, from the point of ultimate limit state, the number of shear connectors in junction part may possibly be reduced.

From serviceability point of view, even though it needs to investigate other factors; under the present study, scope is focused mainly on deflection (deformation) which is governed by instantaneous stiffness (short-term deflection) and time-dependent material properties (influenced by on long-term deflection) such as creep, shrinkage and relaxation. Regarding instantaneous stiffness, the number of shear connectors may have a sensitive impact on it. Therefore, a detail investigation is needed on that impact, as to reduce the number of shear connectors. If it could lead to a solution to reduce the number of shear connectors based on instantaneous stiffness, time-dependent problem would be major issue to investigate. However, there are very few researches that investigate the time-dependent behavior of junction part. Thus, this study focused on the long-term deformation (deflection) behaviour as a very fundamental study. Since, time-dependent deformation under sustained loading is crucial for hybrid girders. investigations must be conducted for quantifying such behaviour and then its application for practical construction may be promoted for sustainable design.

Therefore, experimental investigations have been conducted to quantify the long-term deformation of hybrid girder. Pushout tests with FEA presents the long-term deformations of stud connections that lead to a reduction of stud stiffness. Then a sensitivity analysis is also presented to clarify the impact of reduction of studs and how the instantaneous and time dependent deformations of stud connections influences the deformation of whole structure. A parametric study and an approximate simplified model is proposed to determine the long-term deformation of stud connections under this study although it has some limitations. However, this simplified prediction model could be applied for real structures to determine their long-term deformation behavior.

TABLE OF CONTENTS

LIST OF TABLES

LIST OF FIGURES

CHAPTER 1

1 INTRODUTION

1.1 Background and Motivation

In recent times, steel-concrete composite constructions have gained popularity worldwide. There exist several reasons of combining them as steel presents high tensile strength with ductility and, concrete presents high compressive strength with stiffness. So, while combining them in the composite structures, these two elements act as one, become more effective and beneficial with the properties of both, i.e., can double the flexural strength and stiffness, reduce its span-to-depth ratio with consequent cost savings in real structural construction. In addition, they are lighter, guarantee better quality and have easier and faster erection than concrete structures. They are also expected to reduce noise and vibration levels and therefore, become environmentally friendly. As, steel-concrete composite structures present many advantages, now a day's composite girder bridges are being designed with greater span lengths than those were previously possible with ordinary materials. Moreover, a further innovative idea of hybrid steel–concrete girder system is developed that uses lighter steel girder and inexpensive concrete girder which provides an economical solution for bridge girders. In general, most composite bridge girders are girder composite and box girder composite in nature, which are efficient for longer spans. Considering the longitudinal compositions, prestressed reinforced concrete (PRC) girders instead of concrete girders are preferred because of high stiffness and durability that leads to significant cost savings. However, irrespective of the girder forms, for designing any hybrid or composite girder, the designers have to depend on the behavior of the individual components as well as the bond between them. For hybrid girder, assessing the performances of the junction or overlapping part with different shear connectors is much important, since this lack determines the limited applications of this structural type. Therefore, the bond which must be achieved between the steel-prestressed reinforced concrete (steel-PRC) junction is so crucial for composite action. This bond between these two elements in junction part must be designed to prevent separation between them as well as to ensure resisting both the tensile forces normal to the steel-PRC interface and the shear forces parallel to that. The requirements for such junction shall include easy fabrication, quick construction, high loading capacity and enough deformation capacity. Performance of such girder under any static and dynamic load significantly depends on force transfer mechanism at the junction which is generally achieved by mechanical shear connectors i.e., headed stud connections (connectors), bearing plates, or perfobond strip connectors. As the use of perfobond connectors or bearing plates presents difficulties for confirming the filling of concrete into the hole, headed stud shear connections are most commonly used for this purpose. These connections have additional advantages such as rapid installation, superior strength and stiffness, high ductility, and dowel action. In Japan, the existing

specifications which are used for the design of the connections of hybrid girder considers very limited nominal shear force borne by the connector than its actual capacity and assumes almost insignificant deformation. Therefore, it is considered that the design method which allows effective uses of stud shear strength could be a way forward in perspective of a more rational and economical design for practical applications. To adopt such a design method that allows effective uses of stud strength and incorporates parameters that clarify the influence on its deformation behaviour, and mechanism are very crucial. Due to the local deformation behaviour of stud connections, how they can influence the deformation behaviour of structure as a whole are also an important issue. In reality; for composite girder, the sustained load is explicitly considered in design. However; for hybrid girder, particularly the creep induced long-term deformation behavior of junction under sustained loading is not considered explicitly. For such a long-term sustained loading, although it is considered that the creep of concrete is a major cause of time dependent deformations; there is no existing evidence that it could induce a significant damage and threat to the structures. For the hybrid girder, using of enhanced stud strength in the junction part will reduce the number of shear connections; and owing to the time dependent behaviour, concrete could ultimately lead to weakening the interfacial strength of the stud connections. Since, it is considered that for the time dependent behaviour, concrete loses its strength and consequently with the shear connections, it transfers stresses to the structural steel; for which it is assumed that under the sustained load the stiffness of junction will be reduced even though the capacity might be same. Therefore, owing to the sustained loading action, there is a possibility that the mechanical behavior of stud connections and concrete will have an influence on the overall deformation of the whole structure; and this particular area was not considered in the previous research. The type of junction that adopted for hybrid girder is designed mainly according to structural details which is prescribed based on the results of experimental works and is considered to have greater capacity than the other parts, i.e. steel girder and PRC girder part. Since, there is no way to verify the capacity of the junction, therefore, to ensure a safety-side design approach; so many shear connectors are provided in junction that usually induce a problem in construction works, since the junction part becomes very congested. Thus, the main concern of this study is to reduce the number of shear connectors in junction part; aiming to improve the constructability with a consequent savings of cost.

As per practical consideration and applicability, before reducing the number of shear connectors, it needs to investigate its impact on the structural performance of junction for limit state design considering serviceability and ultimate limits. For serviceability approach, it may influence on deflection, vibration, fatigue, etc and for ultimate limit, capacity will be a major concern. Since, the junction part is a composite section with a same sized concrete cross section with steel girder

section, thus, with reduced number of shear connectors, the capacity of junction may be possibly decreased but still it would have much greater capacity than the general sections like composite girder and PRC girder. Therefore, from the point of ultimate limit state, the number of shear connectors in junction part may possibly be reduced.

From serviceability point of view, even though it needs to investigate some factors such as deflection, fatigue, vibration, etc., under the present study, scope is focused mainly on deflection which is governed by the time-dependent material properties (influenced by on long-term deflection) such as creep, shrinkage and relaxation. Regarding instantaneous stiffness, the number of shear connectors may have a sensitive impact on it. Therefore, a detail investigation is needed on that impact, as to reduce the number of shear connectors. If it could lead to a solution to reduce the number of shear connectors based on instantaneous stiffness, time-dependent problem would be major issue to investigate. However, there are very few researches that investigate the time-dependent behavior of junction part. Thus, this study focused on the long-term deformation (deflection) behaviour as a very fundamental study. As already mentioned, that serviceability includes not only deflection but also fatigue and vibration. So, investigating the remaining factors shall have importance and could be investigated in the future, in order to realize the reduction of the number of shear connectors in junction part. As already mentioned, that time-dependent deformation under sustained loading is crucial for hybrid girders. investigations must be conducted for quantifying such behaviour to obtain a basis and guidelines for designing such innovative girders while considering the long-term response with time effects. Then, the time-dependent deformation behaviour for such a girder under sustained loading can be clarified, and its application for practical construction may be promoted for sustainable design.

1.2 Research Objectives

For hybrid girder, being an important part, the stud connections can influence the overall deformation behaviour of that under a sustained loading condition. To ease the constructability and applicability of such girder, most important concern is to reduce the shear connections at junction part (embedded zone). Therefore, investigation is inevitable to predict their long-term deformation behavior and how stud connections can influence the overall deformation of the girder with instantaneous and time dependent effect; even though, there remains challenges to address the non-linearity and complex mechanism of connections as well as girder behaviour very precisely. Experimental investigations along with a finite element analysis can approximately model those behaviour although it has some limitations to realistically reach to a certain conclusion. However, considering the above avenue and limitations, the objectives of this thesis are as follows:

i. To quantify the long-term deformation of hybrid girder with headed stud connections with a sensitivity analysis how instantaneous and long-term stud deformation can influence the overall deformation of the girder.

ii. To formulate a simplified prediction model for deformation of stud connections to apply for real structures to determine their long-term deformation behavior.

1.3 Dissertation Outline

This dissertation consists of six chapters. The brief summary of these chapters is described here;

Chapter 1: Consists of background and motivation; research objectives and outline of dissertation.

Chapter 2: Consists of introduction, general review of literature on the study focusing the hybrid girder, reviewing the existing design standards and codes on girder design, deformation under sustained loading, finding the research gaps with statement of problem and formulation of research plan to the targeted problem to narrow-down it.

Chapter 3: Consists of general introduction; brief description on investigation on the long-term deformation of stud connections through pushout experiment; specimen assemble, casting and curing; material properties; experimental program, measuring the environmental conditions; test results and discussion focusing on time-dependent slip behaviour, slip displacement and skeleton curve with residual displacement and failure load with its pattern and summary with conclusions.

Chapter 4: Consists of general introduction; description on construction of non-linear FEA program for investigating the long-term deformation as examined in pushout specimen; modeling of concrete; method of modeling considering constitutive law, concrete tension/compression softening parameter, creep deformation etc.; modeling of pushout specimen with analysis procedure and loading method. cases of analysis to validate experimental results; parametric study focusing on influencing factors that affect the long-term slip deformation; with an analogy with the creep deformation model, formulating a generalized time dependent slip deformation model to predict the deformation behaviour of headed stud for the hybrid girder under this study and summary and conclusions.

Chapter 5: Consists of general introduction on long-term deflection of hybrid girder; brief description on design of hybrid girder specimen and connections; specimen assemble, casting and curing process; experimental programme; properties of materials used in specimen; test results and discussions focusing on long-term (time dependent) deformation behaviour with a distinct impact of creep and shrinkage, influence of sustained loading on failure and crack pattern. This also consists of description on conceptual forces acting on junction; finite element approach to calculate shear forces of stud connections; discussions on shear behaviour of connections under sustained

loading, a sensitivity analysis to clarify the impact of instantaneous and long-term stud deformations on hybrid girder with summary and conclusions

Chapter 6: Consists of conclusions of this research and suggestions for future investigations.

CHAPTER 2

2 RESEARCH BACKGROUND AND LITERATURE REVIEW

2.1 Introduction

In bridge composite girders, the concrete and the steel girder are provided with a coupling element such as headed studs, a bearing plate, and a perfobond leiste (PBL)etc., known as shear connector, which provides the anchorage; facilitating the smooth transfer of stress between the connecting elements. In recent years, the demand for simplification and constructability in composite girders has been increased; and now a days, the use of prestressed reinforced concrete (PRC) girder instead of concrete girder has got its widespread acceptance for real structural applications. The concrete mass is casted with the steel girder and shear connectors integrate the concrete to the steel girder and high-strength prestressing tendons are placed at suitable locations, so that under the full composite action, the girder behaves as one and the pre-stressing tendons could counteract deformation due to the applied load. The hybrid steel-concrete girder system is a further innovative design approach that uses the lighter steel girder and the cheaper concrete girder together that provides an economical solution to the bridge girders. Considering the longitudinal compositions of the girders, PRC girders are preferred for hybrid girders because of high stiffness, durability and low material cost. The continuity in the junction part or embedded zone of such hybrid girder between the steel and PRC girder must be designed to prevent separation as well as to resist tensile and shear forces at steel-concrete interface. Headed stud shear connectors are most commonly and widely used in hybrid girder connection design due to many advantages including rapid installation, strength and stiffness with high ductility and dowel action. The deformation behaviour of the junction part as well as the performance of the shear connections are thus important as they can affect the behavior of the different components of the composite section and the hybrid girder as a whole.

2.2 Literature Review

Several reasons exist for combining steel and concrete elements to form composite structures as they have some unique characteristics. Unlike steel elements or reinforced concrete elements, the strength of a composite structure varies along its length, and so the strength at all sections must be compared with applied load along the structure. This can be achieved through combining them as to take the full advantage of the properties of both by resisting tensile forces and compressive forces. This also can double the flexural strength and stiffness as well as can reduce the span to depth ratio with consequent cost savings in real structural construction [(Oehlers DJ, 1995), (Choo JF, 2019)]. Due to the advantageous uses of both materials, composite construction has gained popularity over last few decades. Composite bridges have been designed to span lengths greater than were

previously impossible with ordinary materials that leads to reducing the cost as much as 10 % [(Nie J, 2003)]. The hybrid steel-concrete girder system, an innovative design approach uses the lighter steel girder and the cheaper concrete girder that provides an economical solution to the bridge girders. In general, the most composite bridge girders are girder composite and box girder composite in nature; efficient for long spans. As reinforced concrete girders are mostly economical for short spans and steel girders are for longer spans, to materialize such advantageous features, a first attempt to combine steel girders and concrete girders was realized in 1972 with the construction of the Kurt-Schumacher Bridge, a cable stayed bridge in Germany. Following this milestone, several hybrid bridges have been constructed worldwide over last 30 years including the Normandy Bridge in France, the Tatara Bridge in Japan and the Cheongpung Bridge in Korea. A hybrid girder differs with composite girder in a way that concrete and steel parallel each other in longitudinal direction in composite girder whereas a hybrid girder divides the concrete and steel at each end of the girder [(Choo JF, 2019), (Kim SE, 2012)]. Considering the desired member strength and

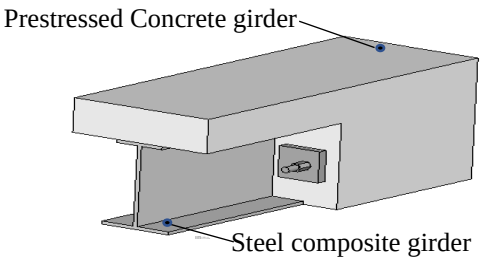

Figure 2. 1: Hybrid girders with PRC.

longitudinal compositions, PRC girders are preferred because of their high stiffness and durability, along with their significant cost savings [(Deng Y, 2013), (Nilson AH, 2010)]. Shinozaki et al. [(Shinozaki H, 2014)] adopted an innovative hybrid girder; they intended to combine a steel girder with a PRC girder applicable for a given span, on both sides of which there existed the same number of steel and PRC girders. Although using such a girder is unpopular, embedding a steel girder into a PRC girder can reduce the section force and weight of the steel material. Figure 2.1 presents that hybrid girder.

In a hybrid girder, the continuity at the junction or embedded zone must be designed to prevent separation as well as resist tensile and shear forces at the steel–concrete interface. The performance of such a girder under a static or dynamic load significantly depends on the force-transfer mechanism at the interface, at which the components are joined by headed stud shear connectors, bearing plates, or perfobond strip connectors [(Oehlers DJ, 1995), (Choo JF, 2019), (Prakash A,

2011)]. As the use of perfobond connectors or bearing plates presents difficulties for confirming the filling of concrete into the hole, headed stud shear connections are most commonly used for this purpose. These connections have additional advantages such as rapid installation, superior strength and stiffness, high ductility, and dowel action [(Shinozaki H, 2014), (Prakash A, 2011), (Allobody, 2014), (Anju T, 2016)]. Hence, Shinozaki et al. designed the connections for the hybrid girder using headed studs that were already installed in a real bridge [(Shinozaki H, 2014)].

Research on headed studs began in the 1950s [(Pallarés L, NSEL Report 2009)], and Ollgaard et al. [(Ollgaard JG, 1971)] proposed the first formulae for calculating the strength of a headed stud in composite action, which was adopted by the American Institute of Steel Construction (AISC) Manual [(Pallarés L, NSEL Report 2009), (AISC, 2016)]. As per the AISC manual, the nominal shear of headed stud is calculated using the following formulae (equation 2.1).

$$Q_a = 0.50\, A_{SC}\sqrt{f_c' E_C} \leq A_{SC} F_U \qquad (2.1)$$

where, A_{SC}: x-sectional area of stud connector, f_c': specified cylinder compressive strength of concrete, F_U: ultimate tensile strength of stud, E_C: modulus of elasticity of concrete. Other design codes and specifications also adopted formulae for determining the headed stud strength for composite construction. According to the EURO code [(Eurocode, 2004)], two empirical formulae are used to determine the design shear strength of headed stud as per equations (2.2-2.3).

$$P_{Rd} = \frac{0.8 f_u \frac{\pi d^2}{4}}{\gamma_v} \text{ (for failure of shank)} \qquad (2,2)$$

and

$$P_{Rd} = \frac{0.29 d^2 (f_{ck} E_{cm})^{\frac{1}{2}}}{\gamma_v} \text{ (for failure of concrete)} \qquad (2.3)$$

where, f_u: ultimate tensile strength of steel ($\leq$500 MPa), f_{ck}: cylinder strength of concrete, E_{cm}: mean secant (elastic) modulus of concrete, γ_v: partial safety factor for stud connector (=1.25). As per the Highway Bridge Specification of Japan Road Association (JRA), Japan [(Japan Road Association, 2002.)] the allowable shear force of headed stud is determined as per equations (2.4-2.5).

$$Q_a = 9.4 d^2 \sqrt{\sigma_{ck}} \qquad (H/d \geqq 5.5) \qquad (2.4)$$

$$Q_a = 1.72 dH \sqrt{\sigma_{ck}} \qquad \left(\frac{H}{d} < 5.5\right) \qquad (2.5)$$

where, Q_a: allowable shear force of stud (N), d: shaft diameter of stud (mm), H: total height of stud (mm), σ_{ck}: specified compressive strength (N/mm^2). And, according to the specifications of Japan

Society of Civil Engineers (JSCE) [(JSCE, 2009)], the design shear strength of headed stud is determined as per equations (2.6-2.8).

$$V_{su} = \min(V_{su1}, V_{su2}) \qquad (2.6)$$

$$V_{su1} = 31A_{ss}\sqrt{\frac{h_{ss}}{d_{ss}}f_c'} + 10000 \quad (N) \qquad (2.7)$$

$$V_{su2} = A_{ss}f_{su} \quad (N) \qquad (2.8)$$

where, V_{su}: shear capacity (N), A_{ss}: x-sectional area of stud (mm^2), h_{ss}: height of stud (mm), d_{ss}: diameter in cross section of stud (mm), f_c': compressive strength of concrete (MPa), f_{su}: tensile strength of stud (MPa).

In Japan, JRA specifications are used for composite and hybrid girder design [(Nagai M, 2010.)]. The stud capacity in the JRA specifications is 0.12, 0.13, and 0.22 times those of the AISC, JSCE, and EURO code specifications, respectively, as shown in Table 2.1. Hence, in the current design method, the nominal shear force borne by the connector is limited to less than 50% of its actual capacity. Thus, the influence of sustained external loads has not been comprehensively studied because of the low design shear force level [(Maki T, 2013)]. As there exist a substantial gap between the JRA and other specifications, an avenue remained for researchers to investigate the issue and realise the effective uses of the stud capacity.

Table 2. 1: Headed stud shear strength as per different specifications and codes.

Headed stud				Concrete		Headed stud shear strength (kN)			
Diameter (mm)	Height (mm)	Area (mm^2)	Tensile strength f_u (MPa)	Desired compressive strength (MPa)	Elastic modulus *Ec* (MPa)	JRA (allowable shear)	EURO Code 4 (design shear)	JSCE (design shear)	AISC (nominal shear)
13	60	132.73	473	33	27000	8	37	61	63
Equivalent shear strength (allowable shear)						8	18	28	37

For the hybrid/composite girder designed with headed stud connections, calculating long-term deformation behaviour under sustained loading is crucial for ensuring serviceability; but in regard to this, limited studies are available that can be discussed with their findings.

(a) Bradford and Gilbert's (1991) study: Bradford and Gilbert [(Bradford MA, 1991)] investigated the behavior of a simply supported T-beam under sustained loading, where uniformly distributed loading condition was applied for a specific time duration as well as the same beam was also subjected to self-weight only to assess the shrinkage deformations and central deflection was measured both experimentally and analytically. The experimental results as presented in Figure 2.2 showed the time dependent increase in deformation as well as shrinkage deformation that can significantly influence the behavior.

(b) S.Al-Deen et.al (2011) study : S.Al-Deen et.al. [(Al-Deen S, 2011)] conducted experiment to evaluation the long-term behavior of steel concrete composite beams where, simply supported beams were designed with headed stud shear connections formed by a steel joist and a solid concrete slab. Then sustained load was applied with concrete blocks for the whole duration of the long-term experiments and shrinkage effects was also measured. The experimental results as presented in Figure 2.3 showed considerable increase in beam deflection over time with sustained loading due to concrete creep and shrinkage.

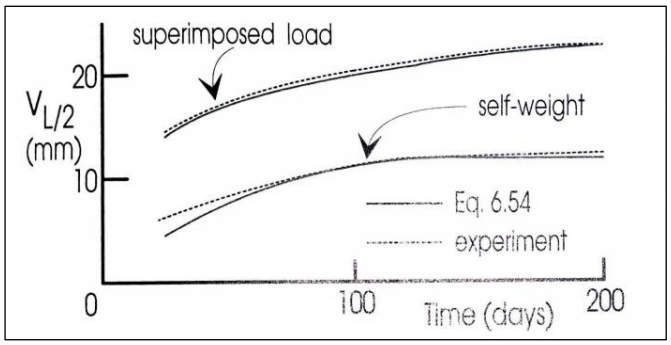

Figure 2. 2: Bradford and Gilbert's (1991) study

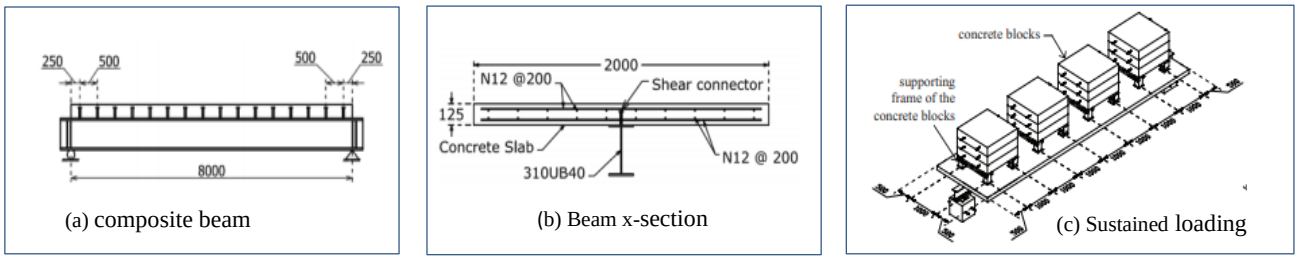

(d) Measured long term (central) deflection of beam

Figure 2. 3: S.Al-Deen et.al (2011) study

(c) Ban et.al (2015) study: Ban et.al. [(Ban H, 2015)]conducted experiment to evaluate the long-term behavior of steel- concrete composite beams where, simply supported beams were designed with shear connections (blind bolts) and sustained load was applied with steel plates for the whole duration of the long-term experiments. The results as presented in

Figure 2.4 showed that time dependent deflection was obvious and showed a considerable increase over time.

(d) Kwak and Seo [2000] study: Kwak and Seo [(Kwak HG, 2000)] developed an analytical model for predicting the long-term behaviour of composite girder bridges. This analytical model investigated the effects of creep and shrinkage of concrete and its contribution to the long-term structural behaviour.

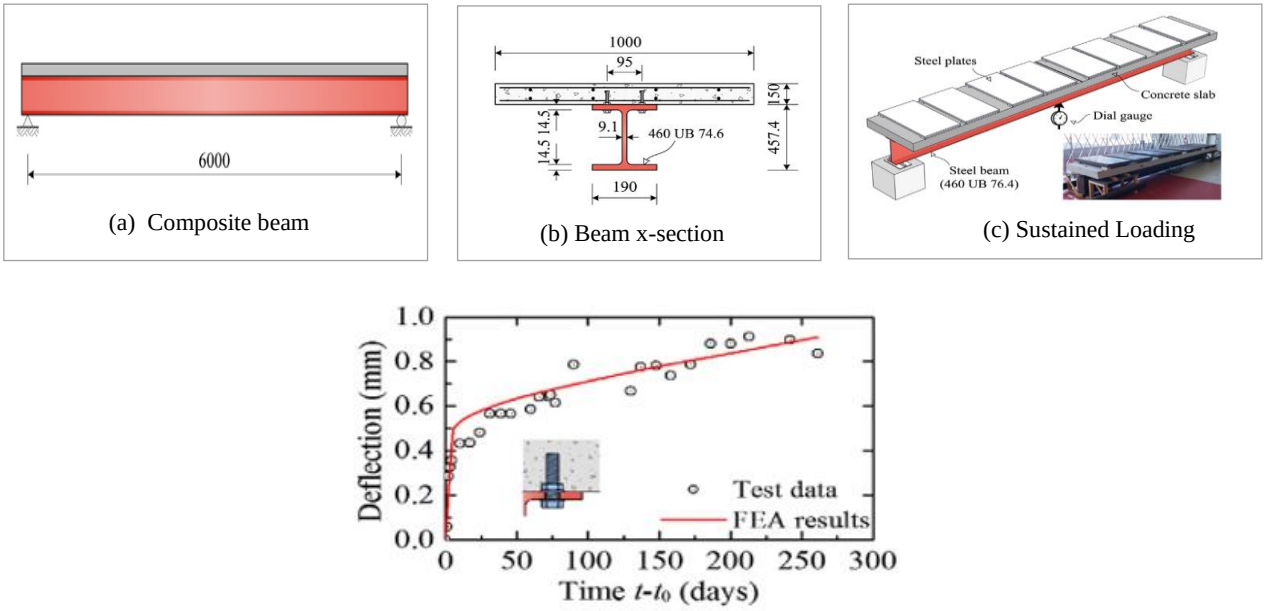

(a) Composite beam

(b) Beam x-section

(c) Sustained Loading

(d) Measured long term (central) deflection of beam

Figure 2. 4: Ban et.al (2015) study

(e) Mirza. O and Uy.B [2010] study: O. Mirza and B. Uy [(Mirza.O, 2010)] , in their study mentioned that even though the combination of steel and concrete enhances the strength and stiffness of composite/hybrid structures, the time-dependent behaviour of concrete may weaken the strength of the shear connection. Due to time dependent creep, when the concrete loses its strength, it will transfer its stresses to the structural steel through the shear connections and this behaviour will reduce the strength of the composite member. Although time dependent deformations for concrete are not a major concern with respect to the collapse of structures; even though the creep of concrete is considered to cause deformations with increasing time, there is no evidence of significant damage to the concrete material but if its long-term serviceability is being compromised accommodating the creep deformation may result in a drastic reduction of their design life as reported in studies by Bazant and Tsubaki (1980) and Mazzotti and Savoia (2003).

Besides the above-mentioned studies on composite structures, few researches were also carried out to investigate the mechanical behavior of headed stud and proposed equations to calculate shear capacity and slip displacement that can be discussed with their findings-

(f) Hiragi et. al [1989] study: Hiragi et. al. [(Hiragi H, 1989)] in their study, discussed the mechanical behavior of the headed stud in the composite steel-concrete beam under both static and fatigue loadings. In case of static loading, static shear decreases if the concrete around the headed stud are not properly connected with the headed stud and it increases in the lateral direction and larger in concrete having no reinforcement. However; in fatigue loading, even though strength decreases if the concrete around the headed stud are not properly connected with the headed stud, it does not have much influence on difference between longitudinal and lateral direction if the spaces of headed studs are kept constant.

(g) Shima et. al [2008] study: Shima et. al [(Shima H, 2008)] in their study, mentioned that existing design method of composite structures assumed as studs are to be free from deformation due to shear forces even though in reality, the studs deform to a considerable extent. Therefore, it will be more rational and if the design method allows the tolerance of the stud deformation for which the equations of expressing the relationship between shear force and displacement are indispensable. Hence, Shima et. al. carried out the experiments by changing the stud diameter, height, concrete strength and proposed a shear force-slip displacement relation formula of the stud. A shear force-displacement relationship for studs has been proposed by many researchers as a load-bearing equation and were not always applicable to other stud of different diameter and height. However, Shima et. al. used the normalized parameters and proposed the following generalized equations (2.9-2.11).

$$V = V_u\left(1 - e^{-\frac{\alpha\delta}{\Phi}}\right)^{2/5} \qquad (2.9)$$

$$\alpha = 11.5(1.1(\gamma - 1)^2 + 1)f_c'/f_{c0}' \qquad (2.10)$$

$$\delta_p = \delta - 0.04\phi(1 - e^{-\frac{24\delta}{\phi}}) \qquad (2.11)$$

where, V: shear force (N), V_{su}: shear capacity (N)\, δ: slip displacement (mm), ϕ: diameter of stud (mm), f_c': compressive strength of concrete (MPa), $\gamma = V_{su2}/V_{su1}$: capacity ratio, δ_p: residual slip displacement (mm).

(h) Maki et. al study: Maki et. al [(Maki T, 2017)] in their study, assumed that sustained loading will influence the displacement behaviour of stud, accordingly pushout specimen with two shear studs were investigated both under static and sustained load. It was confirmed that the effect of sustained loading on the displacement was particularly large. Following this study, later the pattern of loading was changed, and the test was carried out by extending the loading time. As a result of the experiment, it was observed that the amount of deformation

was increased while the load was extended to three months. Moreover, the residual displacement was increased, and the ratio was greater than that of the static load.

2.3 Statement of the Problem: The long-term deformation

As indicated by the afore-mentioned literature review, it is revealed that, the existing design standards what are practiced in Japan allows very limited load carrying capacity of headed studs and assumes almost insignificant deformation of the studs. Therefore, it is considered that the design method which allows effective uses of stud shear strength could be a way forward in perspective of a more rational and economical design with easing the constructability for practical applications. To adopt such a design method that allows effective uses of stud strength and incorporates parameters that clarify the influence on its deformation behaviour, and mechanism are very crucial. Due to the local deformation behaviour of headed studs, how they can influence the deformation behaviour of structure as a whole are also an important issue. As already mentioned in forgoing literature, Shinozaki et al. [(Shinozaki H, 2014)] adopted an innovative hybrid girder, whose junction part or embedded zone is devised with headed stud shear connections as shown in Figure 2.5. The uses of enhanced stud strength in such hybrid girder connections will make it less complex as the number of connections will be reduced and then will increase its constructability. In reality; for composite girder, the sustained load is explicitly considered in design. However; for hybrid girder, particularly the long-term deformation behavior of junction under sustained loading is not

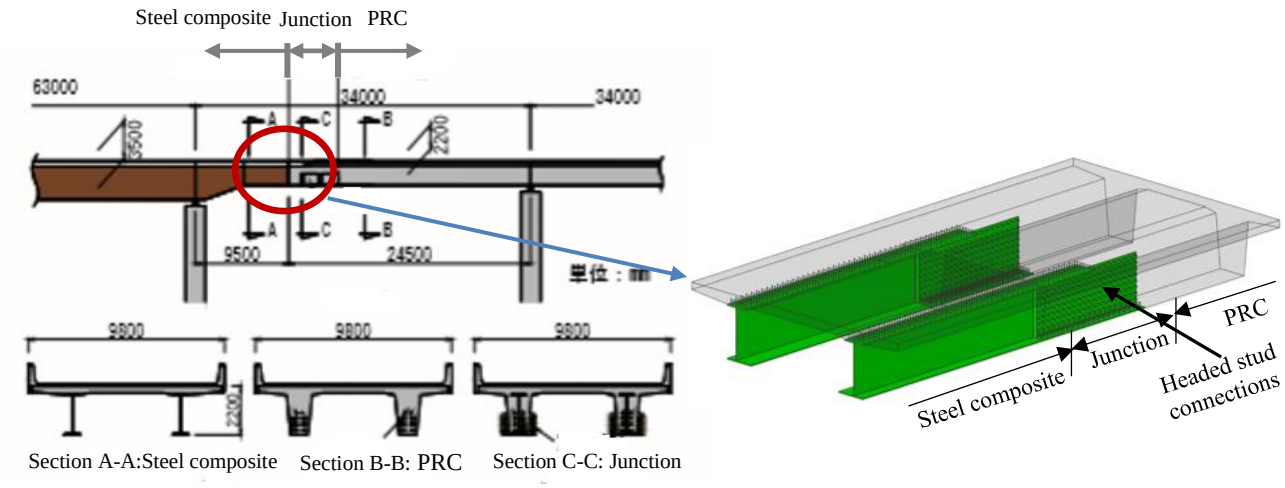

Figure 2. 5: Hybrid girder with headed stud shear connections (***Shinozaki et. al***)

considered explicitly. Although time dependent deformations for concrete are not a major problem or concern with respect to the collapse of structures, they are important issues that need consideration for serviceability and durability of structures. Even though creep of concrete is considered to cause long-term deformations under sustained load, there is no evidence of significant damage to structures [(Mirza.O, 2010)]. For composite structures, if long-term serviceability is

being compromised with the creep deformation may result in a drastic reduction of their design life as also reported in studies by Bazant and Tsubaki (1980) and Mazzotti and Savoia (2003). For the hybrid girder that adopted by Shinozaki et al, due to the uses of enhanced stud capacity; the number of shear connections will be reduced. The time-dependent behaviour of concrete may weaken the strength of the shear connection and when the concrete loses its strength, it will transfer its stresses to the structural steel through the shear connections and it is assumed that under the sustained load the stiffness of junction will be reduced even though the capacity might be same. When the sustained long-term load will act on the junction of the hybrid girder, it is assumed that the compressive force will act on the concrete near the stud as shown in Figure 2.6 below. When cconcrete sustains compressive stress on the junction containing headed stud connections, it might lead to temporal deformation (creep deformation) due to sustained loading action. If the shear force sustained; it is thought, that will develop a continuous compressive force around the stud-concrete vicinity and will lead to a relatively high-level stress generation in that region and consequently creep deformation (slip displacement) will continue for the entire period. Presently, the hybrid

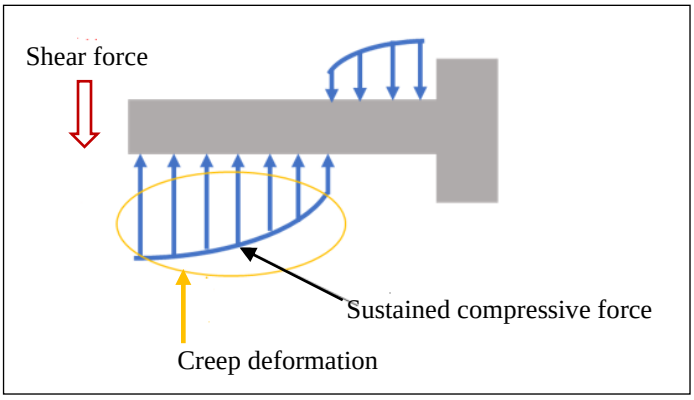

Figure 2. 6: Conceptual diagram on stress distribution around the stud

girder design standard considers the effect of the creep of the concrete for the whole structure only when concrete slab is subjected to compressive force; however, the localized creep that occurs in stud-concrete vicinity mainly due to the stress concentration is still not being considered. The present design method considers the creep effect by the following procedure: by calculating the structure strength including the bending strength, compressive strength etc., and then considers the stress distributed or decreased due to the creep; then the particular strength times the effective coefficient gives the final strength. This coefficient doesn't explicitly reflect the effect of creep occurred at stud-concrete vicinity that might be large or smaller than the actual situation. Thus, the stress aroused from creep is still not calculated precisely. Since, owing to the sustained loading action creep deformation induced in concrete, there is a possibility that this mechanical behavior of

both headed stud and concrete will have an influence on the overall deformation of the whole structure; and this particular area was not considered in the previous research.

The type of junction that adopted for hybrid girder is designed mainly according to structural details which is prescribed based on the results of experimental works. In that concept of design, the junction is considered to have greater capacity than the other parts, i.e. steel girder and PRC girder part. Since, there is no way to verify the capacity of the junction, therefore, to ensure a safety-side design approach; so many shear connectors are provided in junction. Huge number of shear connectors usually induce a problem in construction works, especially in concreting, since the junction part becomes very congested with steel plates, reinforcements, prestressing bars, and headed studs within a narrow space. Thus, the main concern of this study is to reduce the number of shear connectors in junction part; aiming to improve the constructability with a consequent savings of cost.

As per practical consideration and applicability, before reducing the number of shear connectors, it needs to investigate its impact on the structural performance of junction for limit state design considering serviceability and ultimate limits. For serviceability approach, it may influence on deflection, vibration, fatigue, etc and for ultimate limit, capacity will be a major concern. Since, the junction part is a composite section with a same sized concrete cross section with steel girder section, thus, even though the number of shear connectors are reduced in the junction part, the capacity of junction may be possibly decreased but still it would have much greater capacity than the general sections like composite girder and PRC girder. Therefore, from the point of ultimate limit state, the number of shear connectors in junction part may possibly be reduced

From serviceability point of view, even though it needs to investigate some factors such as deflection, fatigue, vibration, etc., under the present study, scope is focused mainly on deflection which is governed by instantaneous stiffness (short-term deflection) and time-dependent material properties (influenced by on long-term deflection) such as creep, shrinkage and relaxation. Regarding instantaneous stiffness, the number of shear connectors may have a sensitive impact on it. Therefore, a detail investigation is needed on that impact, as to reduce the number of shear connectors. If it could lead to a solution to reduce the number of shear connectors based on instantaneous stiffness, time-dependent problem would be major issue to investigate. However, there are very few researches that investigate the time-dependent behavior of junction part. Thus, this study focused on the long-term deformation (deflection) behaviour as a very fundamental study. As already mentioned, that serviceability includes not only deflection but also fatigue and vibration. So, investigating the remaining factors shall have importance and could be investigated in the future, in order to realize the reduction of the number of shear connectors in junction part.

Under the circumstances already mentioned above, owing to sustained loading, the time-dependent behaviour, particularly deformation (i.e., deflection, displacement, strain behaviour, etc.), is crucial for ensuring serviceability for hybrid girders. If this is not exactly predicted, unexpected secondary problems, e.g., over-deflection, increase in impact load, and cracking of concrete, may result in reduction of service life in geometric progression. Therefore, investigations must be conducted for quantifying such behaviour to obtain a basis and guidelines for designing such innovative girders while considering the long-term response with time effects. Then, the time-dependent deformation behaviour for such a girder under sustained loading can be clarified, and its application for practical construction may be promoted for sustainable design.

2.4 References

Oehlers DJ, Bradford MA. "Composite steel and concrete structural members". Kidlington, Oxford, UK: Elsevier Science Ltd.; 1995.

Choo JF, Choib YC, Choic WC, Yoo SW. Behavioral characteristics of hybrid girders according to type of steel–concrete connection. Archives of Civil and Mechanical Engineering 2019; 19:47–62.

Nie J, Cai CS. Steel-concrete composite beams considering shear slip effects. Journal of Structural Engineering ASCE 2003;495–506.

Kim SE, Nguyen HT. Evaluation of connection efficiency of hybrid steel-concrete girder using finite element approach. International Journal of Mechanical Sciences 2012; 61:8–23.

Deng Y, Morcous G. Efficient prestressed concrete-steel composite girder for medium-span bridges. I: System description and design. Journal of Bridge Engineering ASCE 2013;1347–1357.

Nilson AH, Darwin D, Dolan CW. Design of Concrete Structures. New York: Mac-Graw Hill; 2010.

Shinozaki H, Asai H, Kaminaga Y, Maki T, Mutsuyoshi H. A study on joint of composite steel girder and PC girder using shear connecting method. Journal of Structural Engineering JSCE 2014;60A(2014/3):861–871.

Prakash A, Anandavalli N, Madheswaran CK, Rajasankar J, Lakshmanan N. Three-dimensional Fe model of stud connected steel-concrete composite girders subjected to monotonic loading. International Journal of Mechanics and Applications 2011;1(1):1–11.

Allobody E. Finite element analysis and design of steel and steel-concrete composite bridges. Kidlington, Oxford, UK: Elsevier Inc.; 2014.

Anju T, Smitha KK. Finite element analysis of composite beam with shear connectors. International Conference on Emerging Trends in Engineering, Science and Technology (ICETEST - 2015), Procedia Technology 2016;24:179–187.

Pallarés L, Hajjar JF. Headed steel stud anchors in composite structures: Part I–shear. Department of Civil and Environmental Engineering, University of Illinois at Urbana-Champaign, NSEL Report Series 2009; NSEL-013.

Ollgaard JG, Slutter RG, Fisher JW. Shear strength of stud connectors in lightweight and normal-weight concrete. AISC Engineering Journal 1971; 71-10: 55–64.

American Institute of Steel Construction. Specification for Structural Steel Buildings. Chicago: 2016. [14] European Committee for Standardization, Eurocode 4: Design of composite steel and concrete structures-Part 1-1: General rules and rules for buildings. Brussels: 2004.

Japan Road Association. Specifications for highway bridges part-2-Steel bridges. Tokyo: 2002.

Japan Society of Civil Engineers. Standard specifications for steel and composite structures. Tokyo: 2009.

Nagai M, Yamaguchi E, Yoda T, Nogami K. Recent trend on design and construction of steel and composite bridges in Japan. In: IABSE-JSCE Joint Conference on Advances in Bridge Engineering-II. Dhaka: 2010.

Maki T, Watanabe R. Mechanical behavior of stud shear connector under sustained shear and compression forces. Proceedings of the Thirteenth East Asia-Pacific Conference on Structural Engineering and Construction. Hokkaido: 2013.

Bradford MA, Gilbert RI. Experiments on composite T-Beams at service load. Civil Engineering Transactions 1991; CE33 No. 4:285-291.

Al-Deen S, Ranzi G, Vrcelj Z. Long-term experiments of composite steel-concrete beams. The Twelfth East Asia-Pacific Conference on Structural ngineering and Construction. Procedia Engineering 2011;14:2807–2814.

Ban H, Uy B, Pathirana SW, Henderson I, Mirza O, Zhu X. Time dependent behaviour of composite beams with blind bolts under sustained loads. Journal of Constructional Steel Research 2015; 112:196–207.

Kwak HG, Seo YJ. Long-term behavior of composite girder bridges. Computers and Structures 2000; 74:583-599.

Mirza O, Uy B, Finite element model for the long-term behaviour of composite steel-concrete push tests, Steel and Composite Structures, 2010, Vol. 10, No. 1: 45-67

Hiragi H, Matsui S, Fukumoto Y, Derivation of strength equations of head stud shear connectors - fatigue strength, Proceeding of structural engineering, 1989; 1221-1232.

Shima H, Watanabe S, Formulation for load-slip relationships of headed stud connector, Proceedings of JSCE, 2008; 64(4): 935-947.

Maki T, Watanabe R, Zhang P, Deformation of headed stud shear connector under sustained shear forces, 11th Symposium on composite and hybrid structures, 2017.

CHAPTER 3

3 TIME DEPENDENT DEFORMATION OF STUD UNDER SUSTAINED SHEAR FORCE

3.1 Introduction

The hybrid girders that were designed with headed stud connections will be described in chapter later on, that were subjected to long-term experiment under sustained loading. Since, the stud connections are component of that girder it is considered that those will experience the time dependent shear force, this will induce long-term stud deformation inside the specimen, which is difficult to measure directly, but a clear understanding of this behaviour is needed to design a structure more rationally. Therefore, in designing those structures, it is necessary to quantify their time dependent slip-displacement behaviour as well as their strength, both of which are dependent on the loading applied[(Taira Y, 2013), (Ollgaard JG, 1971)]. Because of the large variety with enhanced interface shear resistance and complex dowel action, the strength and ductility of shear connectors are mostly determined experimentally [(Prakash A, 2011), (Allobody, 2014), (Anju T, 2016), (Nguyen HT, 2009)]. The most suitable method to determine shear force-slip relationship is to conduct an experiment on full-scale hybrid structures which might be a time-consuming and costly [(Bouchair J, 2012)]. Therefore, pushout tests are used to obtain such shear force-slip relationship, where the connectors are loaded directly [(Nguyen HT, 2009), (Bouchair J, 2012)] and this mechanical test are performed, where a material is mechanically push out from another with a purpose of measuring the interface de-bonding force and effects of shear between the materials. Although the shear force-slip relationship of shear connector has been widely examined and formulated, a very limited range of nominal design shear force carried by the connector are considered as well as the influence of sustained external loads is neither considered nor has been fully studied [(Ollgaard J.G., 1971), (Maki T, 2013)]. In this study, pushout tests were conducted to dtermine the long term slip behaviour with time effects under the sustained loading and presented in this chapter.

3.2 Design of specimens

The pushout specimens were designed considering the geometry and stud sizes of girder specimen as will be described in a section later on. As per the design method adopted by the JSCE Standard specification for steel and composite structures (JSCE, 2009) [(JSCE, 2009)], the shear capacity of pushout specimen with headed stud shear connector was determined as the minimum of the following two equations (3.1-3.2):

$$V_{su} = \min (V_{su1}, V_{su2})$$

$$V_{su1} = 31A_{ss}\sqrt{\frac{h_{ss}}{d_{ss}}f_c'} + 10000 \quad (N) \qquad (3.1)$$

$$V_{su2} = A_{ss}f_{su} \quad (N) \qquad (3.2)$$

were, V_{su}: shear capacity (N), A_{ss}: cross sectional area of stud (mm2),h_{ss}: height of stud (mm), d_{ss}: diameter in cross section of stud (mm), f_c': compressive strength of concrete (MPa), f_{su}: tensile strength of stud (MPa). The failure mode of the specimen is the demage of concrete in the vicinity of stud when shear force is calculated by equation (3.1) and failure mode become a tensile fracture of stud when the shear force is determined by equation (3.2). The long-term slip behavior of stud shear connector of size ϕ13-H60 was studied over a desired period of sustained loading. Six pushout specimens having identical cross sections labelled as PS I to VI were prepared and tested

3.3 Specimen assemble, casting and curing

The pushout specimens were produced, first by welding the headed stud connectors to the steel plate (H-200×200×8×12) and then casting a concrete slab over the steel plate around the connectors so that the steel and concrete sections are sandwiched with each other. Figure 3.1 shows the schematic view of the specimen used in this study. Each specimen consisting of total two concrete slabs on either side of the T-shaped steel flange surfaces which contains two headed studs each that mainly function to form composite structure by joining each other and prevent sliding. Since, it is difficult to cast the concrete in the H-shaped steel flange as shown in Figure 3.1; therefore, for simplicity, in this experiment, concrete was casted on the flange surface of T-shaped steel and after casting two T-shaped steel were connected by bolts. The joining of T-shaped steel is done with adequate care so that slide can be restricted during loading and shall have the same performance as H-shaped Steel. Formwork was prepared with steel sheet and plywood and putty was used to seal the gaps between them so that during casting concrete cannot come out through leakage. To maintain the clear cover from the concrete surface to the rebars, spacer was used. Since it is necessary to minimize the effect of friction force between steel flange and concrete blocks to obtain realistic value of slip displacement; therefore, grease was applied to the steel girder surface before casting of concrete to remove the steel-concrete interfacial friction. For compressive strength assessment, plastic cylinder molds were used for casting of cylinders. Then, casting was done with a concrete mix of target strength that was poured into the formwork and vibrator was used for compaction. After two days of casting, formworks were removed and the specimen went under a wet curing for 14 days, for which the specimen was covered with wet cloths. The details of the assembling and casting is presented in Figures 3.2 and 3.3.

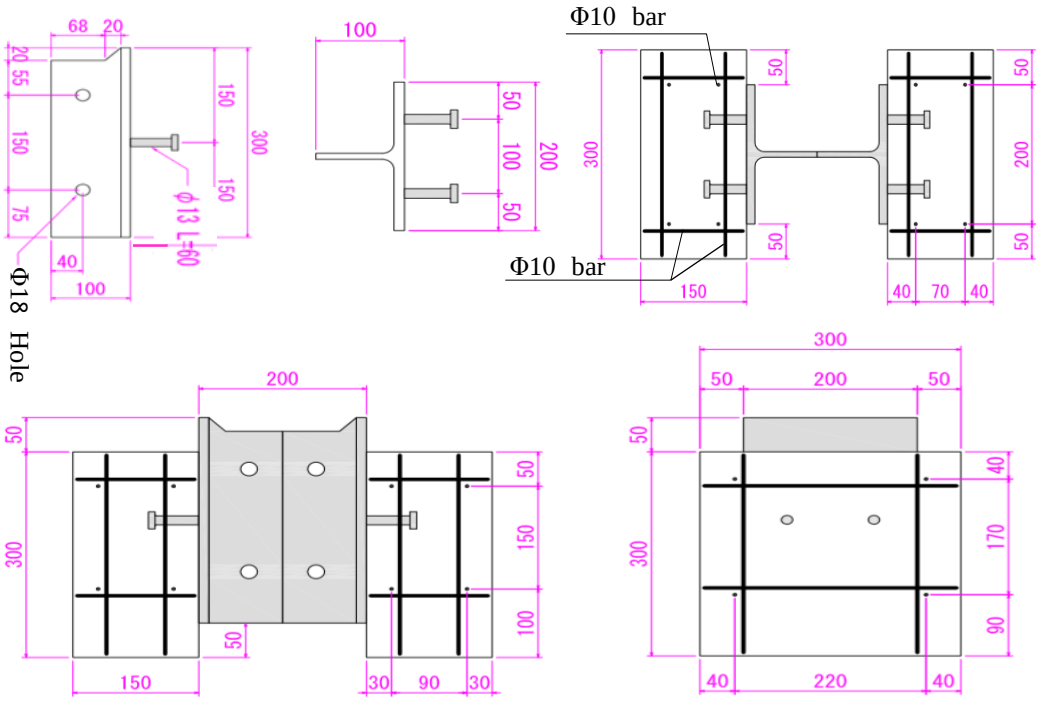

(a) Specimen drawing with steel girder, stud and reinforcement details

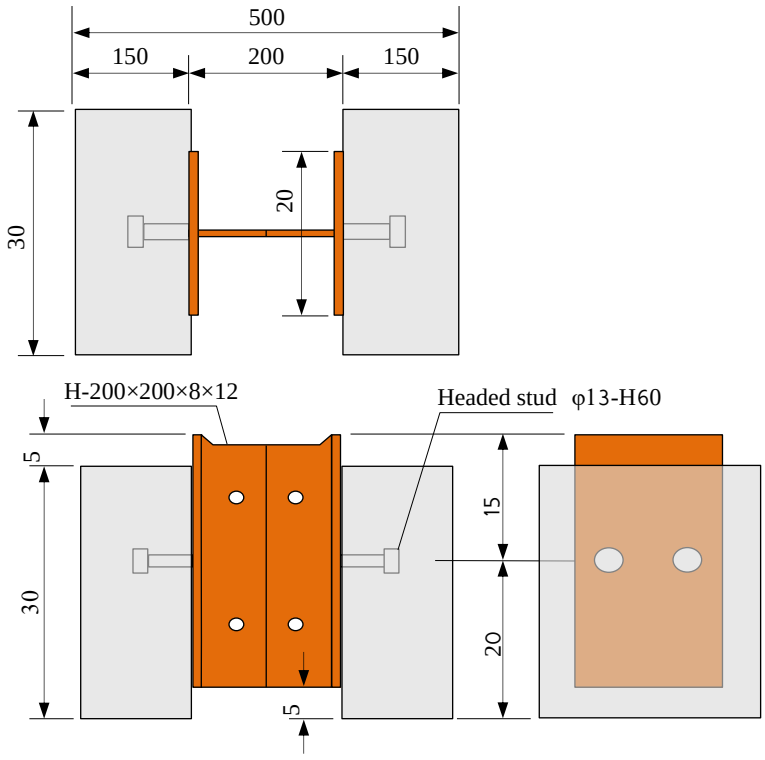

(b) Specimen drawing with steel girder, stud and reinforcement details.

Figure 3. 1: Configuration of pushout test specimen

3.4 Material properties

Six pushout specimens were prepared and cast. The instantaneous compressive strength of the concrete at different ages (time when each specimen was set for loading) for the specimens was

obtained through standard cylinder (200 mm in height and 100 mm in diameter) tests. The material properties of the concrete, steel girder section, and studs are summarised in Tables 3.1 and 3.2.

3.5 Experimental programme

3.5.1 Sensor layout and load setup

For the measurements taken during the pushout tests, sensors were placed at various locations on all specimens. Slip displacement measurement transducers and strain gauges were installed at suitable locations before applying shear force. Layout of such arrangement indicating the loading point and strain gauges locations are illustrated in Figure 3.4. Slip displacement between steel part and concrete slabs was measured by the high sensitive displacement transducers placed at the same height with the location of stud and measured in four locations as shown in the Figure 3. 54. The specimen's slip displacement is taken as the average of the all measured values. The strain gauges were also attached at the upper and bottom part of each stud to measure the strains of headed stud during the sustained loading. Those strain gauges were attached on the headed stud before casting the concrete. In this experiment, the web of steel plate was considered to have stronger stiffness than the flange and considered to have no deformation.

3.5.2 Specimen loading scheme and history

This study investigated the long-term slip deformation of the pushout specimen with headed stud connections (used in the girder specimen as described in sections later on) under a sustained loading to obtain a prediction of realistic behaviour needed to be considered in subsequent design of girders It was thus necessary to apply the loading scheme corresponding to the design load of hybrid girder specimen that can induce axial force to the studs and will induce slip deformation with time. Therefore, 30% of the stud capacity (corresponds to 80 kN design load of hybrid girder) and 15% of the stud capacity (corresponds to 60 kN design load of hybrid girder) was applied in pushout specimen, to which vertical loads were applied through universal testing machine and load cells as shown in Figure 3.5. Stud strength is determined based on its experimental ultimate failure load. Even though it seems that 30% stud strength in real use is excessive with considering the matter of factor of safety; in this study experiment is conducted considering a lower range also, i.e. 15% so that stud strength can be used in a realistic way with an adequate safety margin. In addition, a simplified formulation that will be developed under this study would accommodate a reasonable range of stud shear strength. Among the specimens, PS II to V were subjected to a sustained vertical shear force (i.e., application of vertical load for a specific time duration), and PS I was subjected to a static cyclic loading. The loading level, types and histories for all the specimens are presented in Table 3.3 and 3.4. Static loading was applied to specimen GS I to differentiate its slip behaviour

from the case of sustained loading. PS VI was maintained under self-weight only for the whole duration of sustained period to assess the slip deformation behaviour caused by environmental

(a) Specimen assemble and formwork preparation

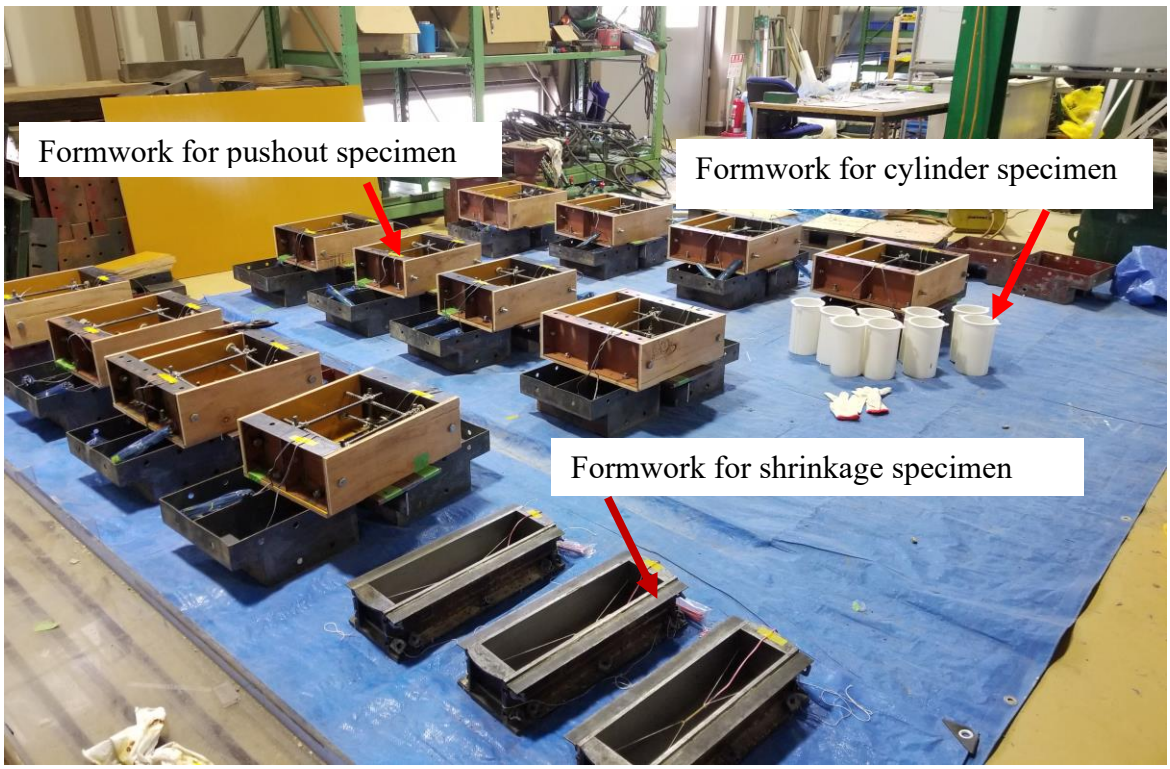

(b) Ready specimen for casting

Figure 3. 2: Pushout specimen assembling and casting preparation

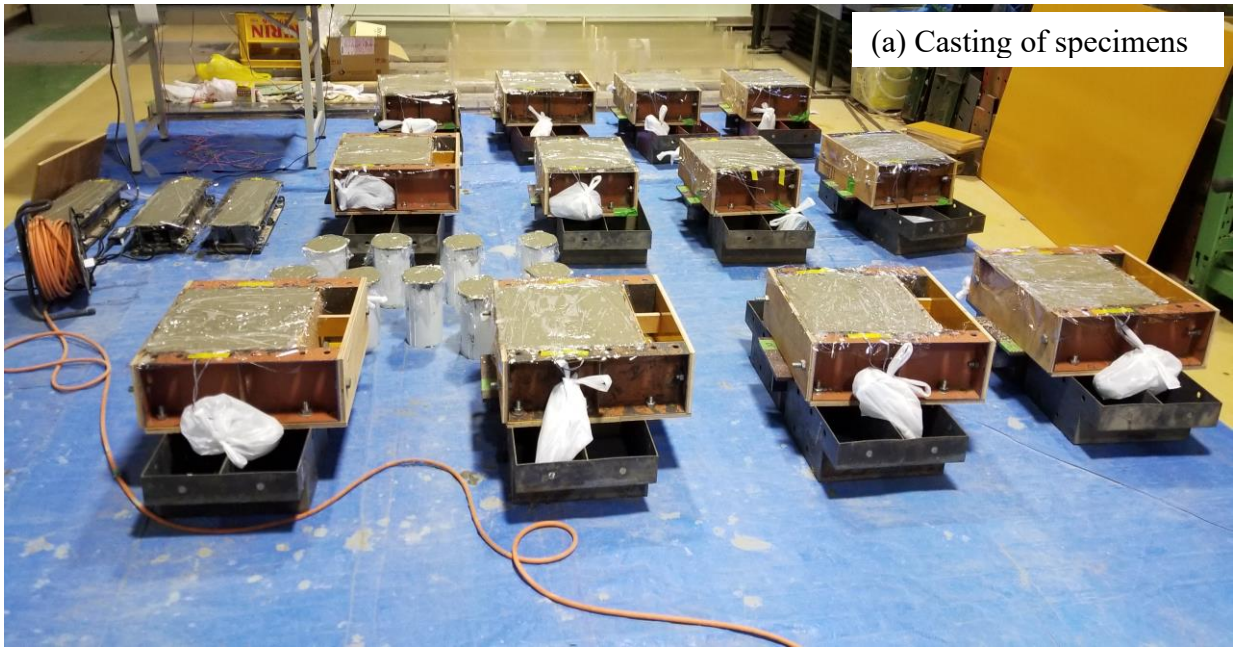

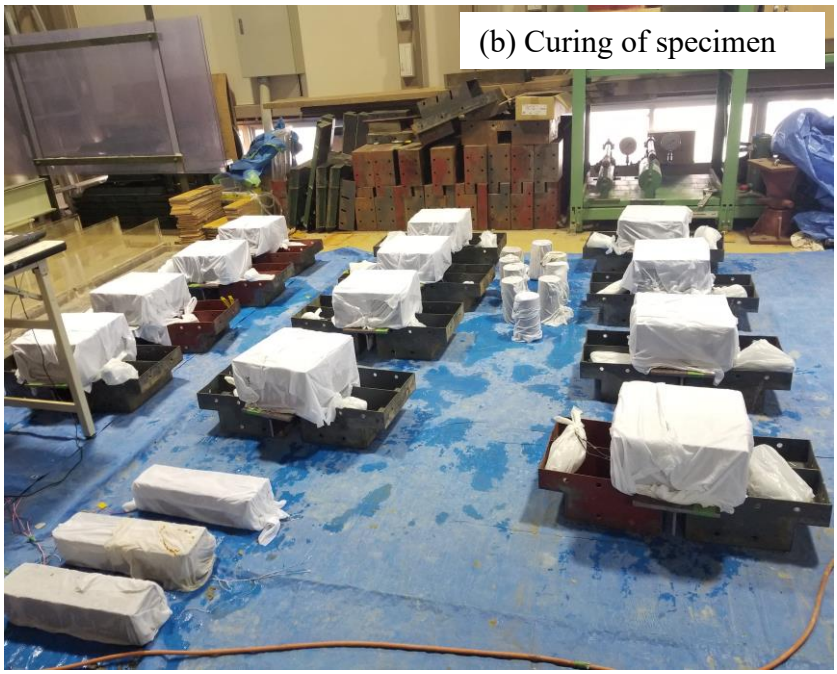

Figure 3. 3: Casting and curing of specimen in (a) and (b)

Table 3. 1: Concrete mix proportions and strength

Specimen	Concrete mix proportions (kg/m3)						Concrete strength MPa)		Type of cement
-	W/C ratio (%)	Cement	Water	Coarse aggr.	Fine aggr.	Air entraining agent	27 Days	87 days	-
PS I to VI	44.5	394	175	990	767	5.12	44.8	49.39	Early strength portland cement

variations. The same concrete as for pushout test specimens was used for preparing specimen for PS I was subjected to static cyclic loading with 5% shear force interval upto failure to obtain the

ultimate strength of the specimen. PS II to V were subjected to sustained loading of designated periods and PS VI was subjected to only under self-weight for whole duration of sustained loading. After the sustained periods, each specimen was subjected to static cyclic loading upto the failure. For PS I, the static cyclic loading was applied through the universal testing machine as shown in Figure 3. 35. The sustained loadings to the specimens were applied as a compressive force through the hydraulic jack on a PC steel bar of 17 mm diameter, and the load block and base block of that assembling as shown in the Figure 3. 5: . The PC steel bar is prestressed by the hydraulic jack and its pre-stressing force is applied as a load on the upper part of the H-shaped steel through the load block. The experimental setup and loading condition were applied as per standard procedure of Japan Society of Steel Construction (JSSC) [(JSSC, 1996)].

3.6 Environmental conditions

During the sustained loading, the environmental conditions was measured to distinguish the behaviour due to sustained loading to that caused by the variations in environmental conditions as shown in Figure 3.6; where, the time depicted indicates time since sustained loading.

Table 3. 2: Material properties of the steel and stud.

Specimen	Yield strength *fy* (MPa)		Tensile strength *fu* (MPa)	
	Steel girder flange	Stud	Steel girder flange	Stud
PS I to VI	353	430	469	493

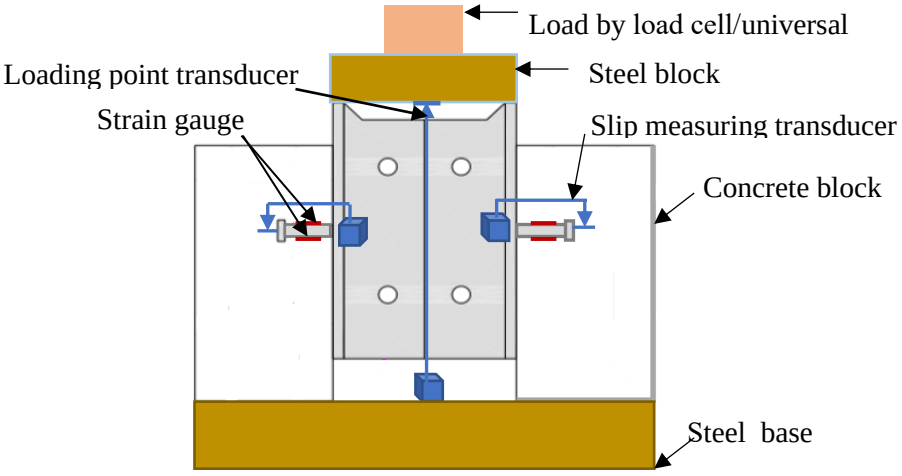

Figure 3. 4: Sensor layout for pushout specimen

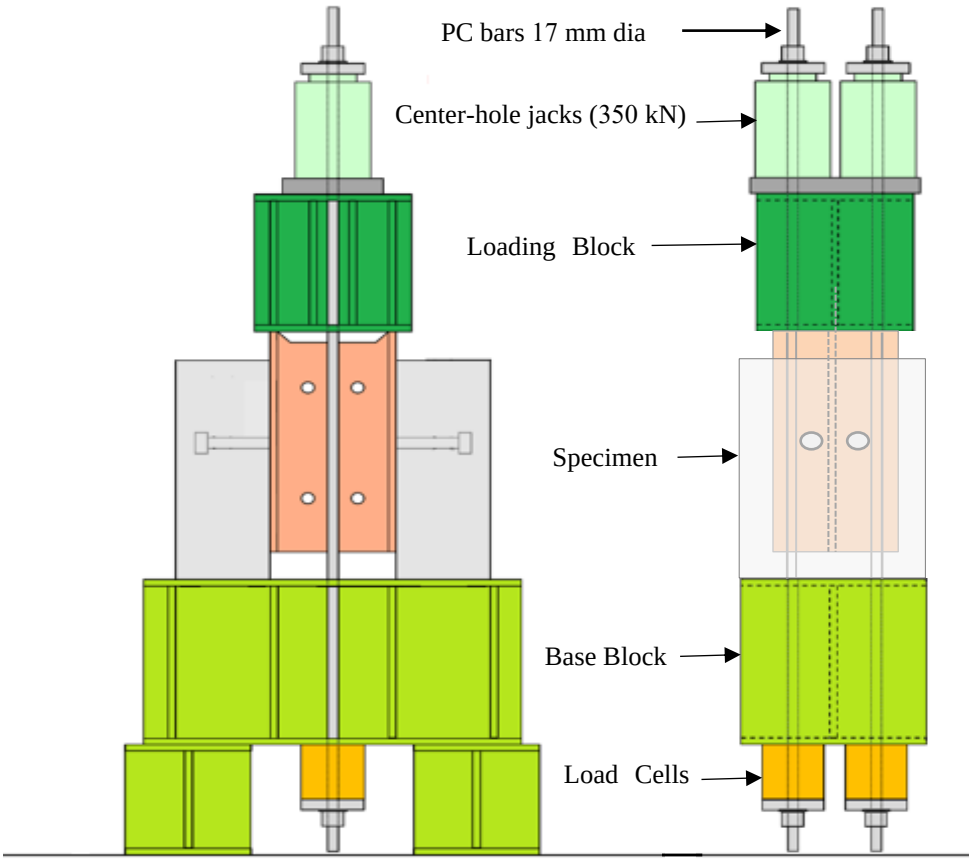

(a) Pushout test loading arrangement with load cells

(b) Practical laboratory load setup for pushout specimen

Figure 3. 5: Static cyclic and sustained load applied to the specimen

Table 3. 3: Calculation of sustained load level

Description	**Unit**	**Value**
Diameter of the stud (D)	mm	13
Length of stud (H)	mm	60
Shear strength (Vsu1)	kN	61.16
Shear strength (Vsu2)	kN	65.39
Shear strength ratio (Vsu2/Vsu1)	-	0.9454
Shear strength (adopted)(Vsu)	kN	65.39
Number of studs used	Nos	4
Total shear strength	kN	261.57
Level of sustained shear force (15%)	kN	39
Level of sustained shear force (30%)	kN	78

Table 3. 4: Specimen loading history

Specimen	Age of specimen from casting (days)	Time of loading (days)			Loading type
		15% Shear force (39 kN)	30% Shear force (78 kN)	Final loading	-
PS I	27	-	-	27th day	Static cyclic
PS II		30	-	57th day	Sustained
PS III		60	-	87th day	Sustained
PS IV		-	30	57th day	Sustained
PS V		-	60	87th day	Sustained
PS VI		-	-	87th day	Self-weight only

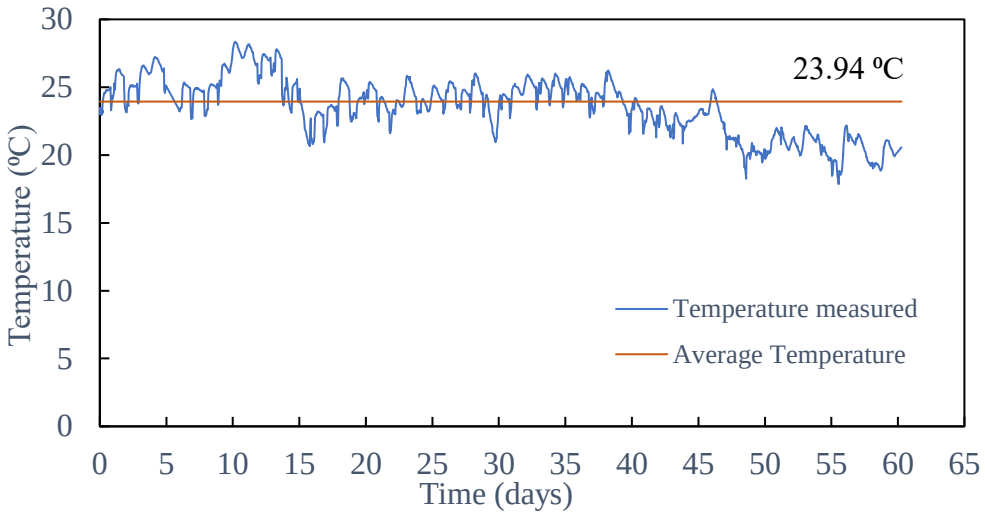

Figure 3. 6: Temperature variations during sustained loading

3.7 Test results and discussions

3.7.1 Time dependent shear force-slip displacement curve

The specimens were subjected to different types of loading as already mentioned in Table 3.4 and then each of them was loaded to failure using an experimental laboratory set-up, which is presented in Figure 3.5. The exhibited shear force-slip displacement relationship of all the specimens are presented in Figure 3.7 and an enlarged view for the low displacement part to distinguish the sustained loading effect is presented in Figure 3.8. For the static cyclic loading specimen PS I, repeated cyclic loading was performed upto the ultimate failure level whereas for the sustained loading specimens PS II-PSV; same cyclic loading process was performed but they differ in that way of subjected to remaining cyclic loading after the elapsed time of sustained periods. For both static and sustained loading, concrete undergone inelastic deformation at ultimate failure load and they exhibited failures through the shearing off the stud shear connectors. The average shear force -slip curves for all the specimens are compared and it seems that each specimen exhibited nearly the same trend with a distinct evidence of increasing long-term displacement for the sustained loading specimens. In the later part of this chapter, the detail will be discussed on long-term behaviour.

3.7.2 Slip displacement over time

Slip displacements at the locations of the pushout specimens were measured using the displacement transducer, as shown in Figure. 3.4 to assess the time-dependent deflection behaviour as reported in Table 3.5 and Figures. 3.9. The experimental results showed that both at 15% and 30% shear force level respectively, the starting slip displacements were not so closer rather varied slightly in the case of sustained loading specimens PS II (0.040 mm, 0.180 mm), PS III (0.051 mm, 0.150 mm), PS IV (0.040 mm, 0.186 mm) and PS V (0.048 mm, 0.144 mm); as those of the static cyclic loading specimens PS I (0.043 mm, 0.205 mm, respectively). Although, all the specimens were loaded in same casting age with same environmental conditions, it become quite complex to identify the reasons which made such differences in slip displacements. Most importantly, static cyclic specimen was tested under universal loading machine where load might be applied in a much-controlled way and for the sustained loading specimens; loads were applied through hydraulic jacks by manual hand control. Therefore, the incremental load steps and peak force level for each cycle varied from each other which might have influence on the differences. This may also have been caused by a lateral uneven distribution of section stress because of the existence of shear connections, resulting in different slip displacements for those specimens [(Haigen, 2015)]. For specimen PS II, at 30% shear force level; the slip displacement relatively higher which might be due the reason that it was subjected to 15% shear force for 30 days before reaching the 30% load

level. This long-term sustained loading might be a reason to induce greater displacement at later stages of loading although this behaviour was not evidenced in PS III. The sustained loading

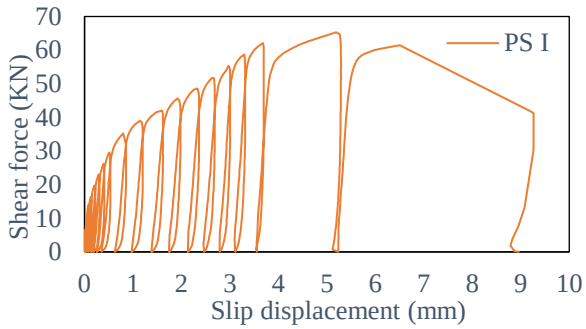

(a) PS I

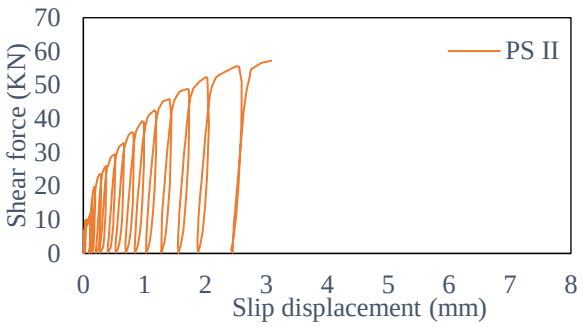

(b) PS II

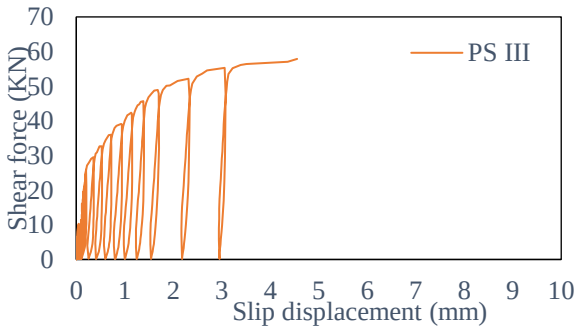

(c) PS III

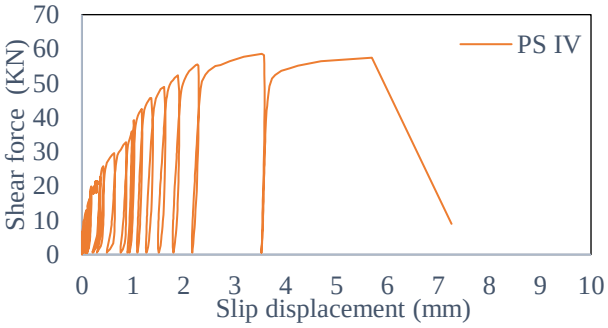

(d) PS IV

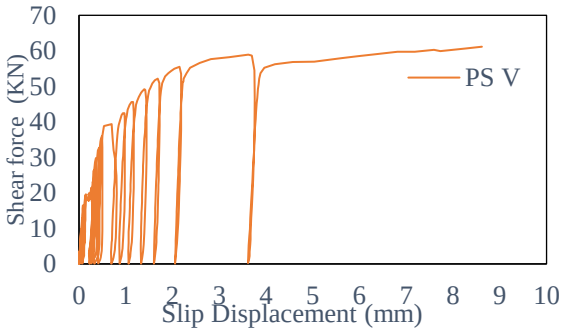

(e) PS V

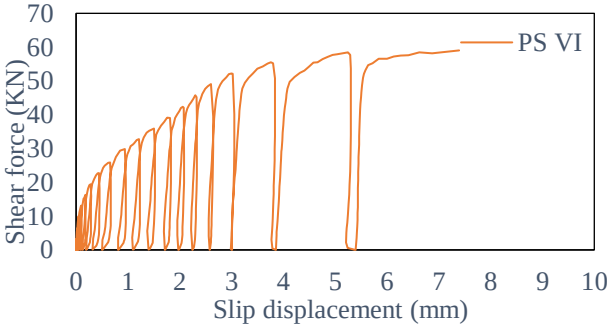

(f) PS VI

Figure 3. 7 Shear force and slip displacement of each specimen

specimen PS II and PS IV were subjected to 15% and 30 % sheaf force respectively for a 30-day period each; both of them exhibited slip displacement increment over time. To assess whether the same behaviour existed for a longer exposure period, specimen PS III and PS V were subjected to same loading condition of 15% and 30% respectively for a period of 60 days each. PS III showed a

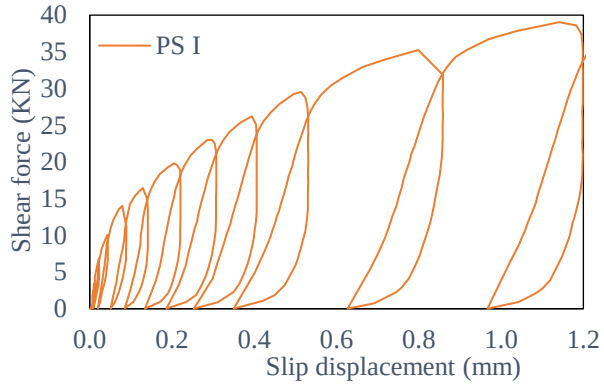

(a) PS I

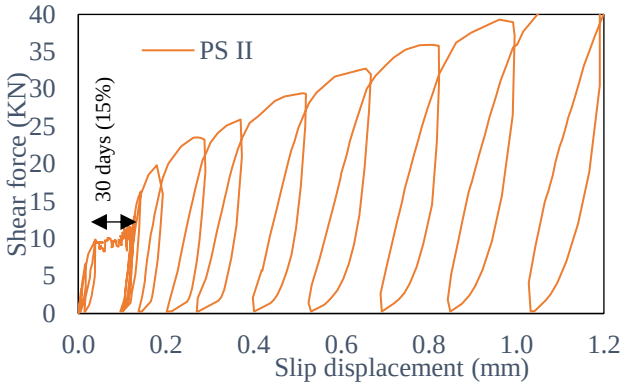

(b) PS II

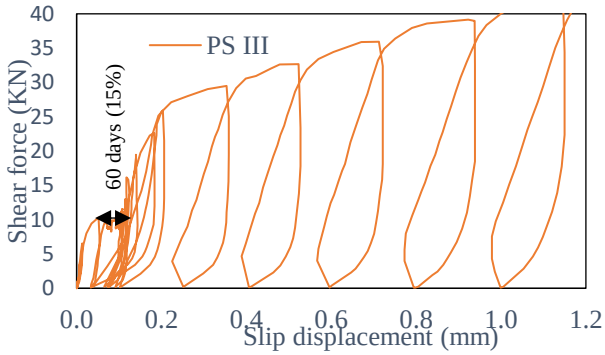

(c) PS III

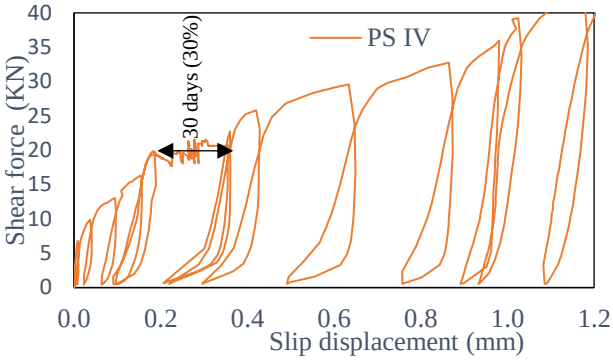

(d) PS IV

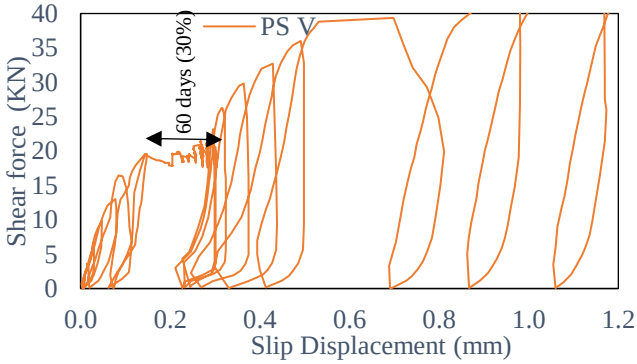

(e) PS V

Figure 3. 8: Shear force-slip displacement of each specimen (low displacement area enlarged)

cumulative increment of 0.033 mm and 0.034 mm for 30 and 60 days respectively and PS V showed a cumulative increment of 0.131 mm and 0.149 mm for the same exposure time respectively. On comparing the incremental displacement values for PS III with that of PS V , it was strongly substantiated that the major part of the displacement occurred at the earlier stages of sustained periods, owing to which, the incremental deflection values decreased with the passing of time at the later stages, which indicated the asymptotical nature of time-dependent displacement behaviour.

The slip-displacement behaviour both in quantity and nature differ slightly from each other in case of 15 % sustained loading-specimens and 30% sustained loading specimens. This might be due to the reason of variations of environmental conditions as shown in Figure 3.6, that caused the fluctuations of load level. Another reason may be that due to unequal load level at any step and due to the existence of shear connections may result in a lateral uneven distribution of the section stress that could have results in differing displacements in each specimen. The mechanism behind the time dependent displacement is mainly the creep of concrete which is purely dependent on the stress that induce the creep strain. As the time elapsed, the creep deformations occur beneath the stud at stud-concrete interface and when stud tends to deform with a upward bending then due to sustained effects this creep induces tensile strain at contact area of two sides of the studs, This deformation is very localized and induce additional stress to the concrete. For 30% shear force, slip displacement become almost double within 30 days which indicates a reduction of stud stiffness about 50%. As the creep and shrinkage of the concrete are considered as the causes of time-dependent behaviour [(Mirza.O, 2010), (Okui Y, 2007)], to differentiate their effects, a comparison of the slip displacement behaviour of PS VI is presented in Figure 3.9. The displacement recorded for PS VI was assumed to be representative of shrinkage due to environmental effects, and the displacement recorded for other sustained loading specimens were due to the combined effect of creep and shrinkage. The shrinkage deflection appeared to be very insignificant but the displacements due to creep (deflection other than shrinkage) in PS II-V were much more dominant than the shrinkage.

Table 3. 5: Slip displacement of specimens under loading

Test specimen and Shear force (SF)	Slip displacement (mm)		Slip displacement for 30 days sustained period (mm)			Slip displacement for 60 days sustained period (mm)		
	15 % (SF)	30 % (SF)	start	end	increment	start	end	increment
PS I-15% (SF)	0.043	0.205	-	-	-	-	-	-
PS II-15% (SF)	0.040	0.180	0.041	0.120	0.079	-	-	-
PS III-15% (SF)	0.051	0.150	0.073	0.106	0.033	0.073	0.107	0.034
PS IV-30% (SF)	0.040	0.186	0.190	0.287	0.970	-	-	-
PS V-30% (SF)	0.048	0.144	0.152	0.283	0.131	0.152	0.301	0.149

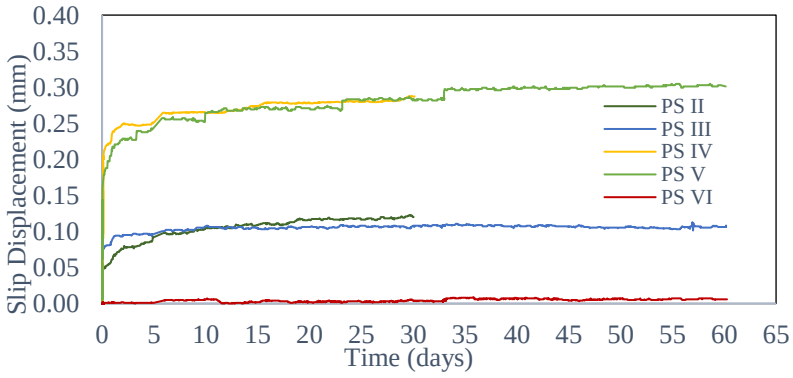

Figure 3. 9: Long-term slip displacement under loading

However, the shrinkage displacement was not identified precisely because similar conditions and arrangement was not achieved as that were for other specimens without the load. During the sustained loading period, if the displacement increment ratio is expressed by the following equation (3.3), the resultant displacement increment behaviour over time is presented in Figure 3.10.

$$k(t - t_0) = \frac{\delta(t) - \delta(t_o)}{\delta(t_o)} \qquad (3.3)$$

Where, $k(t - to)$: slip displacement increment ratio, $\partial(t)$: slip displacement at time t, $\partial(t_o)$: slip displacement at time t_o, and t_o : sustained loading start time. Since, the nature of the curves is very much influenced by the initial displacement at start of the sustained loading, the specimens PS II and PS III under the same 15% shear force, showed different curvatures as their start displacement were significantly differed. The similar behaviour was also observed for other two specimen PS IV and PS V who were subjected to 30% sustained shear force. Convergence tendencies are shown as time passes and for larger the time, the greater the displacement increment ratio which exhibited the trend of creep deformation characteristics of concrete.

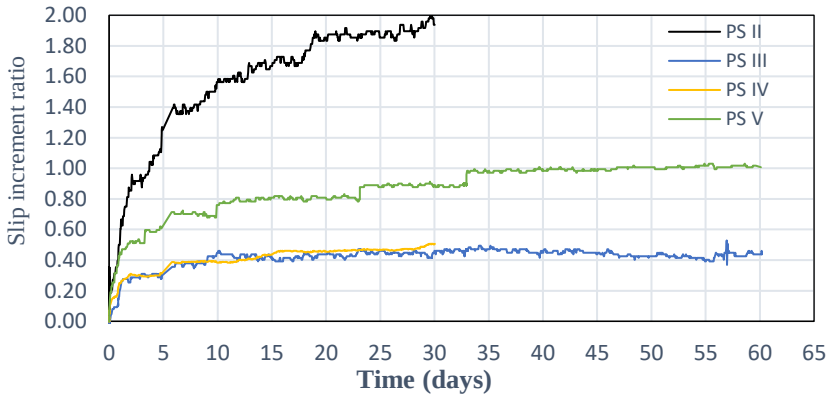

Figure 3. 10: Slip displacement increment ratio over time

3.7.3 Skeleton curve and residual displacement

The skeletal curve of the relationship between shear force and displacement of each specimen and changes in residual displacement during unloading in each cycle is shown in Figure 3.11. The black dotted lines in that figure, show the existing model proposed by Shima et. al. (Hiroshi SHIMA, 2008) and has been formulated by the following equations (3.4) ~ (3.6).

$$V = V_u\left(1 - e^{-\frac{\alpha\delta}{\phi}}\right)^{2/5} \qquad (3.4)$$

$$\alpha = 11.5(1.1(\gamma - 1)^2 + 1)f_c'/f_{c0}' \qquad (3.5)$$

$$\delta_p = \delta - 0.04\phi(1 - e^{-\frac{24\delta}{\phi}}) \qquad (3.6)$$

where, V: shear force (N), V_{su}: shear capacity (N), δ: slip displacement (mm), ϕ: diameter of stud (mm), f_c': compressive strength of concrete (MPa), $\gamma = V_{su2}/V_{su1}$: capacity ratio, δ_p: residual slip displacement (mm). It is observed that, sustained loading specimens have exhibited a shift towards the increasing displacement than the static cyclic specimen and the existing model and a closed-up view of all the specimen is illustrated in Figure 3.11. The residual slip displacement which is defined as a displacement when the applied load was removed in each cycle and that slip displacement that occurs at the maximum load of each cycle is plotted together as shown in Figure 3.12. The black break lines are also obtained from existing model proposed by Shima et. al. (Hiroshi SHIMA, 2008). As the residual slip displacement is governed only by the experienced maximum slip displacement in each cycle, it follows and holds the unique relationship for the control specimen (static case)

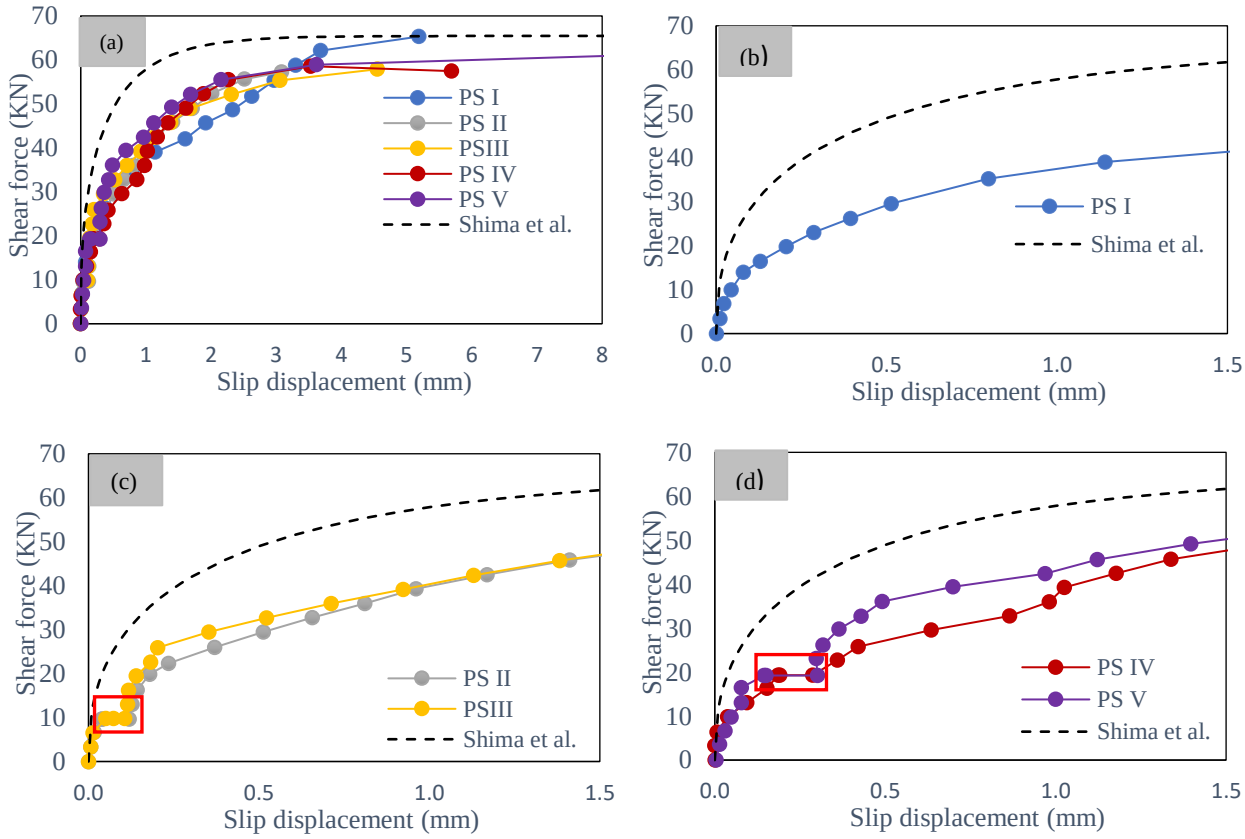

Figure 3. 11: (a) Skeleton curve for shear force-slip displacement relationship with Shima et. al.; (b) For control specimen, (c) For 15% shear force specimen and (d) For 30% shear force specimen

with that proposed by earlier researcher (Hiroshi SHIMA, 2008). In contrary to that the increase in displacement due to sustained loading causes an increase in residual displacement because the creep deformation generated in the concrete near the stud does not recover after unloading.

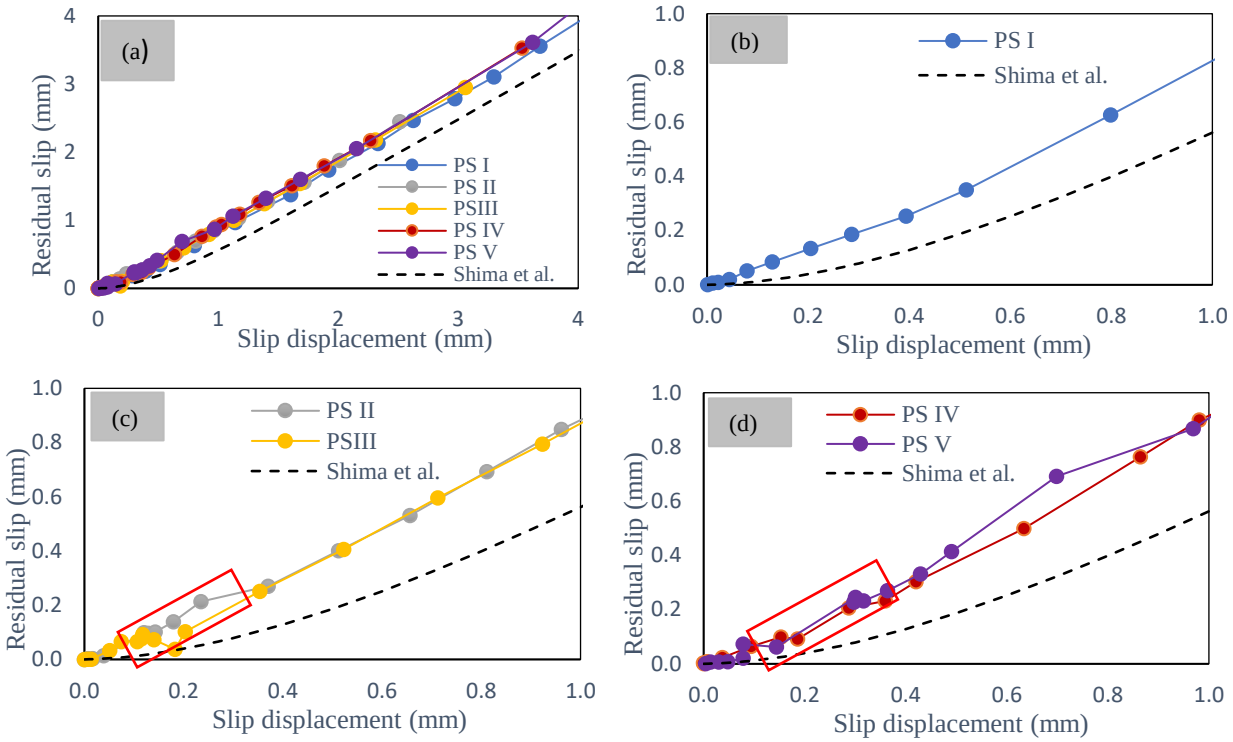

Figure 3. 12: (a) Skeleton curve for residual slip displacement relationship with Shima et. al.; (b) For control specimen, (c) For 15% shear force specimen and (d) For 30% shear force specimen

3.8 Failure load and patterns

Each pushout specimen was loaded to failure using an experimental laboratory set-up, which is presented in Figure 3.5. According to the experimental results presented in Figure 3.7 and Table 3.6, the ultimate failure load ranged from 65.30 kN for PS I to 57.23 kN for PS II. The failure load of static cyclic loading specimen PS I (control specimen) is closest to the specification value. Even though all the specimen were set on loading at same age, the sustained loading specimens were subjected to final loading after the designated sustained period and assumed to gain a little more strength from that of the loading time. Therefore, the sustained loading specimens were assumed to have a higher failure load than the control specimen but showed lesser values than expected. Hence, it is exhibited that sustained loading histories have influenced the failure load. Specimen PS VI also showed a lesser value of ultimate failure load even though it was kept only under self-weight to assess the influence of environmental factors on slip behaviour. Since this specimen was kept without any loading, the shrinkage might have a possible effect to influence the failure load. The failure mode for the sustained loading specimen as presented in Figure 3.13 clearly exhibited that failure behaviour is very much localized beneath and around the headed stud locations. At the beginning, the mechanical behavior of stud connections is influenced by the adhesion force; however, with the increase of shear force, the adhesion is lost, and residual strain increases with every further step of repeated load that leads to much localized deformation. This phenomenon is

considered as the driving mechanism owing to which deformed concrete volume around the stud is increased. Therefore, the creep deformation at the stud-concrete vicinity is more dominant and the slip displacement of whole specimen become larger for a higher level of sustained load. The target strength of pushout specimens was achieved as per equation (3.2); i.e., based on the ultimate strength of headed stud and stud failure is observed as shown in Figure 3.13 which is in line with the specimen design as assumed.

Table 3. 6: Pushout specimens ultimate failure load and pattern

Test specimen	Headed stud shear strength (kN)			Failure mode
	Specification	Experimental	Ratio (Experimental. /Specification)	
PS I	65.39	65.30	0.999	Stud failure
PS II		57.23	0.875	Stud failure
PS III		57.88	0.885	Stud failure
PS IV		57.47	0.879	Stud failure
PS V		61.15	0.935	Stud failure
PS VI		59.02	0.903	Stud failure

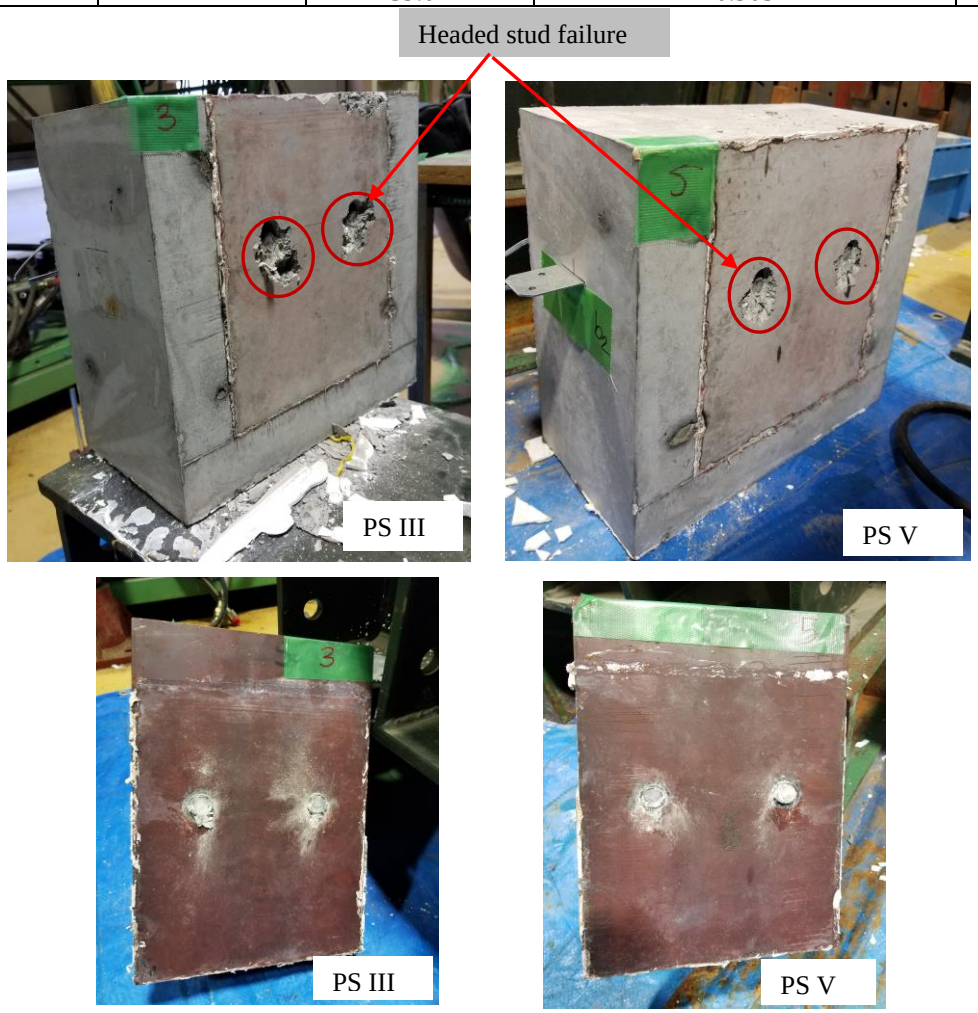

Figure 3. 13: Failure mode of pushout specimen in sustained loading.

3.9 Summary and conclusion

To investigate the the time dependent deformation of the hybrid girder, it is assumed that stud connections would experience long-term shear forces and it is also considered those shear forces will induce long-term stud deformation inside the specimen which is difficult to measure directly. Therefore, understanding of this behaviour is needed to quantify that for the structures in real use. Hence, considering the size of the girder specimens and keeping a consistency with that, six pushout specimens were devised with headed stud shear connections and were subjected to different long-term loading histories. Distinct time-dependent slip displacement and reduction of stiffness was confirmed through the experimental results, and the influence of environmental effects was also determined. Based on the results, the following conclusions can be drawn.

(a) For headed stud connections subjected to sustained shear forces, immediately after the application of force, the displacement increases rapidly at initial stages and continued with time with an asymptotical nature. The higher the shear force level, the increase in displacement is also remarkable. Increase of long-term displacement indicates a reduction of stiffness that accounted almost 50%. The increase is due to creep deformation of concrete around the stud which is very much localized at stud-concrete vicinity.

(b) The residual displacement after unloading with that of slip displacement at peak force of each cycle for static specimen exhibit a unique relationship regardless of the maximum slip displacement that holds the previous relational expression proposed by Shima et al. However; in contrary to that, the increase in displacement due to sustained loading causes an increase in residual displacement because of creep deformation in concrete near the stud that does not recover even after unloading.

(c) The sustained loading specimens showed a lower level of ultimate failure load than the control specimen; which exhibited that sustained loading histories have influenced the failure load.

(d) The failure mode for the sustained loading specimen clearly exhibited that failure behaviour is very much localized beneath and around the headed stud locations. At the beginning, the mechanical behavior of stud connections is influenced by the adhesion force; however, with the increase of shear force, the adhesion is lost, and residual strain increases with every further step of repeated load that leads to much localized deformation.

3.10 References

Haque MN, Maki, T. Experimental study on time-dependent deformation of hybrid steel- PRC girder with headed stud shear connections under sustained loading, Structures, No.22, p.327-340, 2019.9.

Haque MN, Maki, T. Sasaki J, Finite Element Approach to Evaluate Time Dependent Shear Behavior of Connections in Hybrid Steel-PC Girder under Sustained Loading, International Journal of Structural and Construction Engineering, Vol.13, No.9, 2019.10.

Taira Y, Saito S, Watanabe T, Mizoe Y. Shima H, Nakajima A, Furuichi K, Experimental study on shear force-slip relationship of headed stud connectors under controlled shear and axial forces, Proceedings of the Thirteenth East Asia-Pacific Conference on Structural Engineering and Construction. Hokkaido: 2013.

Ollgaard JG, Slutter RG, Fisher JW. Shear strength of stud connectors in lightweight and normal-weight concrete. AISC Engineering Journal 1971; 71-10: 55–64.

Prakash A, Anandavalli N, Madheswaran CK, Rajasankar J, Lakshmanan N. Three-dimensional Fe model of stud connected steel-concrete composite girders subjected to monotonic loading. International Journal of Mechanics and Applications 2011;1(1):1–11.

Allobody E. Finite element analysis and design of steel and steel-concrete composite bridges. Kidlington, Oxford, UK: Elsevier Inc.; 2014.

Anju T, Smitha KK. Finite element analysis of composite beam with shear connectors. International Conference on Emerging Trends in Engineering, Science and Technology (ICETEST - 2015), Procedia Technology 2016;24:179–187.

Nguyen HT, Kim SE, Finite element modeling of push-out tests for large stud shear connectors, Journal of Constructional Steel Research, 65 (2009); 1909-1920.

Bouchair J, Bujnak P, Duratna B, Lachal A, Modeling of the steel-concrete push-out test, Procedia Engineering, Steel Structures and Bridges, 40 (2012); 102 – 107.

Maki T, Watanabe R. Mechanical behavior of stud shear connector under sustained shear and compression forces. Proceedings of the Thirteenth East Asia-Pacific Conference on Structural Engineering and Construction. Hokkaido: 2013.

Japan Society of Civil Engineers. Standard specifications for steel and composite structures. Tokyo: 2009.

Head stud pushout test method (draft), JSSC Technical Report, No. 35, Japan Steel Structure Association, pp. 1-24, 1996.11

Haigen C. Analysis of stress and deflection about steel-concrete composite girders considering slippage and shrink & creep under bending. The Open Civil Engineering Journal 2015; 9:171-176.

Mirza O, Uy B, Finite element model for the long-term behaviour of composite steel-concrete push tests, Steel and Composite Structures, 2010, Vol. 10, No. 1: 45-67

Okui Y, Nagai M. Block FEM for time-dependent shear-lag behaviour in two-I girder composite bridges. Journal of Bridge Engineering ASCE 2007; 12(1): 72–79.

Shima H, Watanabe S, Formulation for load-slip relationships of headed stud connector, Proceedings of JSCE, 2008; 64(4): 935-947.

Maki T, Watanabe R, Zhang P, Deformation of headed stud shear connector under sustained shear forces, 11th Symposium on composite and hybrid structures, 2017.

CHAPTER 4

4 FE ANALYSIS ON TIME DEPENDENT DEFORMATION OF STUD UNDER SUSTAINED SHEAR FORCE

4.1 Introduction

The push-out tests are the most reliable and usually used as to investigate the long-term slip displacement behaviour of headed stud shear connectors under the sustained loading. However, in most of the cases experimenting with a long time frame are not possible as they are often most costly [(Nguyen HT, 2009)]. In reality, the availability of laboratory facility for unlimited time is not possible which mainly limits the scope to a small-scale experiment. Therefore, many recognize the benefits of predicting the headed stud's behavior by conducting a small-scale tests or numerical simulations [(Yanez SJ, 2018)]. Therefore, a dependable analysis tool has become a necessity which can serve as an alternative to analyzing long-term (time dependent) displacement behaviour that can help to predict the behaviour for field structures. Although conducting experimental tests for investigating the pushout specimens are a straightforward job, a finite element analysis (FEA) is always challenging due to some inherent limitations that can have a significant effect on the prediction of the expected behaviour [(Nasrin S, 2019)]. Finite element analysis is a computer-based method of simulating that can analyze the behavior of engineering structures under a variety of initial and boundary conditions to augmenting the experimental testing. In pushout tests, the most effective parameters that have influences on long-term slip behaviour are the size of stud, the load level, time duration and the concrete property etc. Few influences could be obtained easily by experiment, but some are difficult by experiment, especially to ascertain the stress-strain state inside the specimen; as the stress-strain state of the entire specimen obtained from sensors (gauges) don't always give the reliable data due to misalignment or non-functionality of those sensors. During the preparation of the push-out specimens, difficulties were encountered in the installation of the strain gauges on the level of each connector. On the other hand, short term experimental result cannot be representable for the entire service life of a structure that can last upto few decades, for which the longer deformation behavior should also be considered. Therefore, to observe its long-term deformation, the finite element analysis serves better than that of the experimental investigation [(Titoum M, 2016.)]. For this reason, in this study, a three-dimensional finite element model of the pushout specimen is reproduced and analyzed for the experimental cases, while comparing with the experimental results, outcomes are discussed in the subsequent sections.

4.2 Construction of non-linear FEM program

Steel-concrete composite structures or reinforced concrete (RC) structures are made up of two materials having different characteristics, namely, concrete and steel. In RC or composite structures,

steel is considered as a homogeneous material whose material properties are well defined which can resist the tension; whereas, even though the concrete is a heterogeneous material made up of cement, mortar and aggregates; for the convenience of analysis and design, it is often considered as a homogeneous material that resist the compressive forces.

To identify the non-linear behaviour of RC structures, there are two options available that includes experimentation in laboratories and the computational simulation. Although the experimentation gives the best results; it is restricted under some limited conditions of shapes, sizes, loading and boundary conditions. The later involves the virtual creation of RC structures with no limitations of the application; however, the outcome is greatly influenced by the modeling of non-linearity in constitutive laws of materials [(Maekawa K, 2003)]. In RC structures, the nonlinear response is firstly caused by the cracking of concrete in tension, and secondly the yielding of the reinforcement or crushing of concrete in compression. Non-linearity of RC mainly depends on the bond between reinforcement and concrete and shear transfer behaviour between cracks. Therefore, to predict the non-linear behaviour of RC structures, modeling of these behaviour are indispensable [(Okamura H, 1990)]. In nature, the mechanics of concrete is influenced by the temperature, strain rate and ambient conditions. Accounting the long-term creep of concrete is essential for controlling deflections in prestressed concrete structures in its design life. It is well known that elevated temperature may induce volumetric expansion and high rates of creep and shrinkage can cause cracking, which could shorten the life of structures. Therefore, in order to develop a consistent simulation for time dependent deformation under arbitrary boundary conditions; a comprehensive understanding of creep and shrinkage mechanism in non-linearity of RC is necessary [(Maekawa K, 2003), (Asamoto S, 2006)]. Hence, a finite element model (FEM) that describes faithfully the individual material behaviour in a structure suitably can give reliable output.

4.3 Modeling for Concrete

Owing to the low resistance to tensile stresses, the concrete structures suffer cracks even they are subjected to a lower level of load. In case of sustained loading, time dependent behavior reduces the stiffness of concrete and accordingly internal stress distribution changes; and the structures start to exhibit a non-linear behavior [(Maekawa K, 2003)]. Due to such nonlinearity, modeling of a cracked concrete becomes more difficult. There are several models for FEA analysis for RC concrete structures. Although their method of approach may differ based on what set empirical formulae are adopted for each, and it is quite expected that the closer the analytical model has its origin to the problem, the greater would be its efficiency [(Okamura H, 1990)]. However; all those models are composed of three basic components: crack initiation determination, crack

representation and criterion for crack propagation. The most relevant two models are discussed in this sub section.

4.3.1 Discrete Cracking Models

This model is based on the idea of dealing with the portion of the solid that remains continuous without any damages, and for an existing crack, its sides incorporate to the outline of the solid. Cracks are modeled as displacement discontinuities among the finite elements and they must appear across their outlines, that ends up with a restriction in the direction of its propagation [(Maekawa K, 2003)]. The location of cracks is specified in advance, and the other un-cracked portion is treated as a continuum concrete and the local mechanical model for stress transfer at a crack is considered. Stress-strain relationships of concrete are independent of crack coordinate. This model is applicable for those problems having fewer cracks, what actually limits its application in most of the RC structures.

4.3.2 Smeared Cracking Models

The smeared cracking constitutive model is formulated based on a space-averaged stress-strain relation of an RC in-plane element as shown in Figure 4.1. The cracks and reinforcing bars are idealized as being distributed or smeared over the whole element. The non-linearity of cracked RC element is initiated due to cracking, reinforcement plasticity and bond interaction between reinforcement and concrete [(Maekawa K, 2003)]. Although the local stress and strain distribution in cracked RC element is not uniform physically, such locality need not to be considered in analysis through space averaging. The total stress carried by RC elements is the summation of the average stresses of concrete and reinforcement at their equilibrium state and concrete stresses are assumed to be of parallel and normal to cracks and shear stress transfer along cracks on an averaged basis [(Maekawa K, 2003)]. This modeling approach may be categorized as fixed smeared crack and rotating smeared crack. The fixed smeared crack treats a crack as being geometrically and, anisotropy is inherently considered. In contrast, the rotating smeared crack approach assumes that crack direction can be changed depending on the stress condition and principal stress vector always coincide with that of the principal strain. In smeared crack approach, after cracking occurred, the modulus of elasticity of the material is reduced to zero, normal to the principal tensile stress direction. In this model, such versatile options could greatly simplify computations and presents nearly accurate results both under cyclic and monotonic loading, for which it is now regarded as one of the best models for RC structures [(Maekawa K, 2003)].

4.4 Method of Modeling

As shown in Figure 4.2, the RC plate element model is constructed by combining the constitutive law for concrete and that for reinforcing bars and constitutive equations are governed as the relationships of the average stress and average strain. The constitutive law adopted for the cracked concrete is composed of the tension-softening model, the compression model and the shear transfer as shown in Figure 4.3. By combining them with the model for reinforcing bars, the present model for a RC plate element has been constructed. Since, compression softening is mostly dominant, therefore time dependent deformation associated with compressive stress is a major contributor to determine the long-term behaviour [(Bugalia N, 2017)]. Fracture parameter for compression counts the decrease of the time dependent stiffness and plasticity and fracture parameter for tension counts the decrease of time dependent tension stiffness to determine the long-term behavior of RC structures [(Takahashi Y, 2018)].

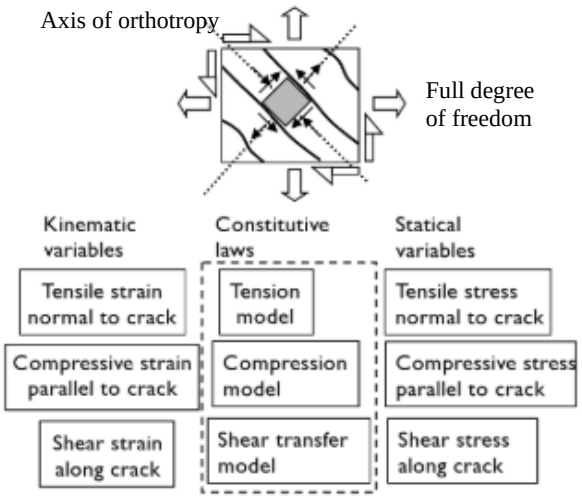

(a) Fixed crack approach

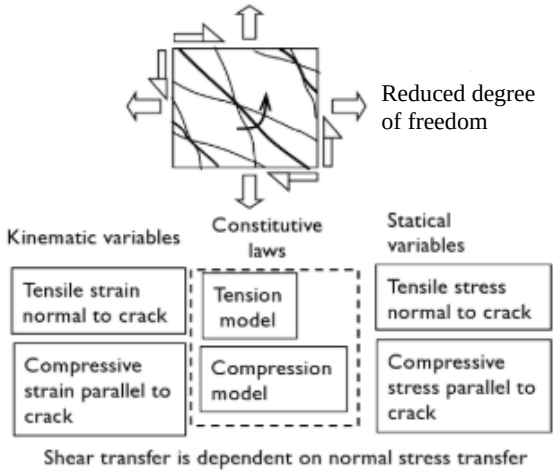

(b) Rotating crack approach

Figure 4. 1: Classification of the smeared crack approach

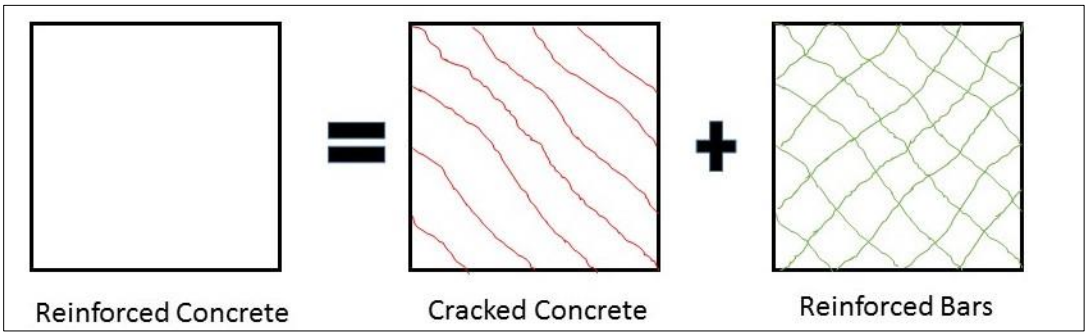

Figure 4. 2: Composition of RC plate element model

.

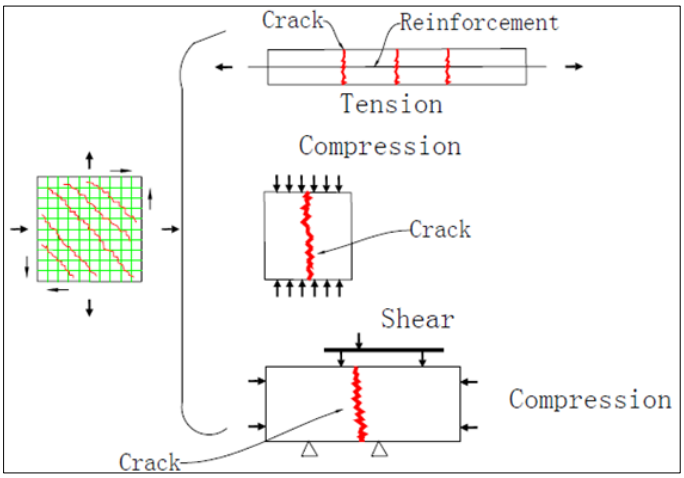

Figure 4. 3: Construction of cracked concrete model

4.4.1 Material Constitutive Laws and Characteristic Value

For the finite element analysis, for creep deformation (with El-kashif's time-dependent model; both elastic and inelastic creep), the nonlinear path-dependent constitutive law of reinforced concrete, proposed by Okamura and Maekawa (Okamura H, 1990) was applied. The yield condition of Von Misc theory was applied for the steel element, and the applied model consists of multi-directional compression-tension-shear transfer model of concrete and reinforcement, with non-orthogonal four-way fixed crack model based on the smeared crack assumption, and it has already been verified for nonlinear behavior of RC structures under various types and combinations of external loads. The compressive strength of RC element, that was obtained in the experiment by column compressive test was inputted and tensile strength was estimated from the compressive strength using the standard evaluation formula as described in the Concrete Standard Specification.

4.4.2 Concrete tension softening behaviour

Concrete tension softening behaviour relies on the concept that concrete in RC members can still support part of the applied tension even after cracking which is known as tension softening effect. Due to bond transfer at the interface of concrete and reinforcement, concrete between cracks can

develop local tensile stresses after the cracks occur. This tension may restrain the free elongation of the reinforcing bars; hence the tension softening effect is known as to increase the overall stiffness of the RC member in tension. Therefore, the stress-strain relation of RC element needs to be precisely simulated at tensile and compression area, since this is considerably influenced by the adhesion force between steel and concrete and also with other effective parameters. For the post cracking concrete tension model; average tensile stress-strain relation of concrete is described in equation (4.1) and shown in Figure 4.4 [(Maekawa K, 2003)].

$$\sigma = f_t \left(\frac{\varepsilon_{tu}}{\varepsilon}\right)^c \qquad (4.1)$$

where, f_t : tensile strength of concrete, ε_{tu} : tensile strain corresponds to softening initiation (normally equals to 2 /E or 0.0002) and c : tension softening factor.

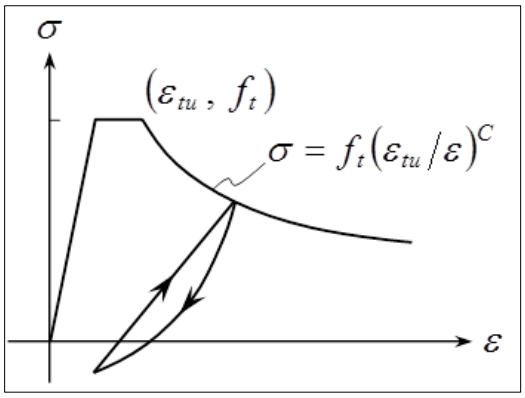

Figure 4. 4: Tensile stress-strain relation in RC element

Since, the cracks are localized in plain concrete subjected to tensile stress; tension softening curve depends on the tensile fracture energy as presented in equation (4.2).

$$G_{ft} = 10\, d_{max}^{\,1/3}\, {f'_c}^{\,1/3} \qquad (4.2)$$

where, G_{ft} : tensile fracture energy (N/m), d_{max} : maximum size of coarse aggregate (mm), f'_c : compressive strength of concrete (MPa). The tensile softening factor can be calculated by equating the fracture energy per unit element length G_{ft}/L_e (L_e: element length) to the absorbed energy per unit volume given as an integration of the tensile stress-strain curve shown in the above figure.

4.4.3 Concrete compressive softening behaviour

The mechanical basis for expressing the non-linearity in elasto-plastic and damage model for concrete compressive softening behavior is presented in Figure 4.5. For a low compressive stress state, the stress-strain relation remains linear; whereas at a high level of stress, it presents nonlinear time dependent behavior with a reduction in elastic stiffness which is seen in the unloading path. This reduced elastic stiffness is described by a fracture parameter and also devised in terms of

intrinsic elasticity. The compression fracture energy can be given as the elastic energy plus the absorbed energy due to compression softening multiplied by the base element size. The compression softening factor equivalent to the compression fracture energy can be calculated according to the element size. The above model is obtained from the experiment with 200-300mm specimens that needs to be corrected according to the element size. Here, compression fracture energy can be given as the absorbed energy per unit volume multiplied by the base element size (200mm). The average compressive stress-strain relation of concrete is shown in the following equations.

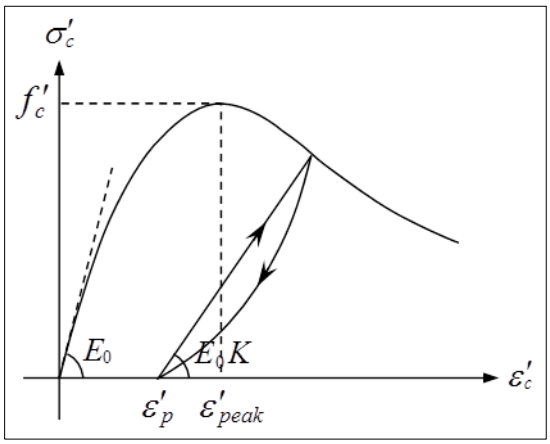

Figure 4. 5: Uniaxial compression stress-strain relation

$$S = E_0 K\left(E - E_p\right) \qquad (4.3)$$

where,

$S = \frac{\sigma'}{f_c'}$: normalized compressive stress

$E = \varepsilon_{max}'/\varepsilon_{peak}'$: normalized compressive strain

$E_{eq} = \begin{cases} E & (E \le 1.0) \\ E^{1+c} & (E > 1.0) \end{cases}$: revised normalized compressive strain

$K = \exp\left[-0.73E_{eq}\left\{1 - exp\left(-1.25E_{eq}\right)\right\}\right]$: fracture parameter

$E_p = E - 2.86\{1 - \exp(-0.35E)\}$: normalized plastic Strain

4.4.4 Creep deformation model

For FEA, the solver program COM3 uses different models for tension and compression to reproduce the creep phenomenon of concrete. For compression creep, the elasto plastic and damage model as summarized in Figure 4. 6 is the mechanical basis for expressing nonlinearity [(Khaled Farouk El-Kashif, 2004)]. The evolved plastic rate of deformation was formulated as elastic strain which represents the intrinsic stress intensity of the damaging continuum and damage is defined as a loss of parallel components; whereas the fracture parameter indicates the ratio of working elements

[(Khaled Farouk El-Kashif, 2004)]. In this study, the time depended plastic rate and supplementary damage with instantaneous strain path dependent nonlinearity is incorporated for the model. Elasto-plastic and damaging concept is schematically consisting of elasto-plastic sliders as shown in Figure 4.7, and the broken elements are represented as damaged ones in past mechanics and the total stress is taken as an integral of internal stresses of remaining elements [(Khaled Farouk El-Kashif, 2004)]. As shown Figure 4.7, the intrinsic stress intensity applied to each non damaged component is directly proportional to elastic strain; then time-elasticity path is thought to be a logical operator to

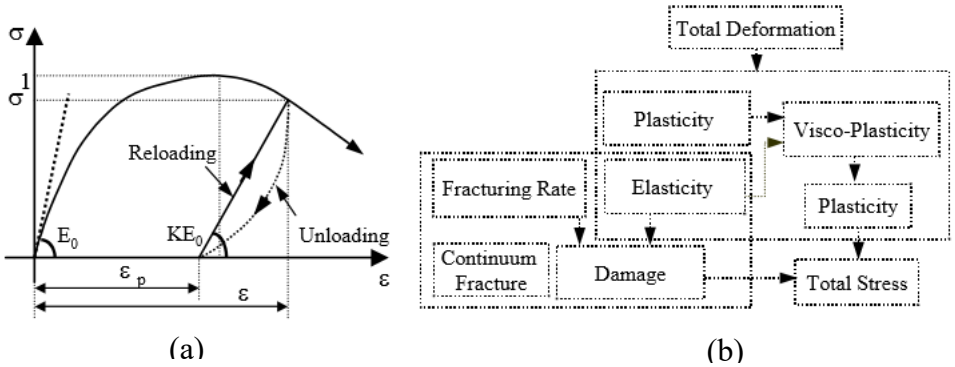

Figure 4. 6: Elastic-plastic and damaging model; (a) Definition and (b) Scheme of formulation

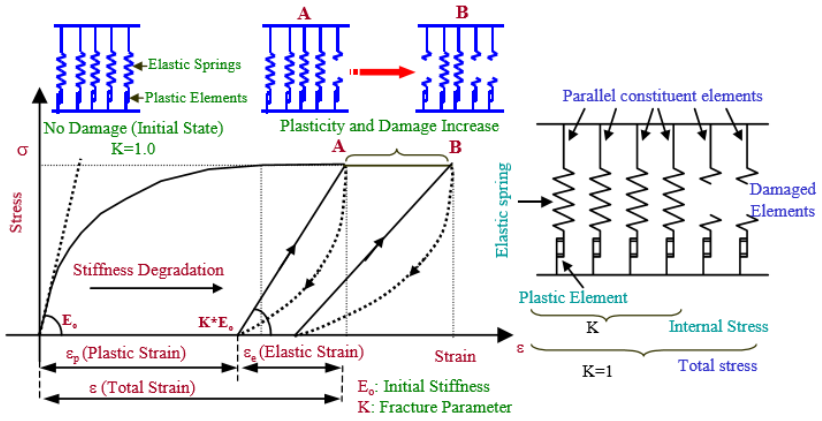

Figure 4. 7: Schematic representation of elasto-plastic and damage concept

rule both plastic and damaging growths [(Khaled Farouk El-Kashif, 2004)]. The basic constitutive equations to express the elasto plastic and damaging concepts and the general Taylor's series of state variables (plastic strain and facture parameter) can be expressed in the following equations.

$$\varepsilon = \varepsilon_e + \varepsilon_p, \sigma = E_o \varepsilon_e K \qquad (4.4)$$

$$d\varepsilon_p = (\partial \varepsilon_p / \partial t)dt + (\partial \varepsilon_p / \partial \varepsilon_e)d\varepsilon_e \qquad (4.5)$$

$$dK = (\partial K / \partial t)dt + (\partial K / \partial \varepsilon_e)d\varepsilon_e \qquad (4.6)$$

The simple combination of elasto-plastic and damage results in partial linearity in unloading-reloading paths without any hysteresis loop. Although this simplicity does not reflect the reality, it is acceptable for structural analysis to verify some limit states of capacity. Generally, the unloading loop tends to deviate from the linear line specified by the facture parameter according to the damage evolution (0.5<K<1.0). This deviation is suppressed by the presence of lateral confinement. Referring to the computation model for cracked concrete, the following fictitious loop stress was incorporated into equation (4.4) as [(Khaled Farouk El-Kashif, 2004), (K.Maekawa, 2006)]-

$$\sigma = E_o \varepsilon_e K + \sigma_{loop}, \quad \sigma_{loop} = E_{loop} \varepsilon_e \qquad (4.7)$$

$$E_{loop} = -\alpha . E_o \left(1 - \left(\frac{\varepsilon_e}{\varepsilon_{e(\max)}}\right)^{\omega}\right) \qquad (4.8)$$

$$\omega = 4 - 2.4K - 1.6K^2, \qquad \alpha = (k - k^2) \qquad (4.9)$$

In regard to tension creep, since the nonlinearity of tensile rigidity depends mainly on cracks, the fracture parameter K was introduced, and the stress-strain relationship was formulated as $\sigma = \boldsymbol{KE\varepsilon}$

4.5 Modeling of pushout specimen

4.5.1 Model Description

The displacement and deformation behavior of headed stud connections under sustained shear force was examined and clarified experimentally using pushout specimens that were experimented in laboratory and already described in chapter 3. It was observed that the slip displacement increment under the long-term sustained loads depends on the applied load level, exposure time and loading history. Since, a single type of stud was used in pushout specimen and all the specimen were experimented parallelly with same material properties and strength it could not be clarified which factors influence the displacement behavior. Furthermore, since multiple studs are used in combination as the connections in the actual structure, the transmission of stress is very complicated. Therefore, it is quite difficult to quantitatively evaluate long term deformation of the stud connections only through experimental examination. From this viewpoint, the applicability of analytical method was verified in this study by reproducing and analyzing the experimental result as presented in chapter 3; by a three-dimensional non-linear finite element analysis (FEA) considering the time-dependent behavior of concrete and the slip-displacement under the sustained shear force. A three-dimensional finite element model of 1/4th part of test specimen was produced as shown in the Figure 4.8. Shear stud, H-shaped steel, concrete blocks, and loading plate are all modeled by isoperimetric element. The elasto-plastic constitutive law based on the yielding condition of Von Mises was provided to each steel material element of stud, H-shaped steel, and loading plate. For concrete elements, the time-dependent non-linear reinforced concrete analysis process developed by [(Okamura H, 1990), (Khaled Farouk El-Kashif, 2004)]was applied. This

model combines discrete crack model, smeared crack model, and nonlinear model of concrete and reinforcing bars with the applicability of reinforced concrete structures in the strong nonlinear region which has already been verified by past researches. As shown in Figure 4.8, the non-linear concrete element around the stud has been modeled as plain concrete while other concrete elements have been modeled as reinforced concrete elements. The reinforcement ratios have been inputted in model and based on the idea of fracture energy, compression and tensile softening coefficients according to element dimensions were set and incorporated in the model as data input. Considering the numerical efficiency, only 1/4th of test specimen has been modeled. The boundary condition was also applied to the model as of all the nodes of bottom surface of concrete have been confined in stud axis, and in horizontal and vertical axis direction. All nodes in the cutting planes (plane for symmetry) has been confined in the direction normal to the planes. The concentrated vertical loading (Y-direction) was applied at the right top node on the top surface of loading plate.

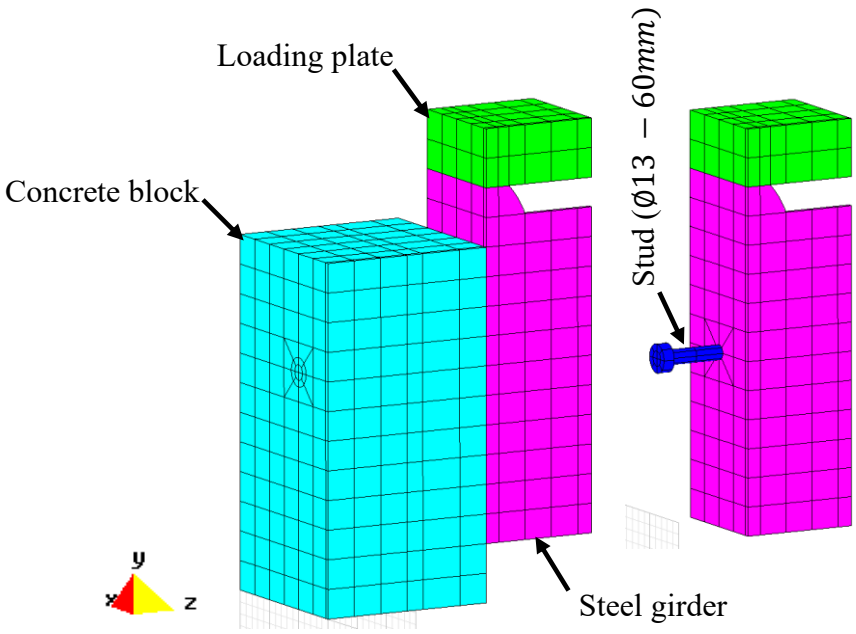

Figure 4. 8: Model of pushout specimen for FEA analysis

4.5.2 Analysis Procedure

The finite element analysis process followed in this study was a bit complex as it was a 3-steps interface process compatibility with pre-processor, solver and post processor which is presented in a flowchart as shown in Figure 4.9. In this analysis, the solver COM3 was used which was developed by professor OKAMURA and professor MAEKAWA of Tokyo University to perform the numerical task. Firstly, the geometric model of the pushout specimen was prepared with a preprocessor GiD (version 9.0.6) where element assemble, boundary condition and materials names were assigned. Sub programs were used separately to assign the interface elements, material

information, softening data, output information and then converted it to COM3 compatible format for finite element analysis. Secondly COM3 was used as a solver and finally, the output results were obtained with the use of GiD (version 9.0.6) software.

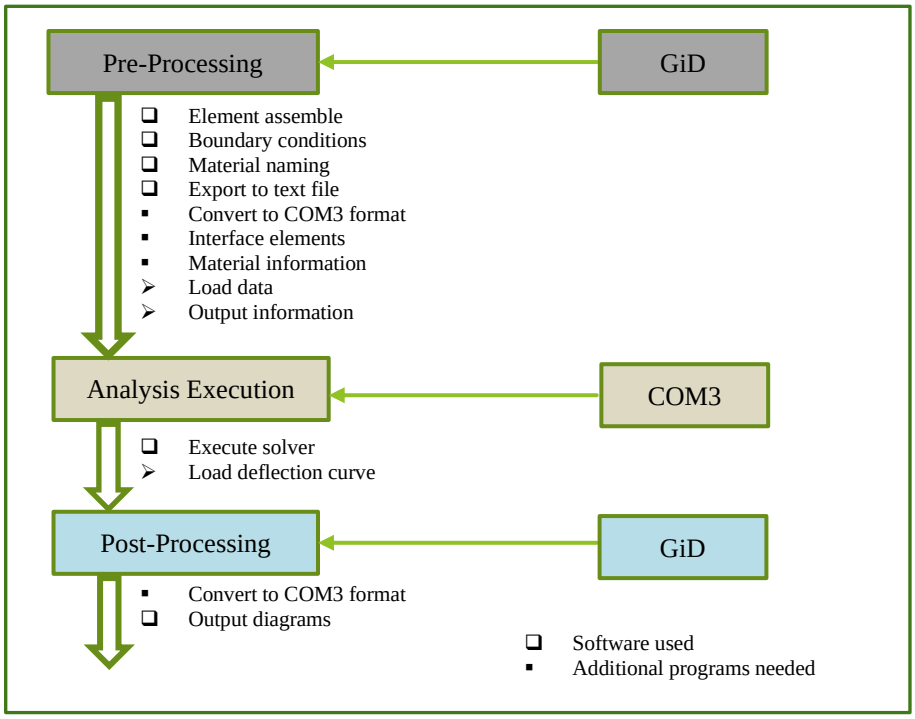

Figure 4. 9: Analysis process flowchart

4.5.3 Loading Method

This analysis is conducted with a consistent and similarity of the loading as that of experimental specimen that were subjected to sustained loading. Hence load (force) control method was applied rather than displacement control. The loading method is similar to the experimental cases which was 5% increment of calculated shear capacity at every cyclic loading path.

4.6 FE analysis result

The long-term deformation behaviour of headed studs used for hybrid girder is experimentally clarified through pushout tests in preceding chapter. For consistency with the sensor layout of the experimental setup, in the FEA analysis, the slip displacement was calculated by obtaining the value of slip displacement at the same position of both steel and concrete side, as they were in the experiment. The difference of the slip displacements of these two positions thus obtained has been considered as slip displacement corresponding to the experiment results. The internal stress-strain state of the specimens was also obtained through the analysis. The pushout specimens those were investigated in laboratory both under static and sustained loading were analyzed through FEA. PS I was subjected to static cyclic loading and PS II-PS V were subjected to sustained loading of

specific duration and specific shear force level. The same compressive strength of specimens as that of those experimental cases were used in the analysis. The analysis cases and loading histories are presented in Table 4.1.

Table 4. 1: Specimen loading history

Specimen (ϕ13-H60)	Specimen details		Time of loading (days)			Loading type
	Age (days)	Strength (MPa)	15% Shear force (39 kN)	30% Shear force (78 kN)	Final loading	-
PS I	27	44.8	-	-	27th day	Static cyclic
PS II			30	-	57th day	Sustained
PS III			60	-	87th day	Sustained
PS IV			-	30	57th day	Sustained
PS V			-	60	87th day	Sustained

4.6.1 Shear force – slip displacement relationship

The shear force–slip displacement relationship of pushout specimens were analyzed through FEA and the hysteresis curve obtained from both experimental and analysis are presented in Figure 4.10. Their corresponding envelope curve of shear force-slip displacement relation are also shown in the Figure 4.11. As per the analysis results presented, they could relatively reflect the stiffness variation with increment of loading with respect to the experiment results. With the further increase of loading level, the difference between FEA and experimental result is more distinct. The envelop curve of FEA shows a transition towards increasing displacement under sustained loading as observed in experimental result although incremental amount is lesser than experimental values. Constitutive laws followed in FEA has some limitations to reproduce the experimental cases exactly as it could not account the variations of the environmental conditions that always exist in laboratory. Even though the FEA could nearly simulate the experimental result at earlier stages of loading, However, when the shear force reaches to higher level, the analysis result became unrealistic. The slip displacement is suddenly showed distinctive increment where recorded loading reaction force became diverged from real value. This phenomenon is caused because of nonlinear mechanical behavior of specimens when loading level increases. The analysis software could not model this mechanical behavior at high level loading which is a major limitation of this model.

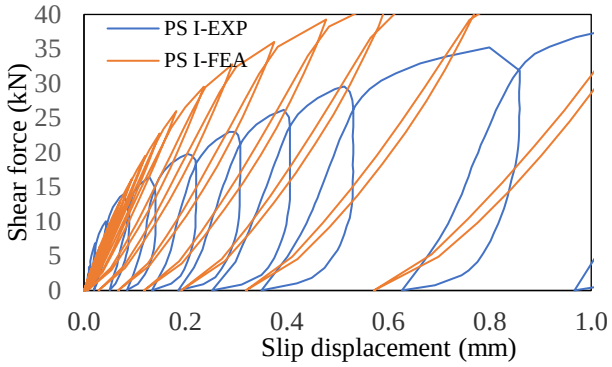

(a) PS I

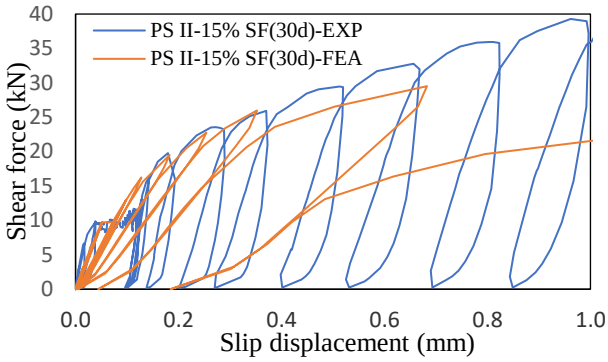

(b) PS II

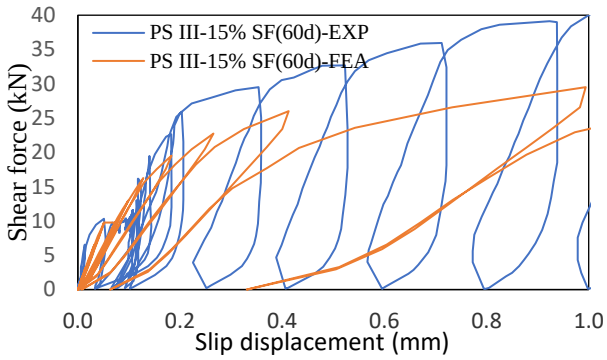

(c) PS III

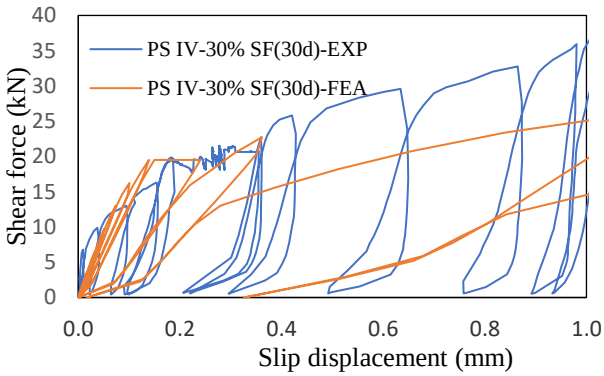

(d) PS IV

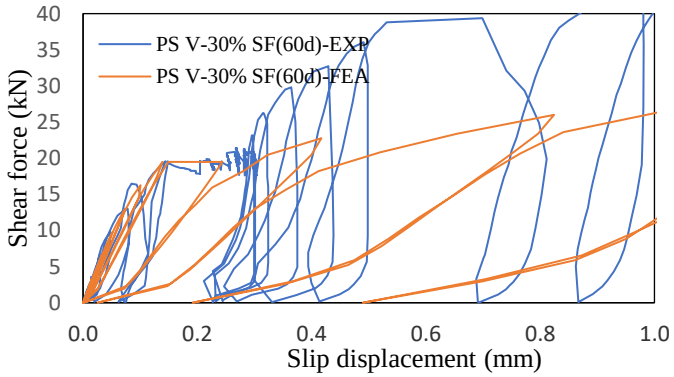

(e) PS V

Figure 4. 10: Hysteresis curve for shear force- slip displacement for experimental and analysis in (a) PS I, (b) PS II, (c) PS III, (d) PS IV and (e) PS V

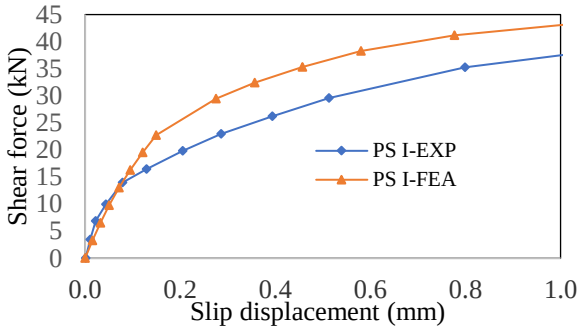

(a) PS I

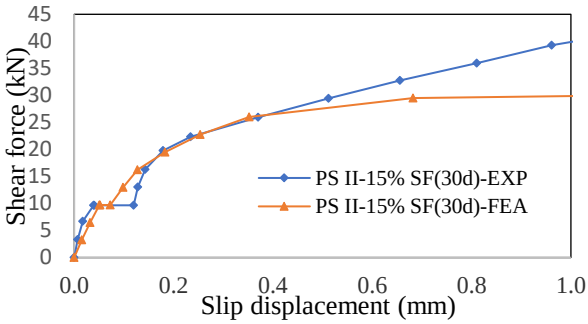

(b) PS I

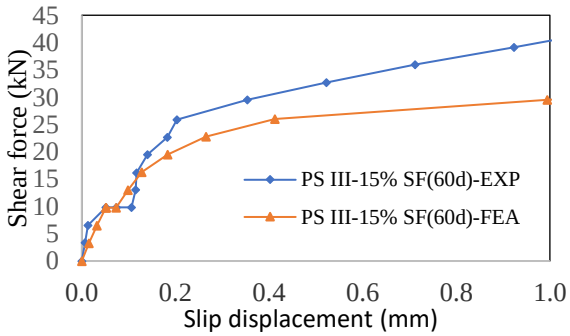

(c) PS III

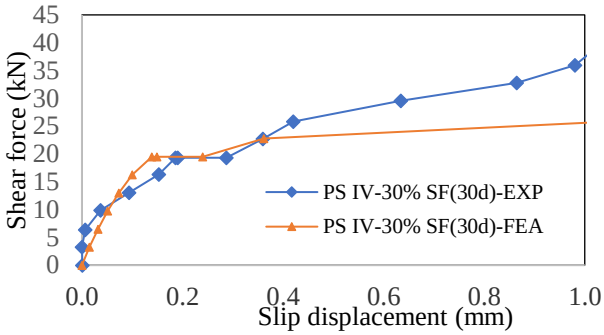

(d) PS IV

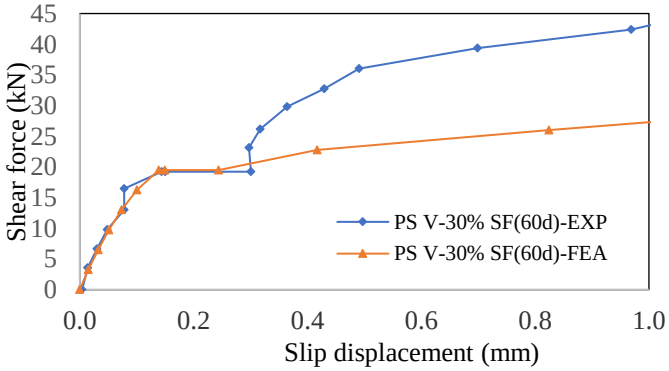

(e) PS V

Figure 4. 11: Shear force- slip displacement envelop for experimental and analysis in (a) PS I, (b) PS II, (c) PS III, (d) PS IV and (e) PS V

4.6.2 Long-term slip displacement: FEA and experimental results

The long-term slip displacements at the locations of the pushout specimens, as those were measured for experimental cases were obtained through FEA analysis and the displacement behaviour is reported in Table 4.2 and Figure 4.12. The experimental and FEA results showed that both at 15% and 30% shear force level respectively, the slip displacements were not so closer rather varied. The

overall slip displacements at the end of sustained loading period were higher in experimental cases than FEA. For a comparative and comprehensive statement of the analysis result, this model was applied similarly to analyze a previously conducted experimental results of Maki et. al.[(Maki T, 2017)] and compared with the experimental results. In those previous experiment, pushout specimen with headed stud of 19 mm diameter with 120 mm height (ϕ19-H120) was subjected to a sustained loading of 30% of shear force for 28 days' time duration and results are presented in Figure 4.13. It is observed that FEA values are lower than the experimental investigation under this present study and a similar result was also obtained in the previous study, which might be due to the environmental conditions as assumed in FEA (20°C and 60% RH) that differ than that exist for the experiment. However; the cumulative slip displacement over time progresses with a slower incremental rate in both experimental and FEA cases as shown in Table 4.2 and this nature of displacement behaviour over time resembles the nature of asymptotical curve. As similar to experimental cases, it is evidenced that for 30% sustained shear force, slip displacement increment within 30 days indicate a reduction of stiffness to approximately 30%.

Table 4. 2: Comparison of slip displacement in experiment and FEA

Test specimen and Shear force (SF)		Slip displacement (mm)		Slip displacement for 30 days sustained period (mm)			Slip displacement for 60 days sustained period (mm)		
		15 % shear force level	30 % shear force level	start	end	increment	start	end	increment
PS III-15% (SF)	EXP	0.051	0.150	0.073	0.106	0.033	0.073	0.107	0.034
	FEA	0.051	0.183	0.059	0.072	0.130	0.059	0.073	0.140
PS V-30% (SF)	EXP	0.048	0.144	0.152	0.283	0.131	0.152	0.301	0.149
	FEA	0.051	0.138	0.149	0.239	0.090	0.149	0.243	0.094

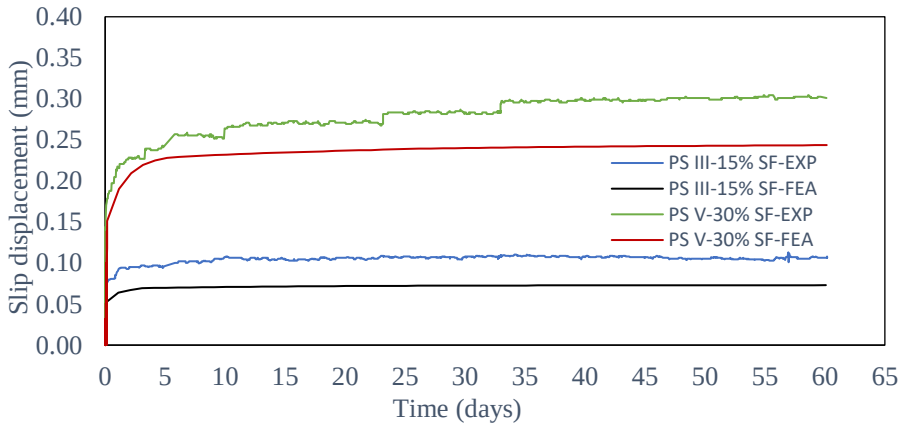

Figure 4. 12: Long-term slip displacement under experiment and FEA

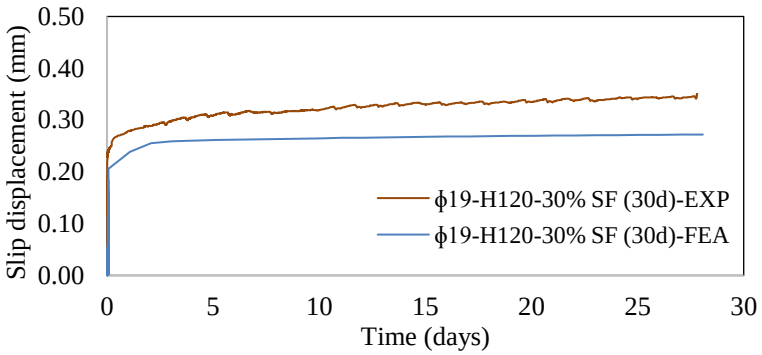

Figure 4. 13: Long-term slip displacement under experiment and FEA ((Maki T, 2017)

4.7 Internal stress- strain state under sustained shear force

Owing to the sustained loading, the internal stress and strain changes from the start of loading; continues throughout the loading period and contour distribution of those strain and stress at concrete-stud vicinity is shown in the Figure 4.14 and Figure 4.15. The strain contour distribution shows that shear stud generated large tensile strain after the sustained load, and due to this tensile strain, the concrete around shear stud have more cracks that can comprehend accelerating the creep deformation of concrete around the shear stud. Similarly, from the stress contour, it is observed that the internal stress condition reaches to a higher value during and after the sustained loading. This also an indication that concrete around shear stud generate creep deformation and have more cracks that indicates the non-linearity really exist in sustained loading.

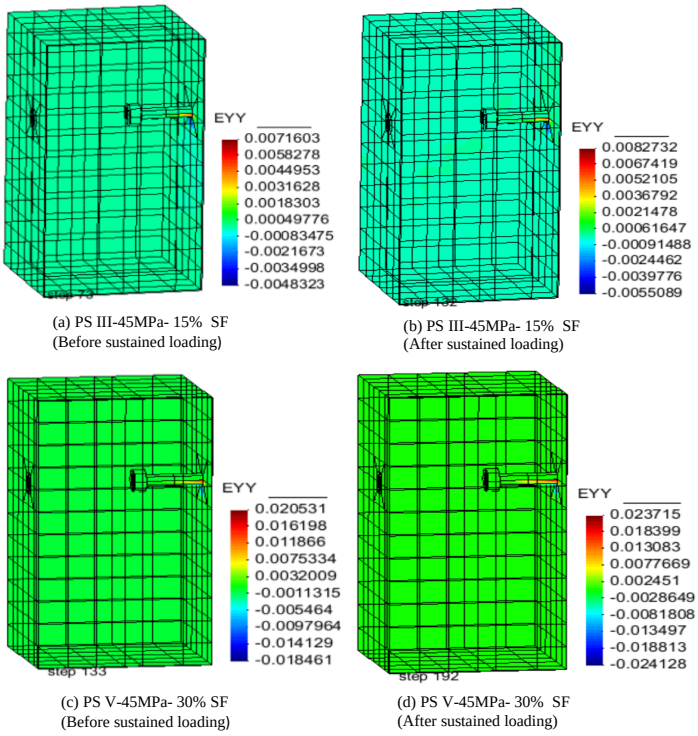

Figure 4. 14: Strain contour distribution for 15% and 30% shear force at before (left) and after (right) sustained loading

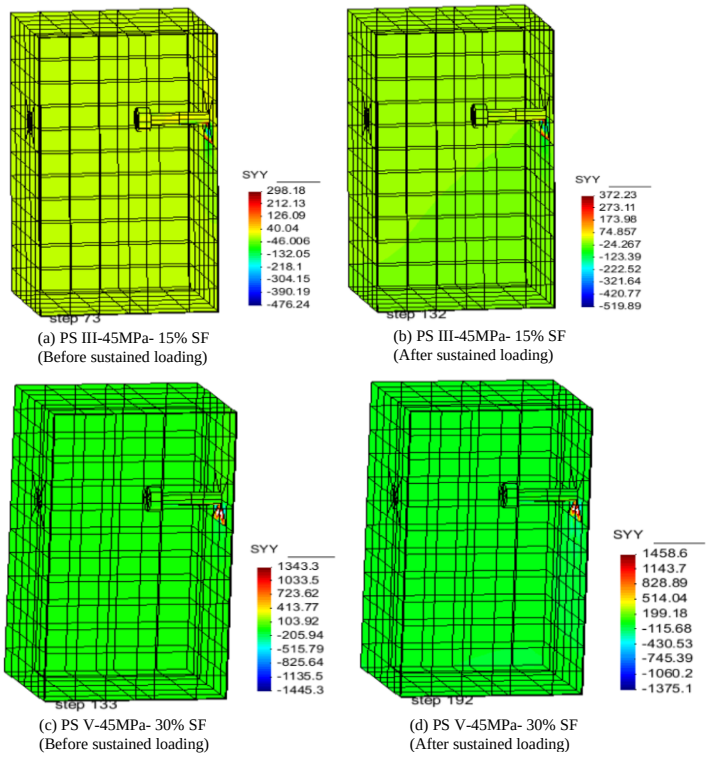

(a) PS III-45MPa- 15% SF (Before sustained loading)

(b) PS III-45MPa- 15% SF (After sustained loading)

(c) PS V-45MPa- 30% SF (Before sustained loading)

(d) PS V-45MPa- 30% SF (After sustained loading)

Figure 4. 15: Stress contour distribution for 15% and 30% shear force at before (left) and after (right) sustained loading

4.8 Parametric study: Factors that influence long-term displacement

Since, conducting pushout experiments to quantify long- term slip behaviour is a straightforward job but costly and time consuming as the laboratory facility for unlimited time is not possible. Finite element analysis can overcome this limitation and can analyze the behavior under a variety of conditions to augmenting the experimental results. Since, slip displacement increment ratio as already expressed in equation (3.3) of chapter 3 and presented as $k(t-t_0) = R = \frac{\delta(t)-\delta(t_o)}{\delta(t_o)}$, which exhibited the trend of creep deformation characteristics of concrete. To model the deformation behaviour of headed studs in hybrid girder that could be realistically useful for the actual structures; using the FEA, a parametric study is conducted on the factors that could influence the long-term deformation behaviour which is described in the following sections-

4.8.1 Compressive strength of concrete

The first parameter investigated was the concrete compressive strength; how it could influence the slip displacement increment ratio (R) for 15% shear force and 30% shear force level as presented in Figure 4.16. R values decrease as concrete compressive strength increases since for lower compressive strength of concrete, the sustained load induces higher compressive strain beneath the

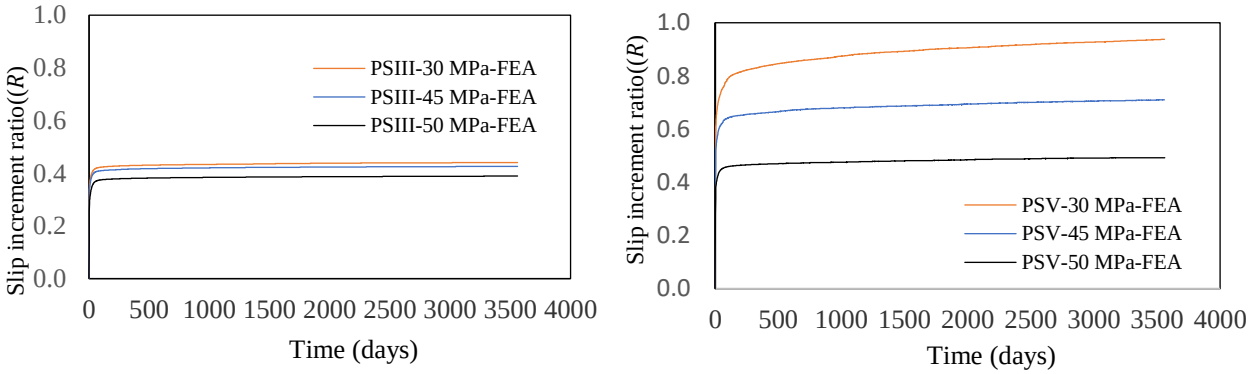

(a) R for 15% shear force (b) R for 30% shear force

Figure 4. 16: Slip increment ratio (R); (a) For 15% shear force and (b) for 30% shear force.

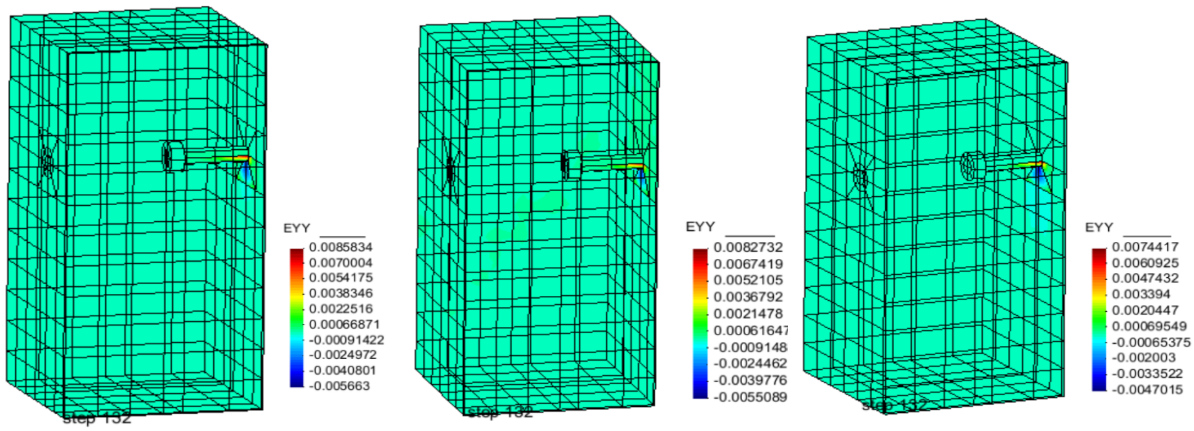

(a) 30 MPa-FEA-15% SF (After sustained loading)

(b) 45 MPa-FEA-15% SF (After sustained loading)

(c) 50 MPa-FEA- 15% SF (After sustained loading)

Figure 4. 17: Strain contour distribution under different compressive strength (for 15% shear force)

stud which leads to much amount of stress and consequent local creep deformation [(Mirza.O, 2010)]. This sustained loading also induces tensile strain at sides of the stud which also increases at lower compressive strength that are reflected in Figure 4.17. If the shear force level increases, R shows relatively higher values which indicates that at higher level of shear force, the localized deformation at stud-concrete vicinity influences surrounding concrete rapidly and aggravate the overall creep deformation.

4.8.2 Height to diameter (h/d) ratio of stud

The second parameter investigated was the effect of height to diameter ratio (h/d) of stud connections on the slip increment ratio (R) for 15% and 30% sustained shear force level as presented in Figure 4.18. R values increase as h/d ratio increases; however, does not show much increases beyond as the creep deformation behaviour is much localized beneath and around the stud

near the stud-steel joint. The localized strain behaviour for 15% shear force is presented in Figure 4.19

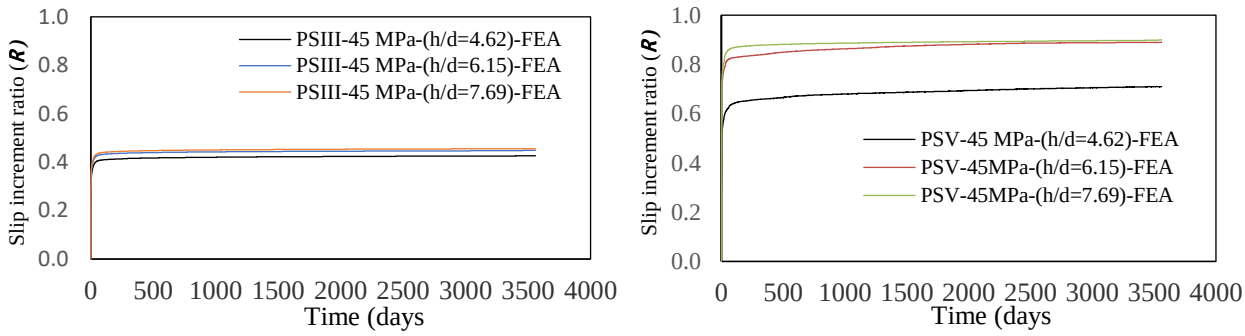

(a) R for 15% shear force (b) R for 30% shear force

Figure 4. 18: Slip increment ratio (R); (a) For 15% shear force and (b) for 30% shear force.

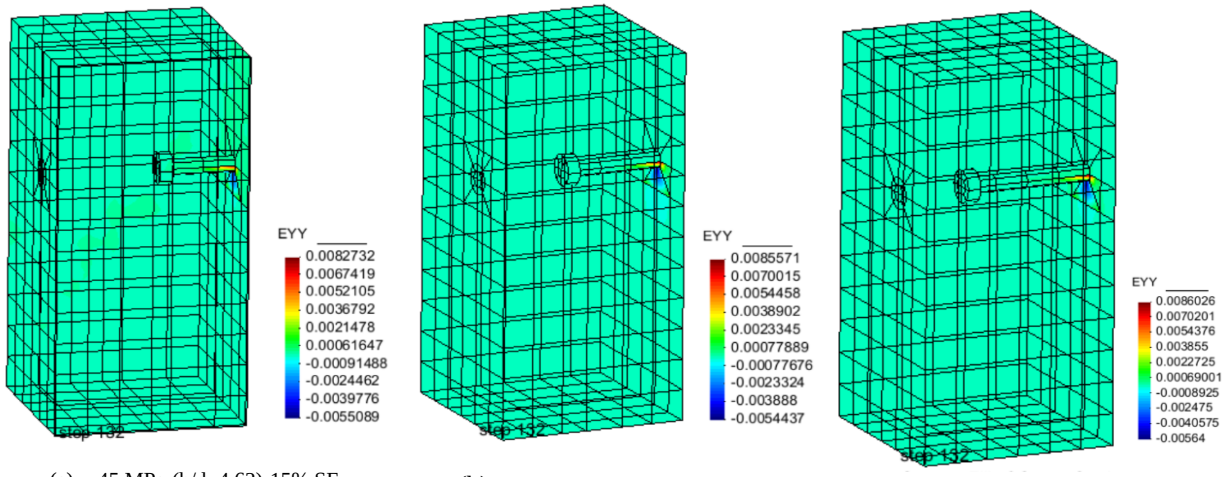

(a) 45 MPa-(h/d=4.62)-15% SF (After sustained loading)

(b) 45 MPa-(h/d=6.15)-15% SF (After sustained loading)

(c) 45 MPa-(h/d=7.69)-15% SF (After sustained loading)

Figure 4. 19: Strain contour distribution for different (h/d ratio) (for 15% shear force)

4.8.3 Headed stud yield strength

The third parameter investigated was the effect of yield strength of stud and how can it influence the slip increment ratio (R) for 15% and 30% sustained shear force level as presented in Figure 4.20. R values increase as yield strength increases. Owing to a relatively high yield strength of stud, concrete beneath the stud and at stud-steel joint area experiences plasticity for which residual deformation at each cycle of loading before reaching to sustained level and then the sustained loading also aggravates this plasticity and creep deformation increases consequently. The localized strain behaviour for 30% shear force is presented in Figure 4.21.

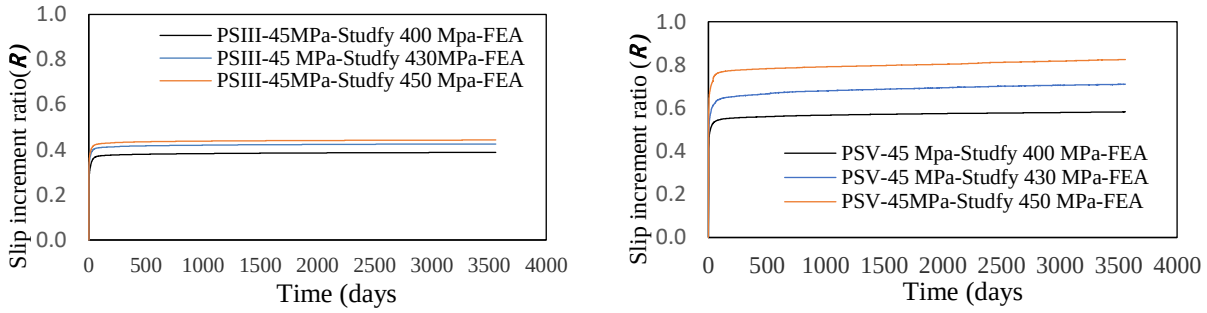

(a) R for 15% shear force (b) R for 30% shear force

Figure 4. 20: Slip increment ratio (R); (a) For 15% shear force and (b) for 30% shear force.

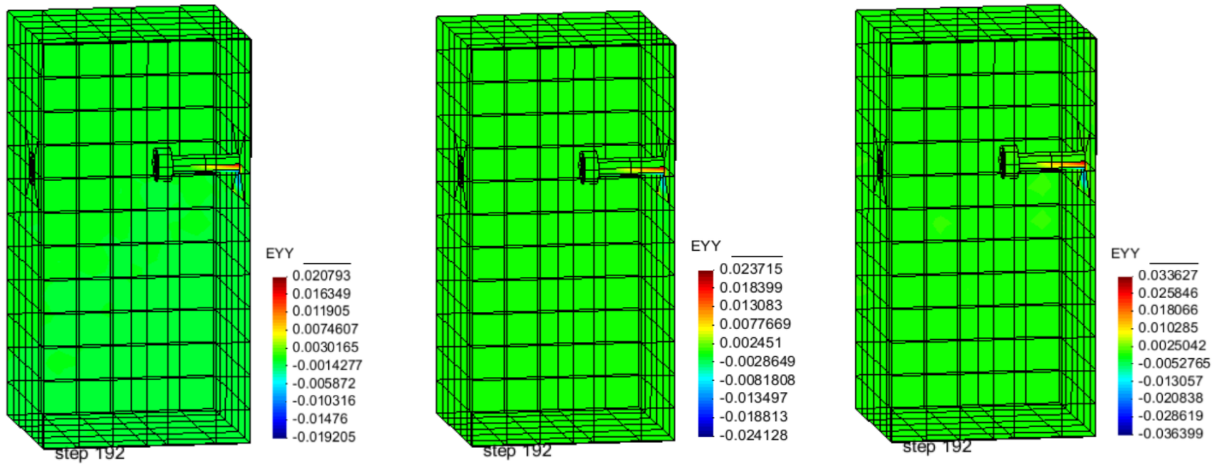

(a) 45 MPa-Studfy 400 Mpa-30% SF (After sustained loading)

(b) 45 MPa-Studfy 430 Mpa-30% SF (After sustained loading)

(c) 45 MPa-Studfy 450 Mpa-30% SF (After sustained loading)

Figure 4. 21: Strain contour distribution for different stud yield strength (for 30% shear force)

4.8.4 Level of shear force (SF)

The fourth parameter investigated was; how shear force level can influence the slip increment ratio (R) for 15%, 20% and 30% sustained shear force level as presented in Figure 4.22. R values increase as shear force level increases. Owing to a relatively high shear force, concrete beneath the stud and at stud-steel joint area experiences relatively higher deformation. Since sustained loading induces continuous creep deformation beneath and around the stud, tensile strain also develops due to which, some cracks would be obvious which induces concrete non-linearity. As some non-linearity exists, then higher level of shear force will induce a relatively higher creep deformation with a non-proportional progress. The localized strain behaviour for 15% and 30% shear is presented in Figure 4.23.

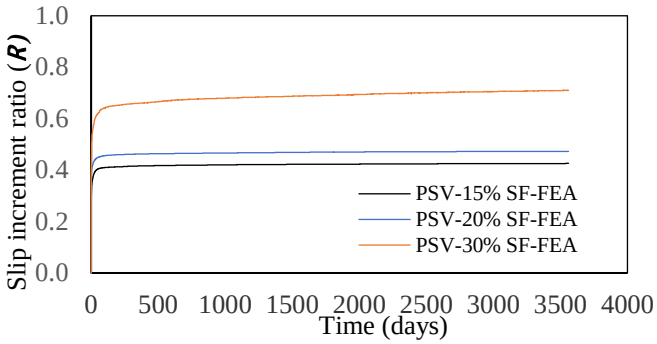

Figure 4. 22: Slip increment ratio (R) for different level of shear force.

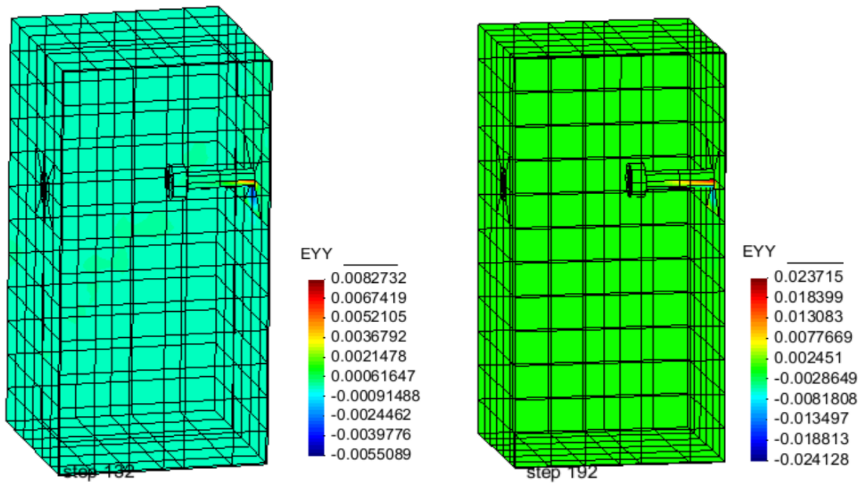

(a) PS III-45MPa-15% SF (After sustained loading)

(b) PS III-45MPa-15% SF (After sustained loading)

Figure 4. 23: Strain contour distribution for 15% and 30% shear force

4.9 Parametric study: Factors that influence initial slip displacement

Since, slip displacement increment ratio as already expressed in equation (3.3) of chapter 3 and presented as $k(t-t_0) = R = \frac{\delta(t)-\delta(t_o)}{\delta(t_o)}$, which exhibited the trend of creep deformation characteristics of concrete. An important component of this R value is initial slip displacement ($\delta(t_o)$). Hence, to model the deformation behaviour of headed studs in hybrid girder; using the FEA, a parametric study is also conducted on the factors that could influence the initial slip displacement which is described in this section. Since, the same factors can influence the $\delta(t_o)$, therefore how these factors can influence is presented in Figure 4.24. Owing to the loading before reaching the sustained load level, the same factors as described for R value, have influences on the $\delta(t_o)$ in a similar way.

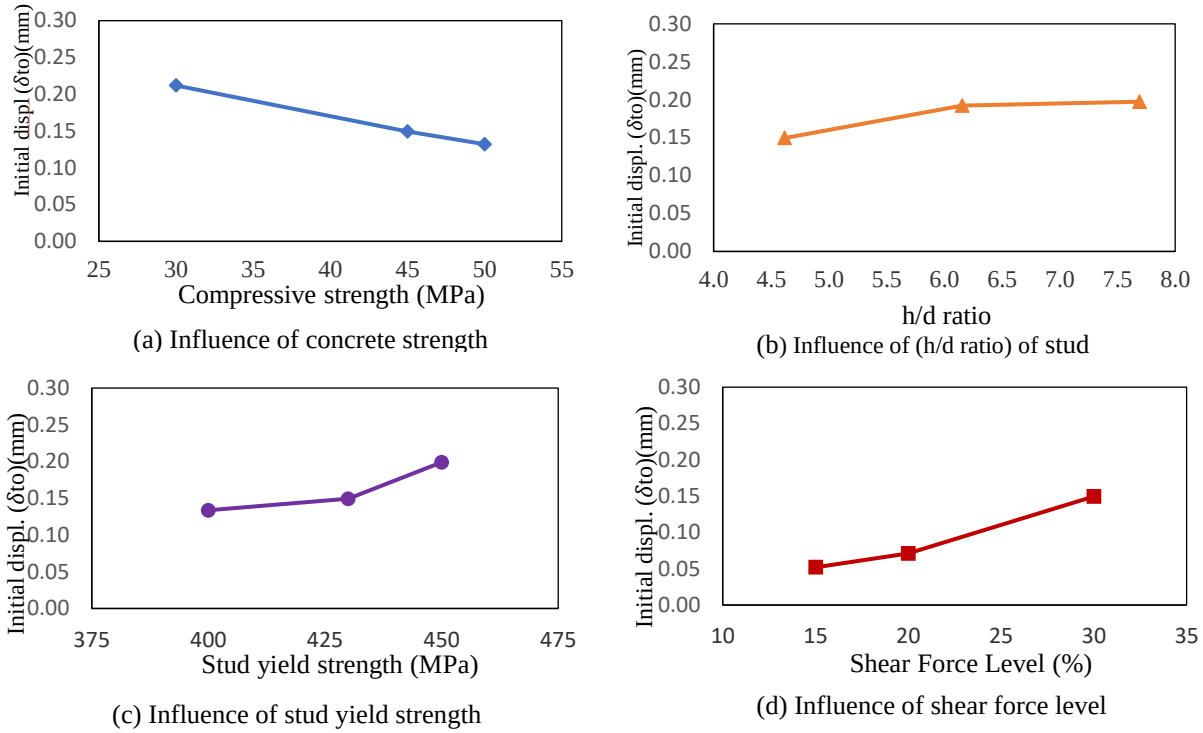

(a) Influence of concrete strength

(b) Influence of (h/d ratio) of stud

(c) Influence of stud yield strength

(d) Influence of shear force level

Figure 4. 24: Factors that can influence the initial slip displacement ($\delta(t_o)$)

4.10 Formulation of a simplified model for long-term deformation behaviour

Since, the relative slip displacement increment ratio as presented as $k(t-t_0) = R = \frac{\delta(t)-\delta(t_o)}{\delta(t_o)}$, that exhibited the trend of creep deformation characteristics of concrete, To propose a formulation on a simplified model for prediction of long-term deformation behaviour, a formulae can be proposed as similar to the long-term creep of concrete (equation 4.10) as per JSCE specification [(JSCE, 2007)].

$$\varepsilon'_{cc}(t,t',t_0)/\sigma'_{cp} = [1-\exp\{-0.09(t-t')^{0.06}\}]\varepsilon'_{cr} \qquad (4.10)$$

where, ε'_{cr}: Final value of creep strain per unit stress [$\times 10^{-10}(N/mm^2)$].

Therefore, to propose a simplified model, a conceptual curve as presented in Figure 4.25 is considered. If R value reaches its final stage at a time t_f with a value of R_{final}, then a formulae as

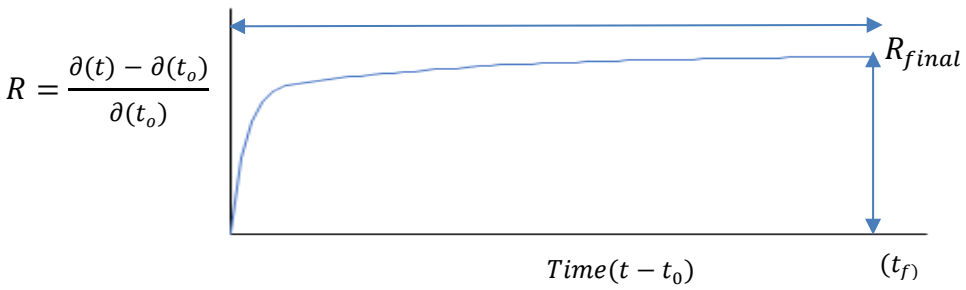

Figure 4. 25: Conceptual curve for proposed simplified model

resented in equations (4.11-4.13) can be considered.

$$R = \frac{\delta(t)-\delta(t_o)}{\delta(t_o)} = R_{final}\,[(1\text{-}\exp\{\beta(t-t_0)^{\alpha}\}] \qquad (4.11)$$

$$R_{final} = f\left(f_c^{'}, \frac{h}{d}, f_{y(stud)}, p\right) \qquad (4.12)$$

$$\delta(t_0) = f\left(f_c^{'}, \frac{h}{d}, f_{y(stud)}, p\right) \qquad (4.13)$$

where, β and α are effective coefficients, $f_c^{'}$ = compressive strength of concrete (MPa), h = height of stud (mm), d = diameter of stud (mm) f_y = yield strength of stud (MPa) and p = percentage of shear force in fraction . From the least square regression analysis with the formulation and FEA values, to obtain a best fit curve, β and α values are fixed as -0.45 and 0.35 respectively and considering the factors that influence the behaviour of R and $\delta(t_0)$, the following final form of the equations (4.14-4.16) are proposed:

$$\frac{\delta(t)-\delta(t_o)}{\delta(t_o)} = R_{final}\,[(1\text{-}\exp\{-0.45(t-t_0)^{0.35}\}] \qquad (4.14)$$

$$R_{final} = 2.9 * \frac{50}{f_c^{'}} * \left(\frac{3h}{40d}\right) * \left(\frac{f_y}{400}\right) * \left(\frac{49p}{25}\right) \qquad (4.15)$$

$$\delta(t_0) = 3.5 * \frac{250}{f_c^{'}} * \left(\frac{3h}{200d}\right) * \left(\frac{3f_y}{2500}\right) * \left(\frac{7p}{10}\right) \qquad (4.16)$$

4.11 Comparison of FEA and prediction model by proposed formulation

Since, a simplified prediction model is proposed to determine the relative deformation (slip-displacement) of stud connections used for the hybrid girder under this study, a comparison is required between the long-term deformation trend of FEA and prediction model. Therefore, a comparison is presented for 15% and 30% shear force for stud connections as shown in Figure 4.26 and 4.27. It is observed that for 30% shear force level; closer agreement exists in prediction model and FEA curves, however for 15% shear force level; prediction model showed higher values than FEA values. Since the expression of $\boldsymbol{R_{final}}$ and $\delta(\boldsymbol{t_0})$ are derived from the linear regression curves

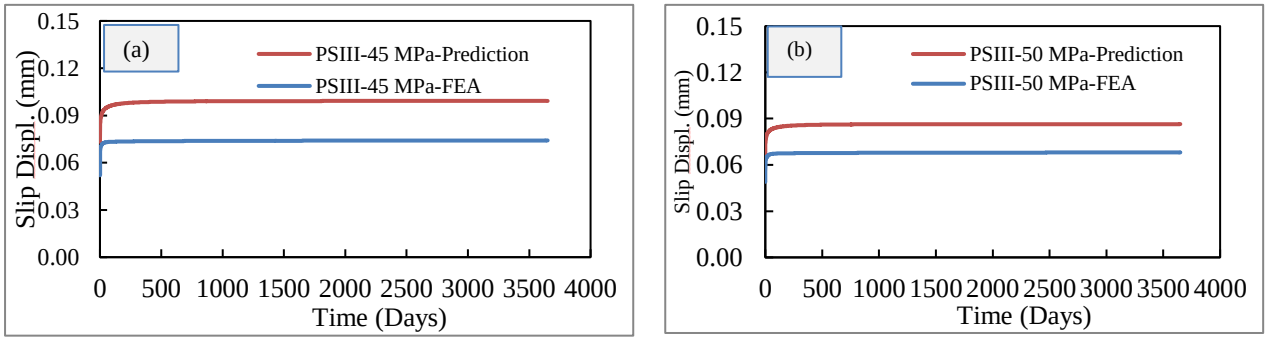

Figure 4. 26: Comparison between FEA and proposed prediction model for 15% shear force for different compressive strength in (a) and (b)

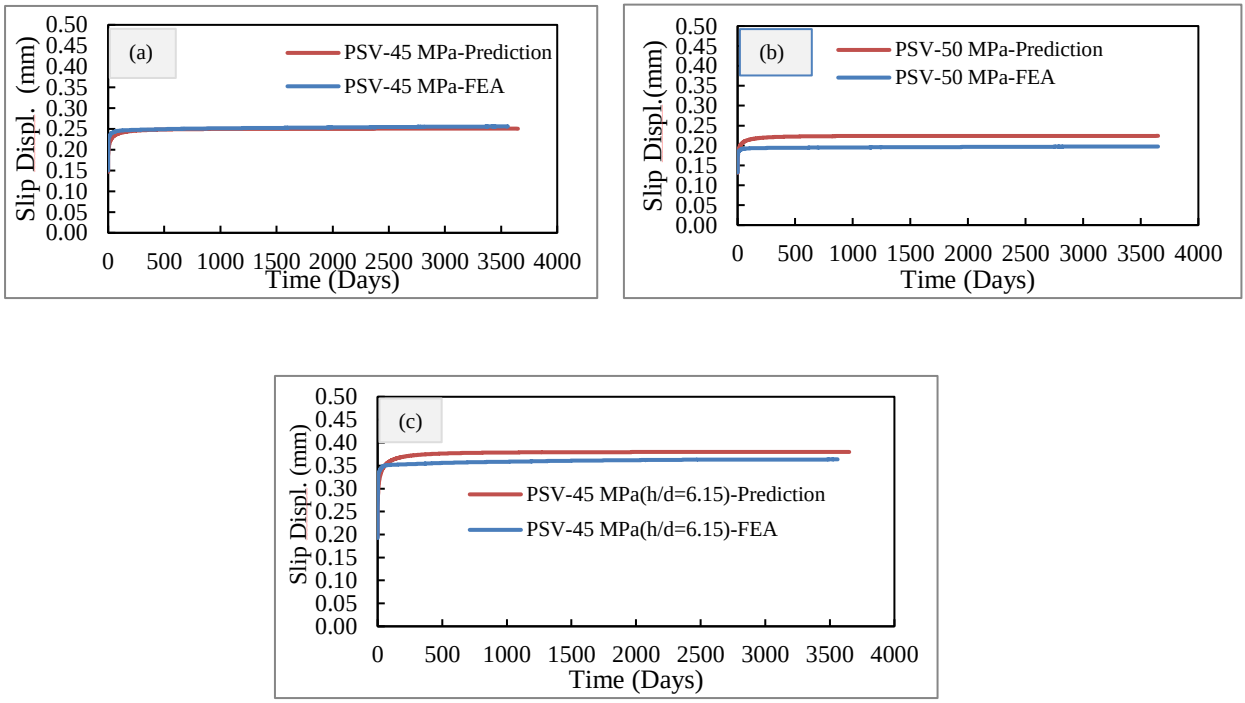

Figure 4. 27: Comparison between FEA and proposed prediction model for 30% shear force for in (a), (b) and (c)

that could not account a relatively lower values at lower level of load as it exhibited in FEA which is a limitation of this prediction model. Since, the long-term deformation is obvious and inevitable in hybrid girder due to sustained loading that induces time dependent shear forces in headed stud connections [(Haque MN, 2019), (Haque MN, 2019.10)]; it is an important issue to quantify the stud deformations for practical structures. Therefore, this model could be applied to quantify the long-term deformation of headed studs in such hybrid girder for practical applications.

4.12 Summary and conclusion

For stud connections which are the major connections devices for hybrid girder, it is considered that owing to sustained loading; the stud connections experience long-term shear forces and it was considered those shear forces will induce long-term stud deformation inside the specimen which is difficult to measure directly. Therefore, pushout experiments were conducted to different long-term loading histories. To reproduce and validate the experimental results, FEA has been also conducted. Based on the results of FEA and consequent parametric study, the following conclusions can be drawn.

4. For shear force-slip displacement envelop curve of FEA shows a transition towards increasing displacement under sustained loading as observed in experimental result although incremental amount is lesser than experimental values. Constitutive laws followed in FEA has some

limitations to reproduce the experimental cases exactly as it could not account the variations of the environmental conditions that always exist in laboratory.

5. It is observed that FEA values for long-term deformation are lower than the experimental investigation under this present study and a similar result was also obtained in the previous study. However; the cumulative slip displacement over time progresses with a slower incremental rate in both experimental and FEA cases and this nature of displacement behaviour over time resembles the nature of asymptotical curve. Long-term slip displacement accounts a reduction of stiffness of shear stud as also observed in experimental cases.
6. The internal stress-strain contour distribution in FEA shows that shear stud generated large tensile strain after the sustained load, and due to this tensile strain, the concrete around shear stud have more cracks that can comprehend accelerating the creep deformation of concrete around the shear stud. This also an indication that concrete non-linearity exist in that state.
7. Using FEA, parametric study has been conducted to identify the factors that influence the long-term deformation behaviour of stud connections, and depending on those factors, a simplified prediction model is proposed that can nearly model the actual behaviour. Even though this model has some limitations, this model could be applied to quantify the long-term deformation of headed studs in hybrid girder for practical applications

4.13 References

Nguyen HT, Kim SE. Finite element modeling of push-out tests for large stud shear connectors, Journal of Constructional Steel Research, No.65, p. 1909-1920. 2009.

Yanez SJ, Pina JC, Saavedra-Flores E, Guzmán CF, Numerical modeling of a new push-out test using non-linear behavior of concrete, Proceedings of the 1st Iberic Conference on Theoretical and Experimental Mechanics and Materials, November 2018. pp. 759-766.

Nasrin S, Ibrahim A, Numerical study on the low-velocity impact response of ultra-high performance fiber reinforced concrete beams, Structures, No.20, p.570-580, 2019.6.

Titoum M, Mazoz A, Benanane A, Ouinas D, Experimental study and finite element modelling of push-out tests on a new shear connector of i-shape, Advanced Steel Construction, Vol. 12, No. 4, pp. 487-506, 2016.

Maekawa K, Okamura H, Pimanmas A, Non-linear mechanics of reinforced concrete, Spon press, London, 2003.

Okamura H, Maekawa K, Non-Linear Analysis and Constitutive Models of Reinforced Concrete, Tokyo 1990.

Asamoto S, Ishida T, Maekawa K, Time-Dependent Constitutive Model of Solidifying Concrete Based on Thermodynamic State of Moisture in Fine Pores, Journal of Advanced Concrete Technology. Pp.301-323, 2006,

El-Kashif KF, Maekawa K, Time Dependent Nonlinearity of Compression Softening in Concrete, Journal of Advanced Concrete Technology, pp. 233-247, 2004.

Maekawa K, Toongoenthong K, Gebreyouhannes E, Kishi T, Direct Path-Integral Scheme for Fatigue Simulation of Reinforced Concrete in Shear, Journal of Advanced Concrete Technology, pp. 157-177, 2006.

Maki T, Watanabe R, Zhang P, Deformation of headed stud shear connector under sustained shear forces, 11th Symposium on composite and hybrid structures, 2017.

Mirza O, Uy B, Finite element model for the long-term behaviour of composite steel-concrete push tests, Steel and Composite Structures, 2010, Vol. 10, No. 1: 45-67

Japan Society of Civil Engineers. Standard Specifications for Concrete Structures, Tokyo, 2009.

Haque MN, Maki, T. Experimental study on time-dependent deformation of hybrid steel- PRC girder with headed stud shear connections under sustained loading, Structures, No.22, p.327-340, 2019.9.

Haque MN, Maki, T. Sasaki J, Finite Element Approach to Evaluate Time Dependent Shear Behavior of Connections in Hybrid Steel-PC Girder under Sustained Loading, International Journal of Structural and Construction Engineering, Vol.13, No.9, 2019.10.

Takahashi Y, Tanaka Y, Maekawa K, Computational Life Assessment of ASR-dmagaed RC Decks by Site Inspection Data-Assimilation, Journal of Advanced Concrete Technology,2018, vol 16, pp. 46-60.

CHAPTER 5
5 LONG-TERM DEFLECTION OF HYBRID GIRDER

5.1 Introduction

In this study, the time dependent deformation behaviour of a hybrid steel-PRC girder was investigated. For which, a scaled down hybrid girder specimen of a real bridge was designed. This hybrid girder composed of steel composite girder at one side and PRC girder at another side. The steel girder segment was embedded into the PRC segment, and they were bonded together using headed stud mechanical shear connections for the purpose of attaining integral behaviour through the transfer of forces. This embedded part or overlapping part connecting these two sides, known as junction. Shear connections were also used at the upper concrete slab of the steel composite part. This specimen was tested both under static cyclic and sustained loading with the purpose of measuring the long-term deformation behavior.

5.2 Design of specimen and connections

The scaled down hybrid girder specimen (one sixth of a real girder) as shown in Figure 5.1 was designed and used in this study, whose dimensions are presented in Table 5.1. The steel composite segment was designed as a compact cross section that satisfied the expression of total plastic moment as specified in the JSCE standard specifications for hybrid structures (2014) [(JSCE, 2014)]. The load value that induced the stress at the upper edge of the concrete slab equal to the allowable stress was set as the design load which was 80 kN. This design load corresponds to dead load components only (service loads includes self-weight and weight of ancillary structures and does not include the traffic load) that account 30% of the total load and remaining 70% is of transient load (live load, impact live load etc.).The PRC segment was designed with a design load of 60 kN, such that with the introduction of a 195-kN prestressing force, the compression stress at the lower fibre of the concrete would be neutralized by the applied decompressive design load [(Nilson AH, 2010)]. This design load corresponds to dead load components that account 50% of the total load and remaining 50% is of transient load which maintains a dead load component ratio to composite to PRC as 3: 5.The headed stud connections at the shear span of the upper flange were designed to sustain the axial force arising owing to the flexural moment for the applied design load. In the junction segment, the same stud connections that were used in the real bridge were employed. The stud strength used for designing the connections was determined as per the JSCE standard specifications for steel and composite structures (2009) [(JSCE, 2009)]. In each specimen, 74 headed stud connections were used, of which 30 were used in the upper flange and 44 were used in the lower flange and web. The specimen was designed while assuming that failure would occur at the PRC segment. Five scaled-down simply supported girder specimens having identical cross

sections and spans labelled as GS I to V were prepared and tested. The detail calculations of the design procedure are described below-

5.2.1 Design of composite girder part

For the composite girder part as shown in Figure 5.2.; with steel girder height 250mm, upper flange width 100mm, lower flange width 150mm, web height 232mm, steel girder thickness 9mm and

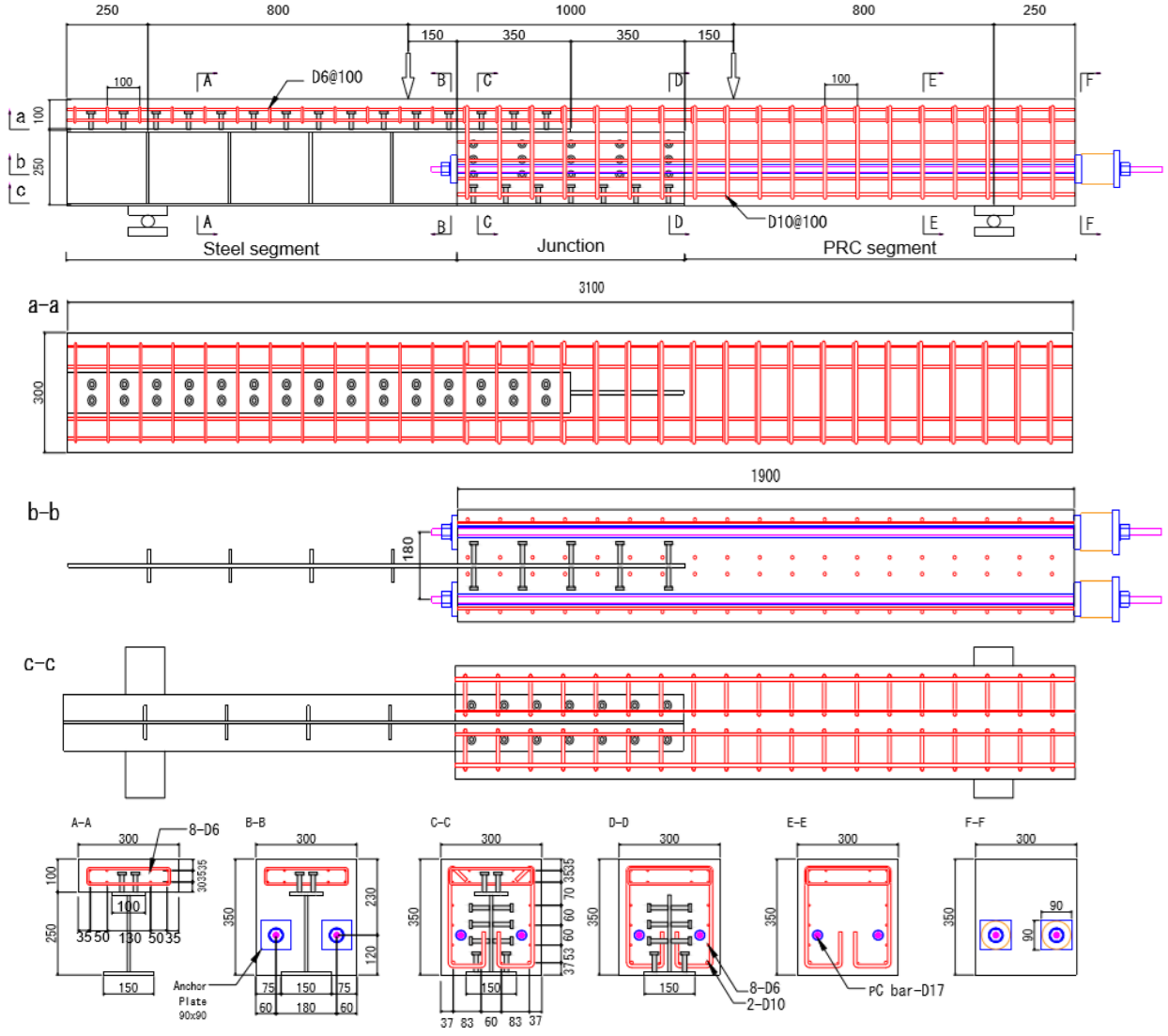

(a) Hybrid girder sectional details.

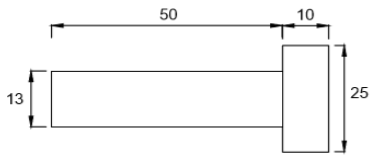

(b) Shape and dimension of headed stud.

Figure 5. 1: Hybrid girder specimen details. (a) Hybrid girder sectional details; (b) Shape and dimension of headed stud.

concrete floor of 200mmx100mm, the material strength was considered as $f'_{cd} = 40\,N/mm^2$, $f_{yd} = 300\,N/mm^2$.

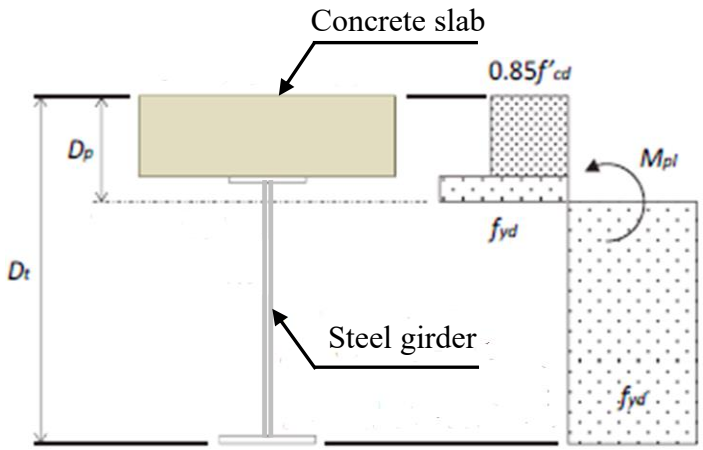

Figure 5. 2: Girder x-sectional view for calculation of sectional forces.

Here,

$$\mathrm{C} = 0.85f'_{cd}A_{c1} + f_{yd}A_{c2} + f_{yd}A_{c3}$$

$$\mathrm{T} = f_{yd}A_{t1} + f_{yd}A_{t2}$$

where, concrete area: $A_{c1} = 100 \times 200$, upper flange area above plastic neutral axis: $A_{c2} = 9 \times 100$, web area above the plastic neutral axis: $A_{c3} = (D_p - 100 - 9) \times 9$, web area below the plastic neutral axis: $A_{t1} = (350 - 9 - D_p) \times 9$, lower flange area: $A_{t2} = 9 \times 150$.

From C=T gives;

$$5400D_p = 670000$$

$$D_p = 124\text{mm}$$

Then, the ratio of the height of the compression zone from the plastic neutral axis (D_p) to the total height of the girder specimen (D_t) is $\alpha = D_p/D_t = 0.354$, and satisfies the following formula.

$$\frac{h_w}{t_w} \leq \frac{2.0}{\alpha}\sqrt{\frac{E_s}{f_{yd}}}$$

Hence, from the obtained value of D_p, the total plastic moment is calculated as-

$$M_{pl} = C_1(D_p - 50) + C_2(D_p - 100 - 4.5) + C_3\left(\frac{D_p - 100 - 9}{2}\right) + T_1\left(\frac{350 - 9 - D_p}{2}\right)T_2(350 - D_p - 4.5)$$

$M_{pl} = 163.8kNm$

Since; 0.15<α<0.4, the ultimate moment is calculated as-

$$M_{ud} = \left(1.05 - 0.33\frac{D_p}{D_t}\right)M_{pl} = 152.8kNm$$

Therefore, a load value corresponding to the bending strength is obtained as-

$$\mathrm{P} = 152.8/0.8 = 191\mathrm{kN}.$$

For designing the headed studs, as the axial force ($0.85f'_{cd}A_{c1}$) that the concrete floorboard takes over during the total plastic moment is 680 kN and for that, 16 studs with strength of 73 kN are placed on the shear span of the upper flange., therefore, every stud is subjected to a force of 42.5 kN. So, the stud arrangement is enough for design requirement.

For determining the stress level at different locations of the composite girder, the Figure 5.3 is considered. The position of the neutral axis of the composite girder is given by the following equation.

$$d_c = \frac{nA_s}{nA_s + A_c} d = 120mm$$

$$d_s = \frac{A_c}{nA_s + A_c} d = 79mm$$

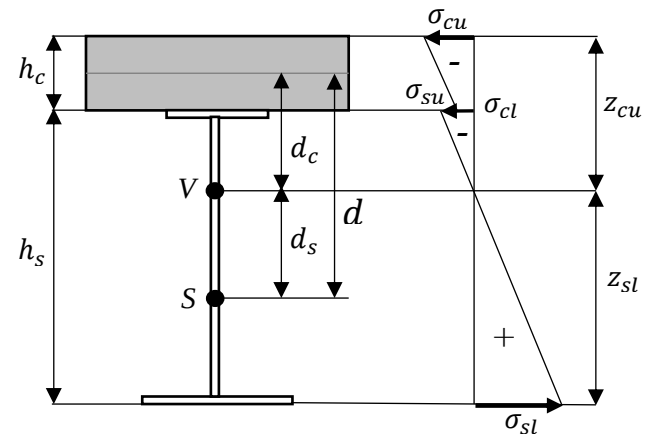

Here;

A_c : Concrete sectional area;
A_s : Steel girder sectional area;
n: E_s/E_c
d : Centroidal distance between concrete section and steel girder section;
d_c : Distance between the centroid axis of composite section and concrete;
d_s : Distance between centroid axis of composite section and steel girder;
I_c : Moment of inertia of concrete;
I_s : Moment of inertia of steel girder;
I_v : Total x-sectional moment of inertia

Figure 5. 3: Girder x-sectional view for stress at different level.

The moment of inertia of concrete is-

$$I_c = \frac{bh^3}{12} = 1.69 \times 10^7 mm^4$$

The moment of inertia of steel is-

$$\mathrm{I} = A_u \left\{\frac{1}{2}(h_w + t_w)\right\}^2 + \frac{t_w h_w^3}{12} + A_l \left\{\frac{1}{2}(h_w + t_l)\right\}^2 = 4.95 \times 10^7 mm^2$$

where, $\mathrm{Q} = 54225$; $\mathrm{e} = \frac{Q}{A} = 13.4$ and $I_s = I - Ae^2 = 4.8 \times 10^7$

Therefore, the moment of inertia of the composite girder is-

$$I_v = I_s + \frac{1}{n} I_c + A_s d_s^2 + \frac{1}{n} A_c d_c^2 = 1.19 \times 10^8 mm^4$$

Now, the edge stress of each member at 191.9 kN load is determined from the total plastic moment

$$\sigma_{ca} = 13.4\, n/mm^2 \;\; \sigma_{ta} = 185\, N/mm^2 \;\; \sigma_{ba} = 177\, N/mm^2$$

Stress at concrete slab upper edge is-

$$\sigma_{cu} = \frac{M}{nI_v} z_{cu} = 31.2\, N/mm^2 > \sigma_{ca}$$

Stress at concrete slab lower edge is-

$\sigma_{cl} = \frac{M}{nI_v} z_{cl} = 12.8\, N/mm^2 < \sigma_{ca}$

Stress at steel girder upper edge is-

$$\sigma_{su} = \frac{M}{I_v} z_{su} = 89.9\, N/mm^2 < \sigma_{ba}$$

Stress at steel girder lower edge is-

$$\sigma_{sl} = \frac{M}{I_v} z_{sl} = 231\, N/mm^2 < \sigma_{ta}$$

Here, the load value that makes the stress at the upper edge of the concrete slab equal to the allowable stress is obtained and the load value is set as the design load.

When the load value is 85 kN (M = 68 kNm);

Stress at concrete slab upper edge is-

$$\sigma_{cu} = \frac{M}{nI_v} z_{cu} = 13.8\, N/mm^2$$

Stress at concrete slab lower edge is-

$$\sigma_{cl} = \frac{M}{nI_v} z_{cl} = 5.71\, N/mm^2$$

Stress at steel girder upper edge is-

$$\sigma_{su} = \frac{M}{I_v} z_{su} = 40\, N/mm^2$$

Stress at steel girder lower edge is-

$$\sigma_{sl} = \frac{M}{I_v} z_{sl} = 102.9\, N/mm^2$$

Since the compressive stress at the upper edge of the concrete slab is almost equal to the allowable compressive stress, the design load is set to P = 85 kN.

5.2.2 Design of PRC girder

For the PRC girder part, the ratio of the strength of the composite part to the strength of the PRC part is kept reasonable so that prestress could be introduced through the PC steel material which cancels the lower edge stress. It is assumed that the specimen will be destroyed at the PRC part, and design load is set to 55 kN.

Here, 17mm prestress bar is used with σ_{pi}=$195kN/227mm^2$=$859.0\,N/mm^2$. It is assumed that after the introduction of prestress, the loss of PC steel stress are considered as-

Reduction due to friction of PC steel and fixing device: $20\ N/mm^2$

Reduction due to elastic deformation of concrete: $20\ N/mm^2$

Reduction due to fixation: $10\ N/mm^2$

Total loss of prestress: $50\ N/mm^2$

Therefore, effective prestress: $\sigma_{pt} = 859.0 - 50 = 809.0\,N/mm^2$. Hence, for the eccentricity $e = 55\ mm$, the effective prestress force: $P_i = N \cdot A_p \cdot \sigma_{pt} = 36.7 \times 10^4 N$

Therefore, bending moment due to prestressing force : $M_{pt} = 36.7 \times 10^4 \times (-55) = -20.2 \times 10^6 N \cdot mm$.

Now, concrete upper edge prestress: $\sigma'_{ct} = \frac{P_t}{A_c} + \frac{M_{pt}}{Z_c} = 0.197 N/mm^2$ and

Concrete lower edge prestress: $\sigma_{ct} = \frac{P_t}{A_c} - \frac{M_{pt}}{Z_c} = 6.793\,N/mm^2$

Assuming that compression edge concrete crushes after the PC steel yield. For $f_{psy} = 1083\,N/mm^2$,$A_{ps} = 227 \times 2 = 454mm^2$;

$$C = 0.85f'_c \cdot 0.8x \cdot b$$

$$T = A_{ps}f_{psy}$$

$$x = \frac{A_{ps}f_{psy}}{0.68bf'_c} = 60.3\text{mm}$$

Therefore, ultimate bending moment: $M_u = A_{ps}f_{psy}(d - 0.4x) = 101.2kNm$ and the bending strength: P = $\frac{M_u}{\text{a}} = 126\text{kN}$.

For shear strength; using two D6 bars and two D10 bars as main bars and D10 for stirrup reinforcement.

$$V_c = 0.2f_c'^{\frac{1}{2}}(100p_w)^{\frac{1}{3}}\left(\frac{1000}{d}\right)^{\frac{1}{4}}\left(0.75 + \frac{1.4d}{a}\right)b_w d = 141.2\text{kN}$$

$$V_s = \frac{A_w f_{wy} jd(sin\alpha + cos\alpha)}{s} = 119\text{kN}$$

Hence, the shear strength: $V = V_c + V_s = 260kN$

Therefore, the bending strength of composite part is 191.9 kN and for PRC part is 126 kN.

5.3 Specimen assemble, casting and curing

For preparing the specimen, a steel girder of designated dimensions as shown in Figure 5.1 was produced with the stud connections welded to that. Then rebars and stirrups were assembled, and strain gauges were installed at the surface of top and bottom flanges and web of steel girder as well as studs and rebars. Formwork was prepared with steel sheet and plywood and putty was used to

seal the gaps between them so that during casting, concrete cannot come out through leakage. To maintain the clear cover from the concrete surface to the rebars and stirrups, spacer was used. Grease was applied to the steel girder surface to remove the interfacial friction between steel and concrete. Steel hollow tubes were also placed at designated locations, so that after casting PC bars could be inserted through them. For compressive strength assessment, plastic cylinder molds were used for casting of cylinders. Then, casting was done with a concrete mix of target strength that was poured into the formwork and vibrator was used for compaction. After two days of casting, formworks were removed and the specimen went under a wet curing for 14 days, for which the specimen was covered with wet cloths. The details of the assembling and casting is presented in Figure 5.4 and 5.5.

5.4 Material Properties

Five girder specimens were prepared and cast in two different batches over two consecutive years. In the first batch, specimens GS I to III were cast on the same day of the first year and in the second batch, specimens GS IV to V were cast on the same day of the second year. The instantaneous compressive strength of the concrete at different ages (time when each specimen was set for loading) for the five girder specimens was obtained through standard cylinder (200 mm in height and 100 mm in diameter) tests. The material properties of the concrete, steel girder section, prestressing bars, and studs are summarised in Tables 5.2 and 5.3. The steel girder sections, prestressing bars, and studs for these specimens were produced separately for each batch. Therefore, the strengths varied from one batch to another. For concrete with the same material composition and lower air entraining agent (AEA), a relatively lower compressive strength was obtained for GS IV and V than for GS I to III. The different environmental conditions under which the two batches of concrete were cast and cured caused the differences in strengths. The extent to which this lower concrete strength can influence the deformation behaviour is discussed later in the results and discussion section.

5.5 Experimental Programme

5.5.1 Sensor layout and load setup

For the measurements taken during the loading, sensors were placed at various locations on all specimens. Deflection measurement transducers and strain gauges were installed at suitable locations before applying the four-point bending loading. Layout of such arrangement indicating the loading point and strain gauges locations are illustrated in Figure 5.6. In house laboratory setup of specimens is presented in Figure 5.7

Table 5. 1: Dimensions of hybrid girder and structural component

Item	Unit	Amount
Total Length	mm	3100
Length between supports	mm	2600
Length of steel composite segment	mm	1200
Length of PRC segment	mm	1200
Length of junction/overlapping segment	mm	700
Steel composite segment section dimensions	mm	Steel section; H x t_w x t_f =250 x 9 x 9, slab; W x H=300 x 100
PRC segment section dimensions	mm	W x H=300 x 350
Re-bar diameter at upper slab	mm	6
Re-bar diameter at PRC segment	mm	6,10
Transverse re-bar diameter at upper slab	mm	6
Transverse re-bar diameter at PRC segment	mm	10
Prestressing bar diameter	mm	17
Stud size	mm	d x h=13 x 60

Figure 5. 4: Assembling of specimen. (a) steel girder with welded studs; (b) pasting of strain gauges and placement of rebars; (c) setting of formworks.

Figure 5. 5: Casting of specimen. (a) Hybrid girder; (b) Cylinder.

Table 5. 2: Concrete mix proportions and strength.

Specimen	Concrete mix proportions (kg/m3)						Concrete compressive strength		Type of cement
-	W/C ratio (%)	Cement	Water	Coarse aggregate	Fine aggregate	Air entraining agent	Strength (MPa)	Age from casting (days)	-
GS I	44.5	394	175	990	767	5.12	49.0	14	Early strength Portland cement
GS II							50.8	16	
GS III							54.8	46	

5.5.2 Specimens loading scheme and history

This study mainly focused on investigating the fundamental behaviour of long-term deformation of the hybrid girder (used in a real bridge) with headed stud connections under a pure bending condition to allow for subsequent design considerations; even though the real girders are subjected

to bending as well as shear. It was thus necessary to model an approximate loading scheme capable of illustrating the loading condition of a real bridge girder. Therefore, a four-point bending condition was applied in a scaled-down (one sixth of the real girder), simply supported girder specimen, to which vertical loads were applied through two designated points as shown in Figure 5.6. However, the actual loading conditions and moment distribution may differ for a real bridge girder. For the investigations, all specimens were under prestress for the entire duration of the loading. Among the specimens; GS II, GS III, and GS V were subjected to a sustained vertical load (i.e., application of vertical load for a specific time duration), and GS I and GS IV were subjected to a static vertical load following the designated number of days since prestressing. The loading types and histories for all the specimens are presented in Table 5.4. Static loading was applied to specimen GS I to differentiate its deformation behaviour from the case of sustained loading. GS IV was maintained under prestress to assess the deformation behaviour caused by environmental effects and was installed and loaded beside GS V

Table 5. 3: Material properties of the steel girder, prestress bar, and stud.

Specimen	Yield strength *fy* (MPa)				Tensile strength *fu* (MPa)			
-	Steel girder web	Steel girder flange	Prestress bar	Stud	Steel girder web	Steel girder flange	Prestress bar	Stud
GS I	429	383	1198	408	550	535	1290	473
GS II								
GS III								
GS IV	396	347	1189	440	536	446	1277	487
GS V								

Table 5. 4: Specimens loading history.

Specimen	Time of loading (days)							Loading type
-	Prestress (195 kN)	30 kN	40 kN	50 kN	60 kN	80 kN	Final loading	-
GS I	2	-	-	-	-	-	2nd day	Static loading
GS II	30	-	-	-	14	14	30th day	Sustained loading
GS III	72	14	14	14	14	14	72nd day	Sustained loading
GS IV	39	-	-	-	-	-	39th day	Prestress only
GS V	42	-	-	-	28	-	42nd day	Sustained loading

5.6 Environmental conditions

During the sustained loading, the temperature was measured for specimens GS IV and GS V to distinguish the behaviour due to sustained loading from behaviour caused by the variations in environmental conditions. Figure 5.8 shows temperature variation with time; the time depicted indicates time since prestressing.

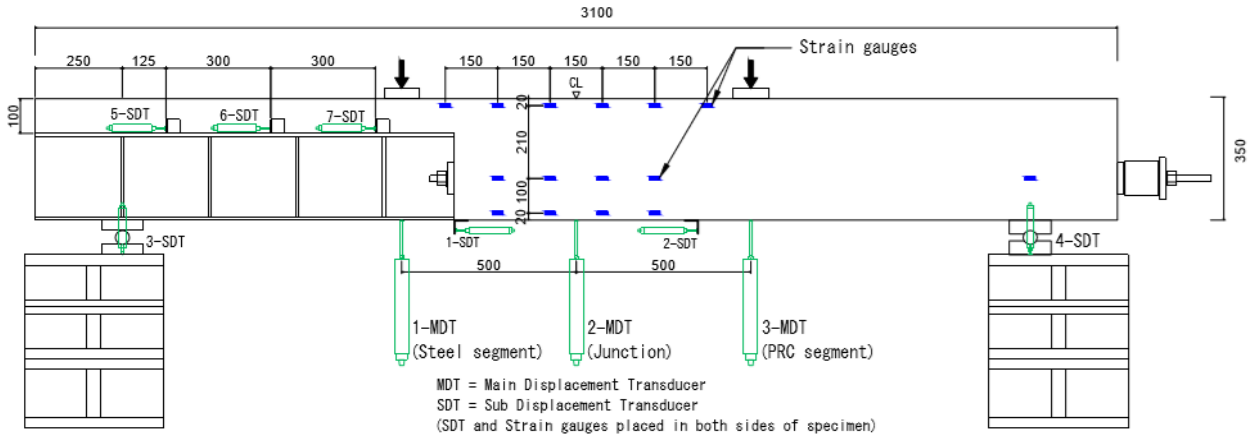

(a) Layout of loading point, transducers and sensors installed on the outer surface of the specimen.

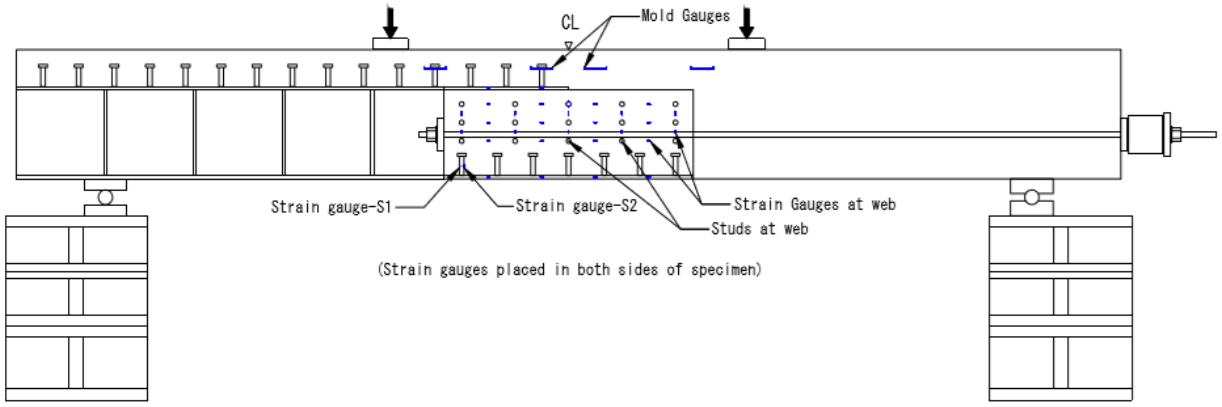

(b) Layout of sensors installed inside the specimen.

Figure 5. 6: Layout of loading arrangement, sensors and transducers for the test specimens: (a) transducers and sensors installed on the outer surface, (b) sensors installed inside the specimen.

5.7 Test results and discussions on hybrid girder

All hybrid girder specimens were subjected to four-point bending after introduction of the prestressing force, as shown in Figure 5.6. Concrete creep and shrinkage are important phenomena that must be considered when examining time-dependent behaviour [(Kwak HG, 2000), (Al-Deen S, 2011)]. Therefore, specimen GS IV was subjected to prestress only to assess such effects. The overall deformation behaviour is discussed in the following sections, with a primary focus on time-dependent behaviour under sustained loading.

5.7.1 Long-term deflection of girder

Deflections at three locations—the steel segment, PRC segment, and junction—were measured using a main displacement transducer (MDT, Figure 5.6(a)) to assess the time-dependent deflection behaviour, which is reported in Table 5.5 and Figures 5.9(a)–(c). The experimental results indicated

Figure 5. 7: Laboratory test set up for specimen

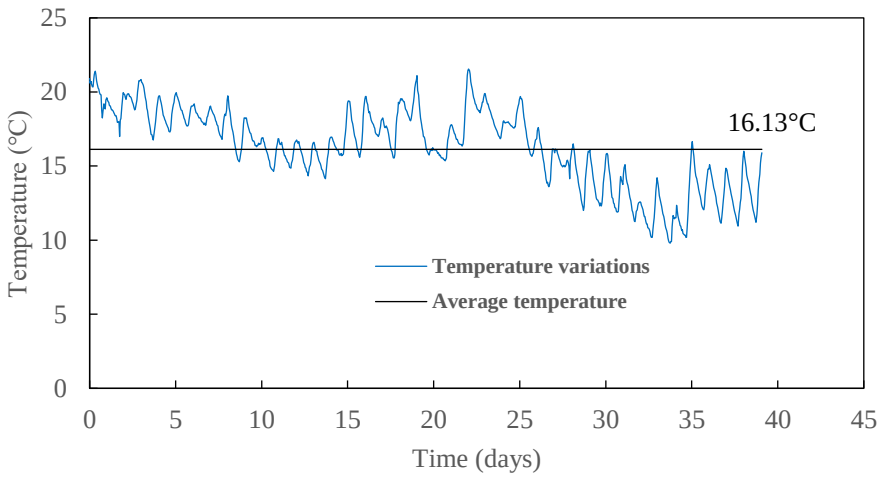

Figure 5. 8: Temperature variations with time

that at a 60 kN load, starting deflections in each segment of steel, PRC, and junction were closer with the sustained-loading specimen GS II (1.19, 0.86, and 1.17 mm, respectively) than those with the static-loading specimen GS I (1.17, 0.95, and 1.14 mm, respectively). At an 80 kN load, the starting deflection values in each segment of GS II (2.05, 1.68, and 2.15 mm) were distinctly different from those of GS I (1.66, 1.42, and 1.69 mm). This difference was observed because GS

II was subjected to a 60 kN sustained load for 14 days prior to the 80 kN load, causing it to undergo additional time-dependent deflections of 0.45, 0.42, and 0.52 mm at the steel, PRC, and junction segments, respectively. The static-loading specimen GS I, however, was not subjected to additional prior loading. A comparison of GS III and GS II reveals that the starting and ending deflection values for each segment under a 60 kN sustained load were significantly higher for GS III, despite lower incremental values for GS III (0.16, 0.15, and 0.19 mm) than for GS II (0.45, 0.42, and 0.52 mm). This was because of the prior sustained loading history for GS III, as the specimen had already undergone three-stage additional intermediate sustained loading of 14 days each at 30, 40, and 50 kN, while GS II was loaded for 14 days total. Therefore, time-dependent creep and shrinkage deformation occurred at each stage of sustained loading, and the cumulative deflection reached higher start and end values at the 60 kN loading stage for GS III. Although these intermediate loading levels were lower than the design load, creep deformations caused by sustained load in the stud–concrete vicinity may have been the primary cause of the increased deflection values. The same phenomena were observed for GS III and GS II at the 80 kN sustained loading stage. Comparing incremental deflection values for GS III and GS II confirmed that the previous sustained loading steps had induced some deflections, causing a decrease in incremental deflection values over time in the later stages of sustained loading. This indicated the asymptotical nature of time-dependent deflection behaviour.

To determine whether an asymptotical nature existed or a nearly constant value was reached, specimen GS V was maintained under a sustained load of 60 kN for a longer period than GS II. For GS V, the start and end values at a 60 kN sustained load, as well as the incremental deflection for each segment (steel, PRC, and junction), were far higher than those for GS II. This was mainly because of the previous loading history and exposure time of GS V. Despite identical load levels, GS V was maintained under prestress for 14 days before the 60 kN load was applied, whereas GS II was maintained under prestress for only 2 days before reaching the same load level. In GS V, the long-term prestress coupled with the low compressive strength influenced the interfacial local deformation in the stud–concrete vicinity, which was further increased when a vertical load was applied opposite to the prestressing force. This resulted in a higher deflection value at the 60 kN load level. The incremental deflection values were also higher for GS V (0.68, 0.68, and 0.81 mm) than for GS II (0.45, 0.42, and 0.52 mm), as under the same load level, the longer the period of sustained loading, the higher the deflection values of each increment. The deflection behaviour of GS V was also asymptotical in nature.

As concrete creep and shrinkage are considered causes of time-dependent behaviour [(Okui Y, 2007)], the deflection behaviours of GS IV and GS V were compared to differentiate their effects

as shown in Figure 5.9(d). The recorded deflection for GS IV was assumed represent shrinkage caused by environmental effects, while the recorded deflection for GS V was caused by the combined effects of creep and shrinkage. The shrinkage deflection appeared significant, but the creep deflection (deflection other than shrinkage) in GS V was significantly more than that caused by shrinkage. However, the shrinkage deflection was not identified precisely, because the effect of the prestress remained and could not be separated. These two specimens were subjected to side-by-side experiments using the same prestress loading for 14 days, however their deflections were slightly different. This may have been caused by differences in the prestress force acting on the two specimens, as shown in Figure 5.10. As noted in a previous study, this may also have been caused by a lateral uneven distribution of section stress because of the existence of shear connections, resulting in different deflection values for the two specimens [(Haigen, 2015)].

Table 5. 5**:** Deflection of specimens under loading.

Specimen		Deflection (mm) at 60 kN				Deflection (mm) at 80 kN				Loading type/days
-		Start	End	Increment	Time (days)	Start	End	Increment	Time (days)	-
GS I	Steel segment	1.17	-	-	-	1.66	-	-	-	Static (after 2 days under prestress)
	PRC segment	0.95	-	-		1.42	-	-		
	Junction	1.14	-	-		1.69	-	-		
GS II	Steel segment	1.19	1.64	0.45	14	2.05	2.35	0.30	14	Sustained /28 days (after 2 days under prestress)
	PRC segment	0.86	1.28	0.42		1.68	1.95	0.27		
	Junction	1.17	1.69	0.52		2.15	2.52	0.37		
GS III	Steel segment	1.67	1.83	0.16	14	2.28	2.49	0.21	14	Sustained /28 days (after 2 days prestress plus 42 days intermediate sustained loading)
	PRC segment	1.37	1.52	0.15		1.98	2.22	0.24		
	Junction	1.68	1.87	0.19		2.37	2.62	0.25		
GS V	Steel segment	1.45	2.13	0.68	28	-	-	-	-	Sustained /28 days (after 14 days under prestress)
	PRC segment	0.90	1.58	0.68		-	-	-		
	Junction	1.41	2.21	0.81		-	-	-		

Figure 5.9 (d) shows another effect. Although the prestress force followed a descending curve with time as shown in Figure 5.10, the deflection curves for GS IV and GS V, up to 39 and 14 days, respectively, did not exhibit such behaviour. Rather, they had nearly uniform values with slight fluctuations caused by temperature variations. This phenomenon indicates that after the application of the sustained load, the time-dependent ascending (asymptotical) nature of the deflection value was due to the creep only.

The trends of the deflection-time curves were similar for the three sustained-loading specimens, GS II, GS III, and GS V. The prestress force was applied to the section including the PRC segment and junction. Hence, at the prestressing load, the bottom-level axial force was most dominant in the PRC and underwent greater upward deflection than the junction. As the three segments were part

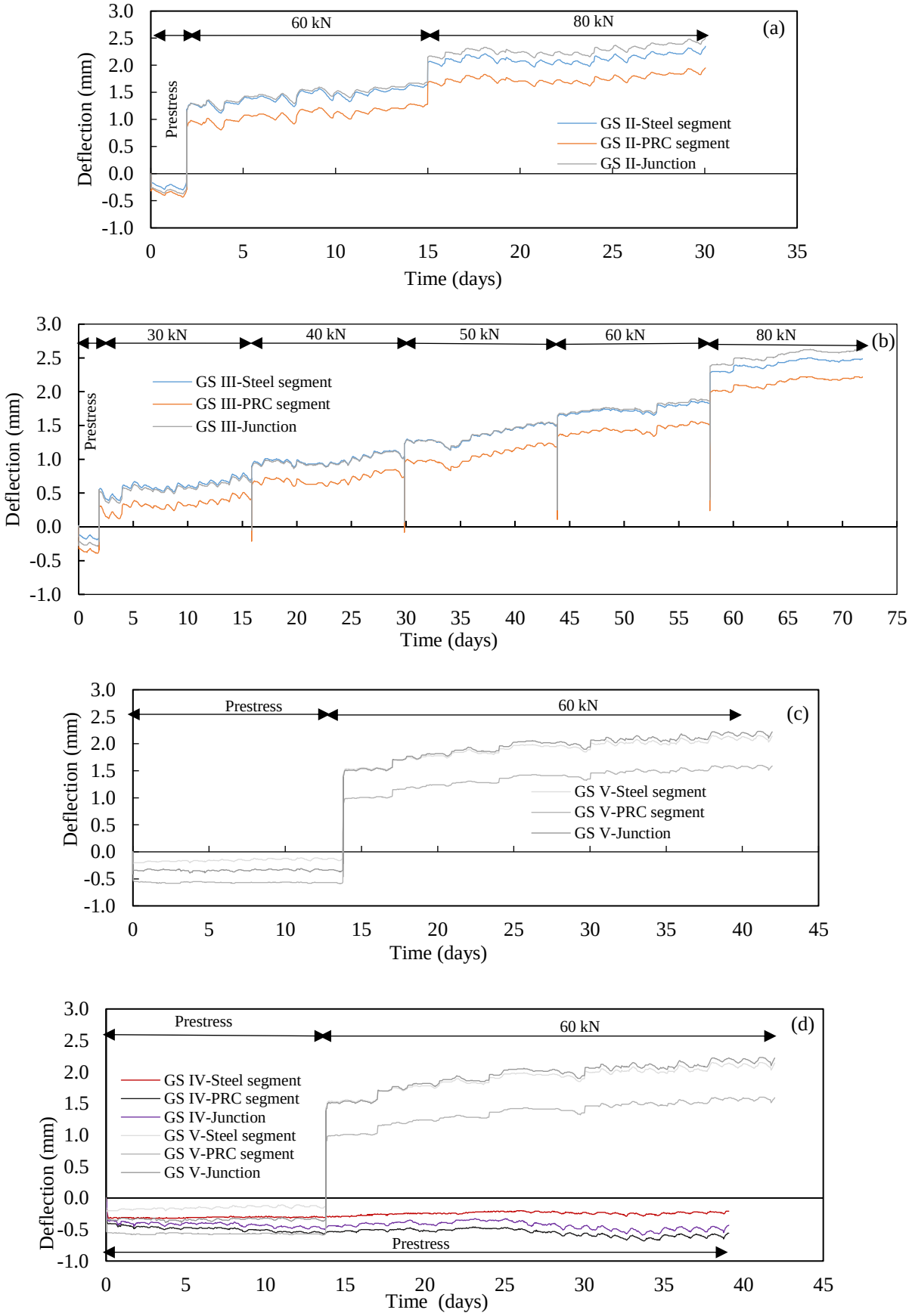

Figure 5. 9: Time-dependent deflection under loading: (a) GS II, (b) GS III, (c) GS V, (d) GS IV and GS V.

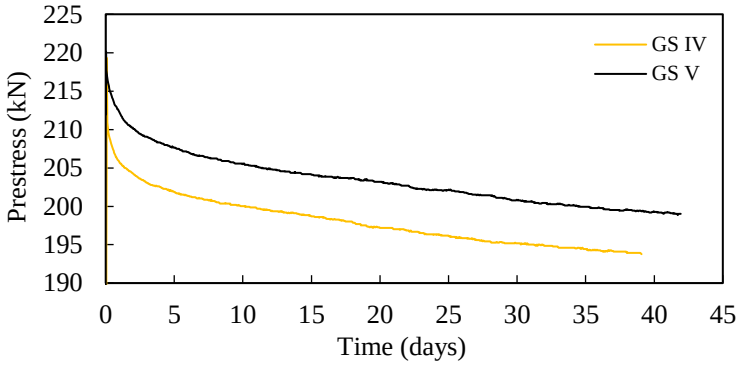

Figure 5. 10: Prestress profile with time for specimens GS IV and GS V.

of the girder, the steel segment exhibited similar behaviour with smaller deflection. As soon as the vertical load was applied, prestress became more dominant to counteract the applied load, resulting in a smaller deflection in the PRC segment. For junction, although prestress played an active role, it was directly influenced by bending that caused slip and localized creep deformation at the stud–concrete interface. Thus, the deflection level was higher than those of the other segments. As the steel segment remained primarily in the shear zone of the hybrid girder, the bending influence was less prominent, resulting in an intermediate level of deflection compared with the junction and PRC. Despite different experimental conditions and loading patterns, the trend of deflection–time curve for sustained loading obtained herein matched the behaviour observed in previous studies by Bradford and Gilbert [(Bradford MA, 1991)], AL-Deen et al. [(Al-Deen S, 2011)], and Ban et al. [(Ban H, 2015)].

5.7.2 Long-term slip displacement

The relative slip displacement between steel and concrete was recorded using a displacement transducer 1-SDT at the bottom of the junction, as shown in Figure 5.6 (a). The time-dependent behaviour is illustrated in Figure 5.11 (a). The slip-displacement values for GS III at 60 and 80 kN were marginally higher than those in the case of GS II. This was because of exposure time and previous loading history of GS III under sustained loading as explained in the previous section. In the case of GS V, slip-displacement was significantly larger than GS II and GS III for the 60 kN load, and even higher than those at the 80 kN load. Prestress application over a longer duration and the subsequent application of vertical loading as a decompression force resulted in local deformation at the stud–concrete and steel-concrete interface. This interfacial deformation, coupled with the low compressive strength of the concrete, aggravated the overall slip displacement. Further, before the design load (60 kN) was reached, intermediate sustained loadings did not result in slips as significant as those caused by long-term prestress. The relative slip displacement at the stud level at the upper slab of composite part was also recorded with the displacement transducer 6-SDT

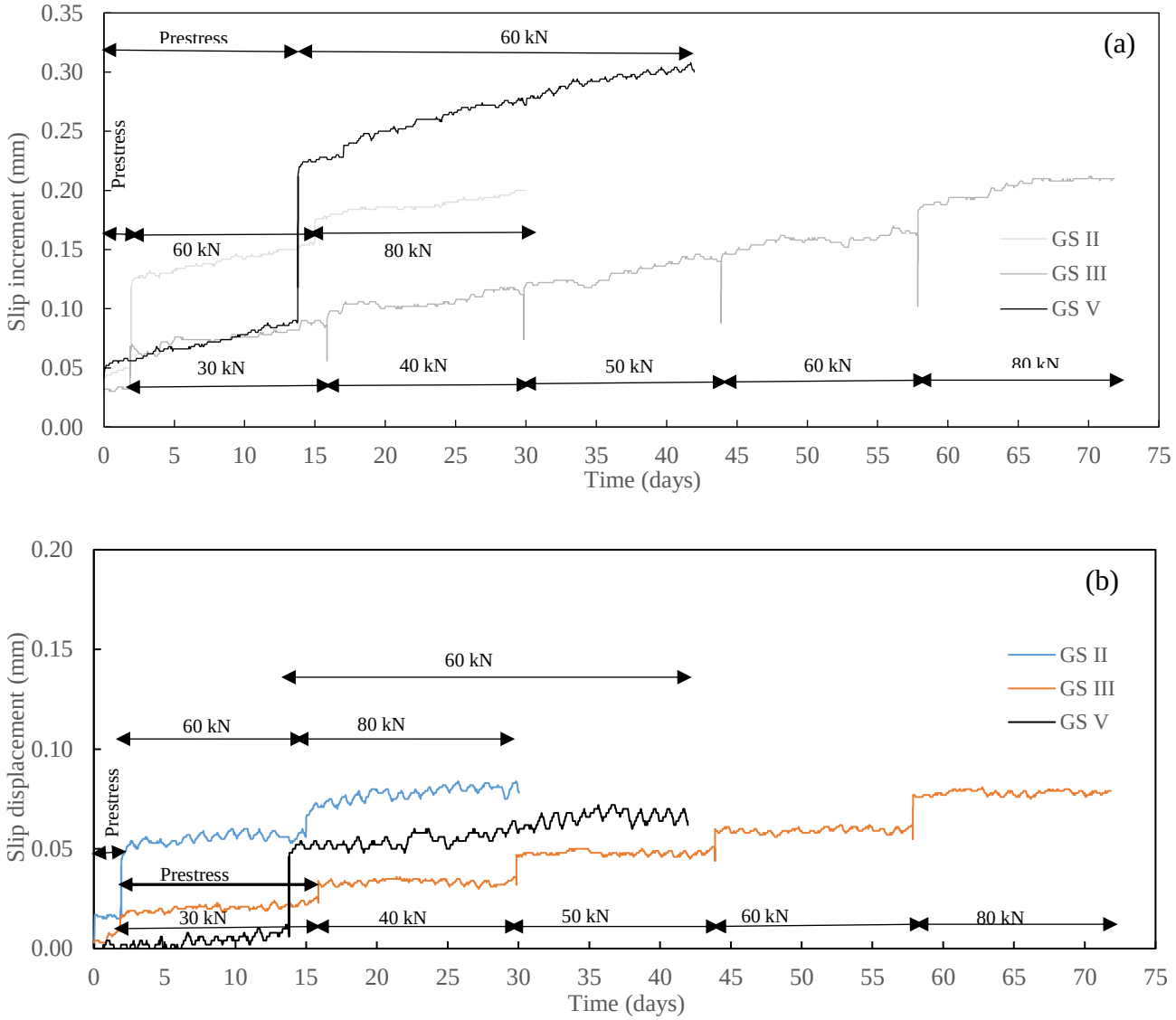

Figure 5. 11: Slip displacement over time in (a) and (b).

as shown in Figure 5.6 (a) and the behaviour obtained is presented in Figure 5.11 (b). Since, the junction part was mostly influenced in terms of deformation with the active influence of flexures; and this slip displacement was measured in the shear zone of the specimen, its values were significantly less even though the similar time dependent behaviour observed.

5.7.3 Strain behaviour with respect to loading and time

As shown in Figure 5.6 (a), strain gauges were placed on specimen surfaces to record concrete strain history under sustained loading. Figure 5.12 shows the strain behaviour at the upper row of the strain gauges. Under the same sustained loading, specimens GS II, GS III, and GS V exhibited larger amounts of strain than the static-loading specimen GS I. Comparing strains of the sustained-loading specimens showed that sustained loading had a distinct effect on the concrete strain increment. A few gauges in GS III exhibited inconsistent values because of inaccurate gauge placement and non-functionality. Specimen GS V exhibited a relatively high strain value, as it was

under prestress for a long duration, and its concrete strength was relatively low. It was assumed that the simple introduction of prestress would not induce compressive strain in the upper concrete surface, but compressive strains appeared in some positions because of inaccurate longitudinal positioning of the specimen during the load setup. The strain development behaviour inside the concrete was recorded with mold strain gauges placed inside the upper concrete slab, as shown in the upper row of Figure 5.6 (b). The results are presented in Figure 5.13 (a). Under 60 and 80 kN loads, GS III exhibited a slightly higher strain than GS II because of longer exposure time and previous sustained-loading history. GS V exhibited significantly higher strain than other specimens under the 60 kN load owing to long-term prestress and low compressive strength. A comparison of the strains of GS IV and GS V is presented in Figure 5.13 (b) to illustrate the environmental effects. A significant amount of strain was developed because of the environmental effects, compared with the creep strain caused by sustained loading.

Figure 5.15 shows strain changes observed in the steel girder section A-A of Figure 5.14 at the junction. A similar tendency as the one previously noted for the concrete strain phenomena was observed in the steel girder, confirming the impact of sustained loading over time.

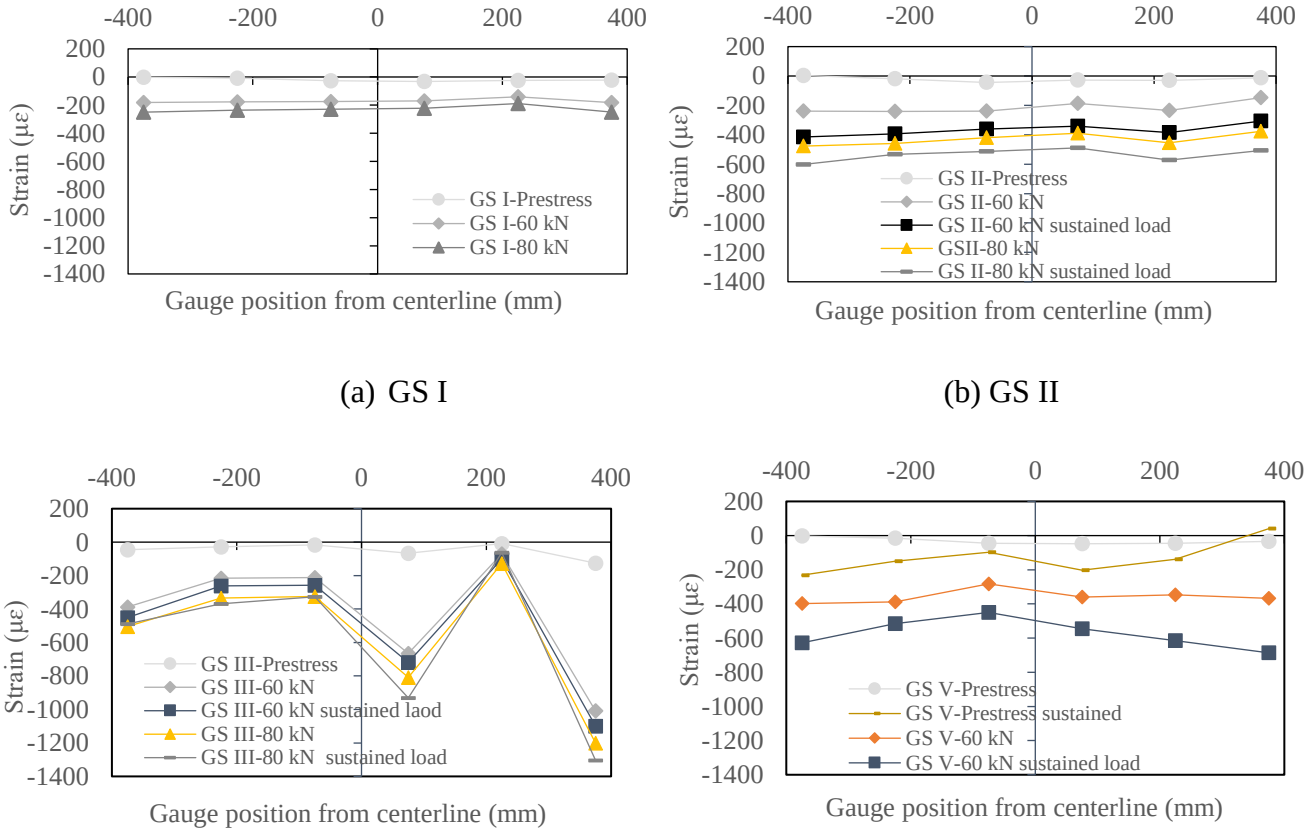

(a) GS I (b) GS II

(c) GS III (d) GS V

Figure 5. 12: Concrete surface strain under sustained loading; (a) GS I, (b) GS II, (c) GS III, (d) GS V.

Because of sustained loading, stud strain changes over time were recorded with strain gauges attached to the leftmost stud of the lower flange in GS V, as shown in Figure 5.6 (b). The results are presented in Figure 5.16. Two strain gauges, S1 and S2, were attached vertically to the left and right sides, respectively. The introduction of a prestress caused compression at the bottom part of the girder, but because the stud was very close to the anchor plate and prestress bar it bent slightly at the upper part towards the inner direction, exerting tensile strain on the side with S1 and compressive strain on the side with S2.

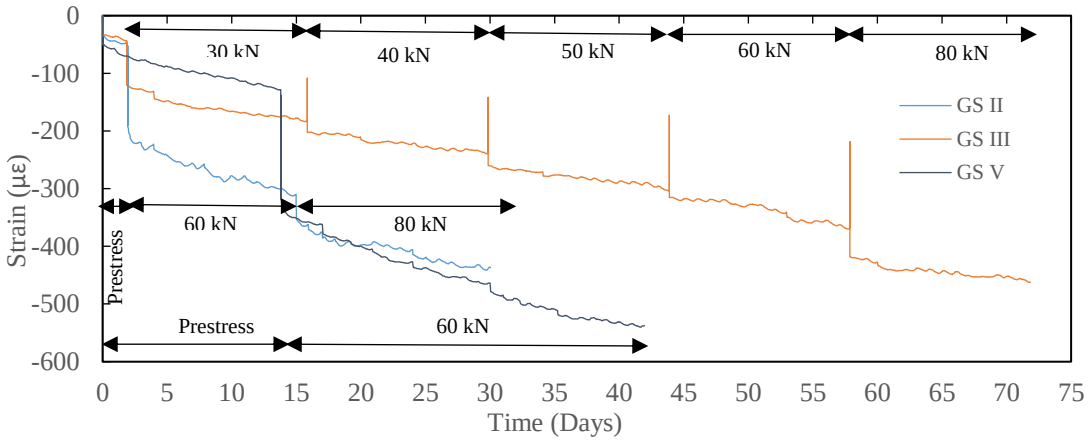

(a) Concrete strain inside specimens GS II, GS III, and GS V.

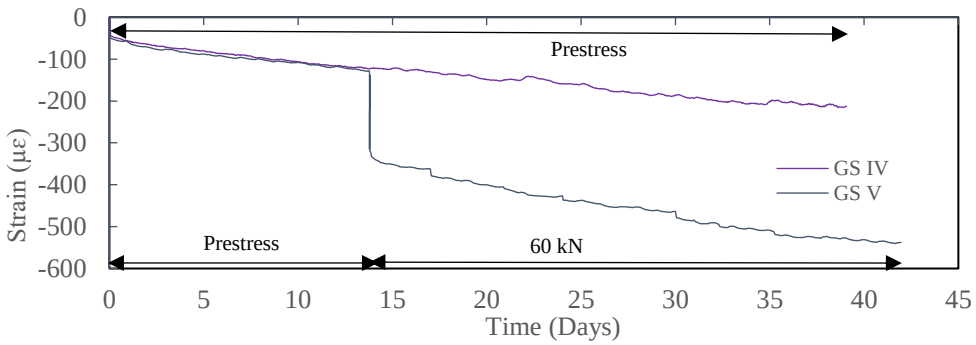

(b) Concrete strain inside specimens GS IV and GS V.

Figure 5. 13: Concrete strain inside specimens: (a) GS II, GS III, and GS V, (b) GS IV and GS V.

The same strain behaviour continued with a rise in strain values when the external load was applied over a long duration. This caused the lower flange to bend outside towards the tensile force, whereby the stud continued to bend in the same direction. The strain values exhibited the increment over time owing to the sustained-loading effect. This indicated how stress was transferred through the shear connections under a composite action. The strain values were different on the two sides owing to the influence of other studs at the flange and at the web close to that stud.

The change in strain was also recorded at the outermost bottom main rebar at the junction in GS IV and GS V to assess the effects of sustained-loading and environmental factors. The results are

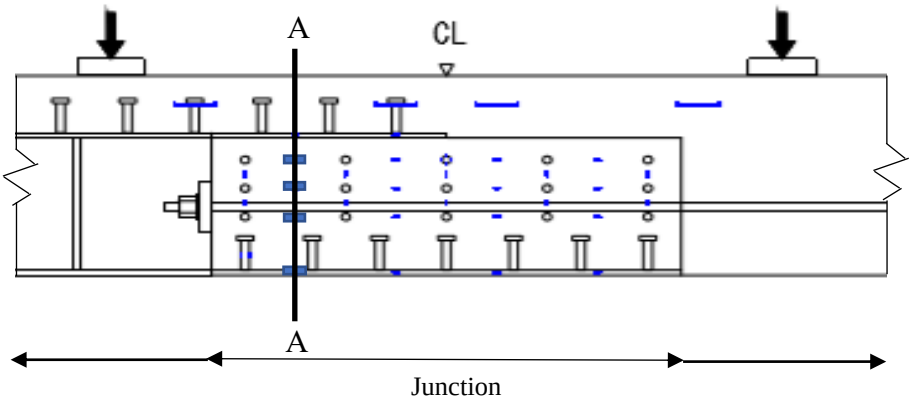

Figure 5. 14: Steel girder strain gauge position in section A-A.

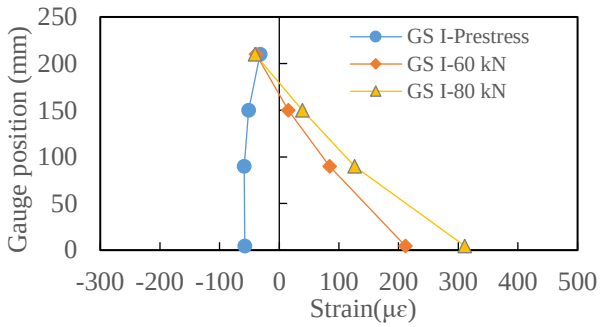

(a) GS I

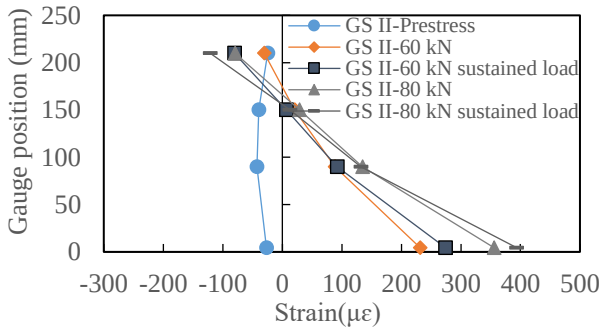

(b) GS II

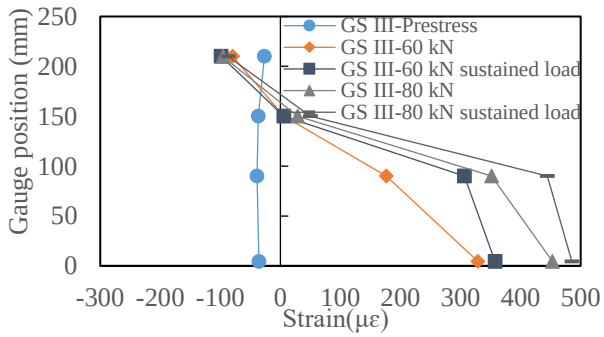

(c) GS III

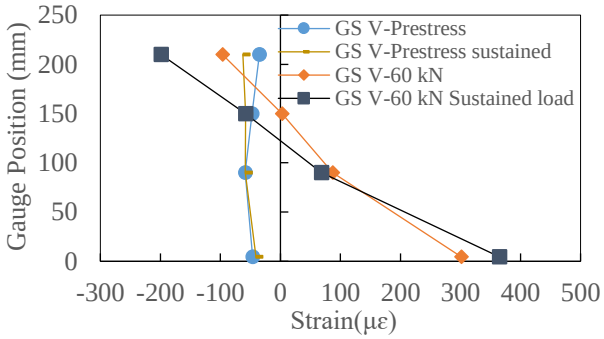

(d) GS V

Figure 5. 15: Steel girder strain inside the specimen in section A-A; (a) GS I, (b) GS II, (c) GS III, (d) GS V.

shown in Figure 5.17. Because of prestressing, the starting strain level and slope were very similar for GS IV and GS V. The design assumed that introducing a 60 kN load after prestressing would induce zero strain in the rebar, which was observed a few days later. This is because the prestress level was slightly higher than the design level, as shown in Figure 5.10. However, the strain reached zero and increased over time because of creep induced by sustained loading. These phenomena confirmed the intended stress transfer and composite actions through connections in the hybrid girders.

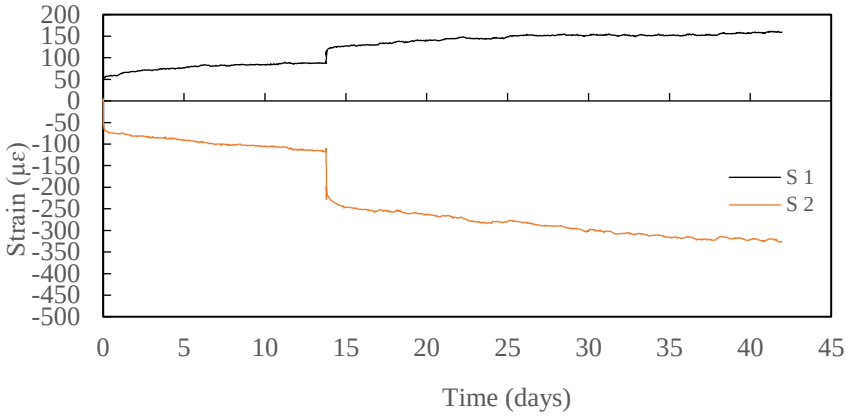

Figure 5. 16: Stud strain in GS V.

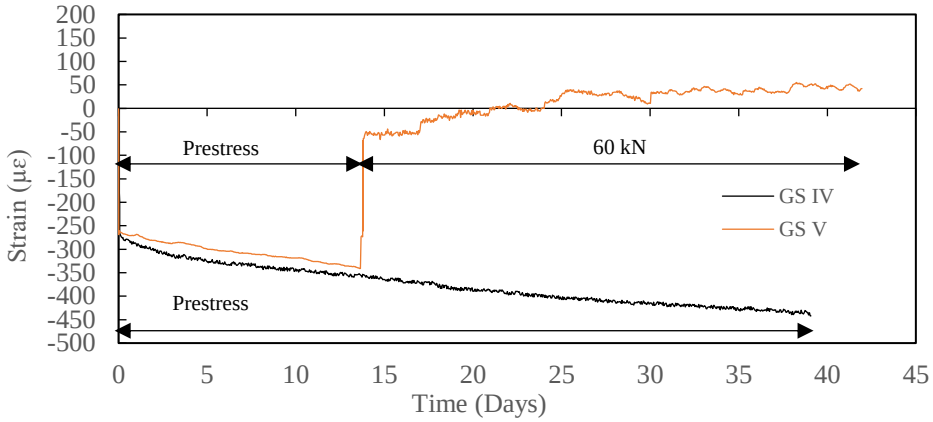

Figure 5. 17: Rebar strain in GS IV and GS V.

5.8 Load–deflection, crack, and failure patterns

Each specimen was loaded to failure using an experimental laboratory set-up, which is presented in Figure 5.7. According to the experimental results presented in Figure 5.18 and Table 5.6, the ultimate failure load of the hybrid girder specimens ranged from 190 kN for GS V to 204 kN for GS II. It was difficult to differentiate which factors influenced the failure load, but potential influencing factors include previous loading history, effective prestress force at final loading, and compressive strength of the concrete. The smallest deflection (9.87 mm) in the steel segment was observed for GS I, which was subjected to a static load, compared with GS II, GS III, and GS V, which were subjected to various durations of sustained loading. Behaviour under sustained loading for the hybrid girder significantly depended on connections behaviour in response to the applied load and the effective prestress force (defined as the instantaneous prestress force and expressed as a percentage of the transferred peak prestress force) on that time. Both prestress force and concrete compressive strength influenced the deflection behaviour in the PRC segment and junction. The PRC segment and junction exhibited the largest deflections (16.11 and 15.81 mm, respectively) for GS III. They exhibited deflections of 14.11 and 14.75 mm, respectively for GS V and 13.40 and 13.71 mm, respectively for GS II. Specimens GS III, GS V, and GS II were subjected to sustained loading for 70 days, 28 days (with an additional 14 days prestress), and 28 days, respectively, before

final static loading. Final loading was then applied with effective prestress forces of 0.88 Fp , 0.90 Fp, and 0.91 Fp, respectively. In the case of GS V, low compressive strength was also responsible for large deflection. In the case of sustained loading, creep and shrinkage deformation in the concrete–stud vicinity resulted in earlier appearance of cracks (discussed later in this section) than under circumstances, which also affected the deflection. In the PRC segment, GS I had a larger deflection than GS II and GS V because final loading was applied to GS I relatively early. Specimen GS IV exhibited a relatively large deflection because it was subjected to prestress force for a longer duration than the other specimens. As a result, several small cracks appeared after the load reached 100 kN at the PRC-side loading point, along with low effective prestress and low concrete compressive strength. However, the consistency and coherent behaviour of the load–deflection curves for the three segments indicated successful intended load transfer through the headed stud shear connections in the junction or embedded zone.

Table 5. 6: Deflection of specimens at ultimate failure load, crack, and failure pattern.

Specimen	Effective prestress force at time of final loading (kN) [F_p = Peak prestress force]	Measured load (kN)		Deflection at ultimate failure load (mm)			Failure pattern
-	-	Flexural crack	Failure	Steel segment	PRC segment	Junction	-
GS I	0.93 F_p	100	194	9.87	14.32	13.84	Flexural failure near PRC side loading point
GS II	0.91 F_p	80	204	10.17	13.40	13.71	Flexural failure near PRC side loading point
GS III	0.88 F_p	60	196	11.41	16.11	15.81	Flexural failure near PRC side loading point
GS IV	0.88 F_p	80	192	11.28	14.74	15.23	Flexural failure near PRC side loading point
GS V	0.90 F_p	80	190	11.10	14.11	14.75	Flexural failure near PRC side loading point

Table 5. 7: Influence of sustained loading on girder deflection.

Specimen	Loading phases	Deflection (mm)			Remarks
		Steel segment	Junction	PRC	
GS I	Prestress (phase 1)	-0.130	-0.250	-0.260	Static loading case
	60kN load (phase 2)	1.170	1.140	0.95	
GS II	Prestress (phase 1)	-0.17	-0.280	-0.260	Sustained loading case (14 days)
	60kN load (phase 2)	1.64	1.69	1.28	
Change in deflection		(+40.17%)	(+48.24%)	(+34.73%)	

To determine, how the sustained loading can influence the deflection behavior of the whole girder; the deflection values of the two pahses, i.e, prestressing and loading (both static and sustained) phases are presented in Table 5.7. It is clearly evidenced that sustained loading only for 14 days could lead to an increase of deflection upto 48% at junction part than the static case and other parts were also influenced with a remarkable level of deflection increment. The crack and failure patterns presented in Figure 5.19 and Table 5.6 indicate that the flexural cracking load for sustained loading varied between 60 and 80 kN. For the static-loading specimen GS I, crack appearance was first confirmed at 100 kN. The cracks gradually expanded until the load reached 140 kN and expanded

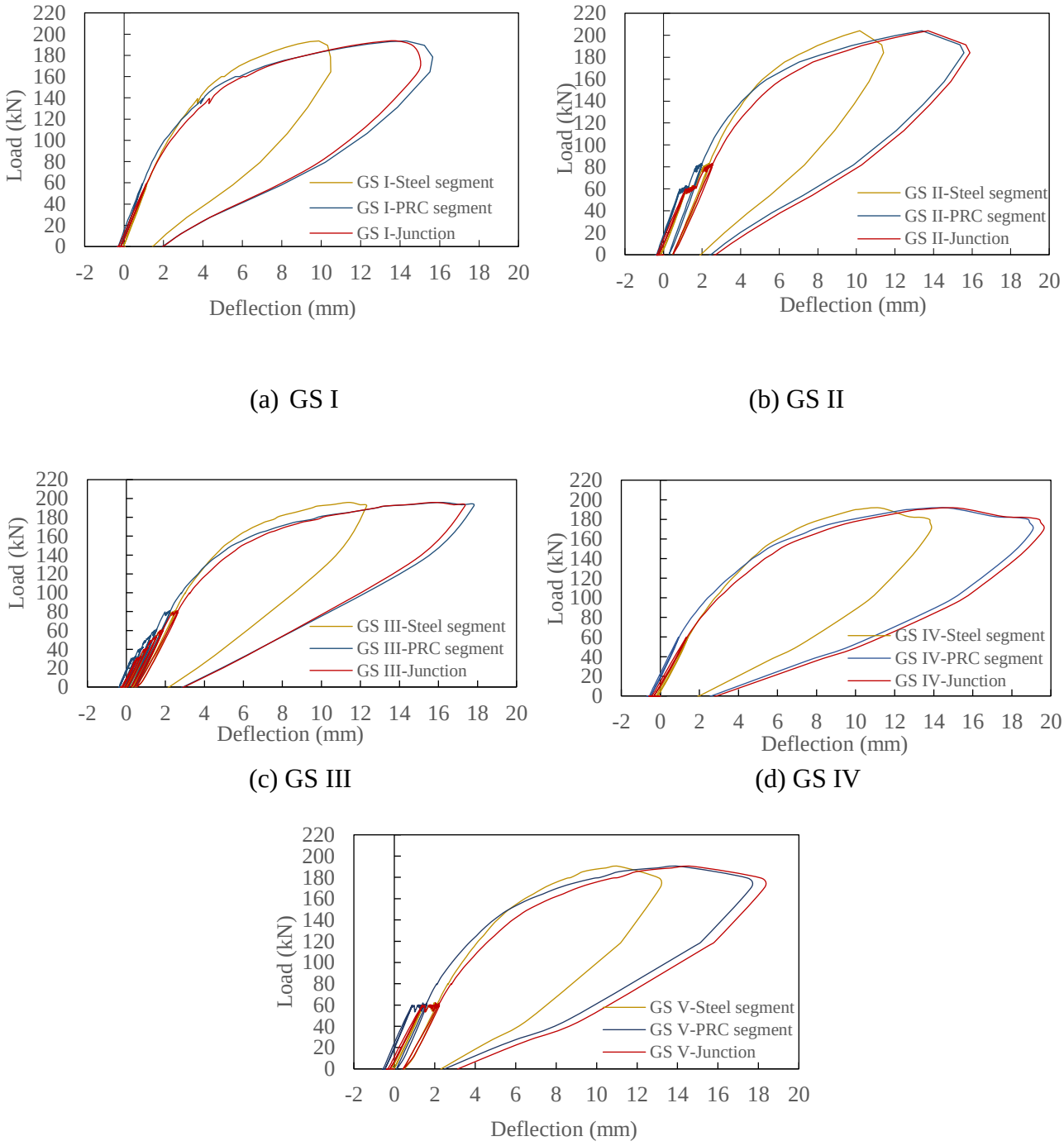

Figure 5. 18: Load-deflection curves; (a) GS I, (b) GS II, (c) GS III, (d) GS IV, (e) GS V.

rapidly beyond 160 kN. The cracks began at the lower edge of the loading point on the PRC side, and bending failure was observed on the same side at 194 kN. Although cracks appeared around the boundary between the PRC and the junction, no cracks were observed at the boundary between the steel girder and the junction. The sustained-loading specimen GS II exhibited the first crack at 60 kN, after only 2 days of loading. The cracks started in the horizontal direction, indicating the influence of shrinkage. The tensile and compressive stresses acted on the concrete near the stud

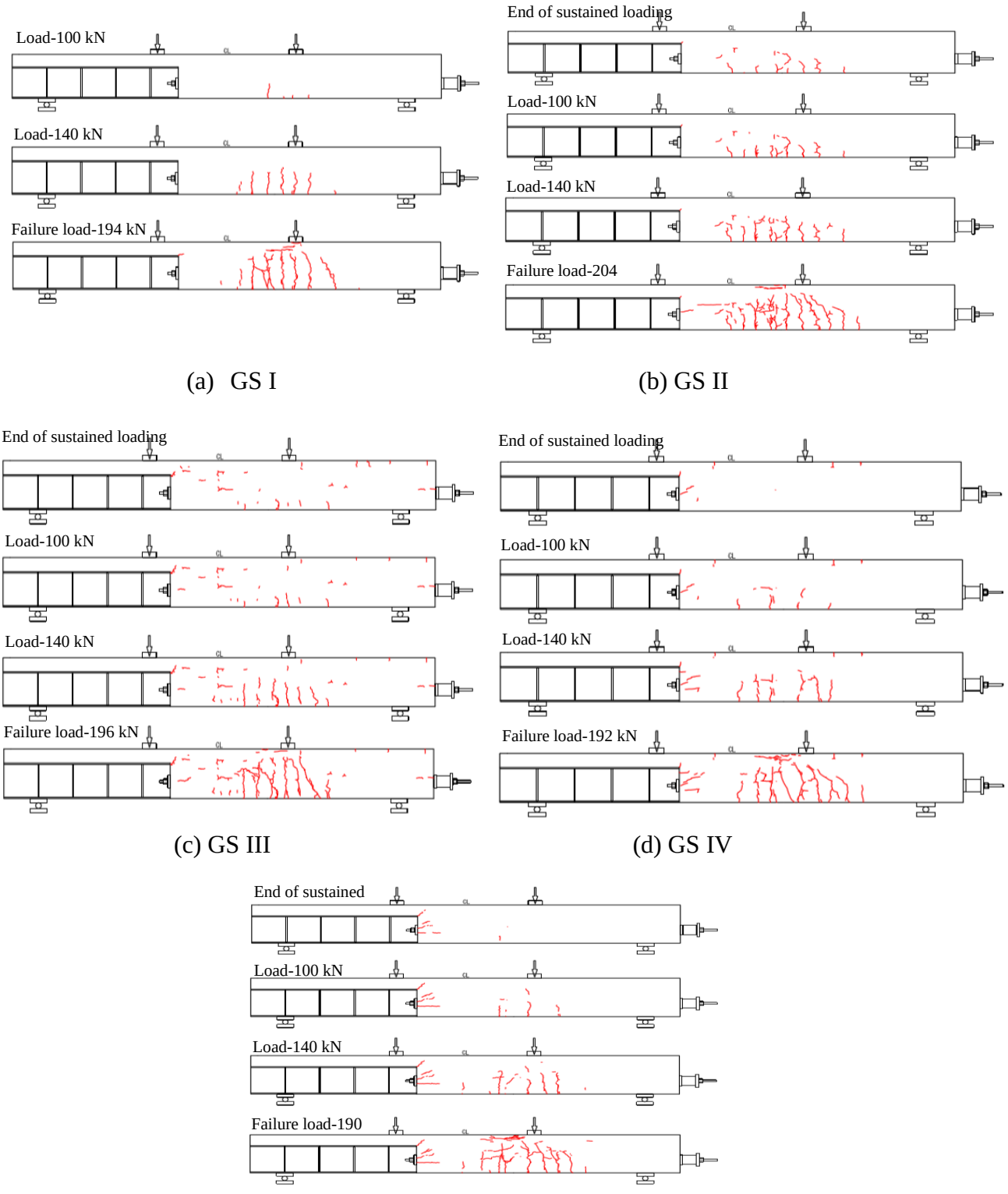

Figure 5. 19: Crack and failure pattern: (a) GS I, (b) GS II, (c) GS III, (d) GS IV, (e) GS V.

because of prestress. Further, the sustained load was accompanied by a constraining force from the neighbouring studs or rebar because of shrinkage, which resulted horizontal cracking. Bending cracks occurred from the lower edge when the load was increased to 80kN, which is reasonable

with respect to the design considerations. After sustained loading, the load was removed once before the final load was applied. Thus, the horizontal cracks expanded further because of the contraction and bending failure eventually occurred on the PRC side at 204 kN. In the case of GS III, cracks from the lower edge were not confirmed until the sustained load reached 60 kN, probably because the internal rebar and stud restrained the contracted concrete. The number of cracks was greater than in other specimens; this specimen was aged for 46 days and was affected by shrinkage as well as intermediate stage sustained loadings. The number of cracks increased at 80 kN and flexural failure occurred on the PRC side at 196 kN. Specimen GS IV exhibited cracks on the upper edge with sustained prestress. Subsequently, bending cracks on the lower edge were confirmed with static loading of 80 kN and extended by 300 mm from the lower edge until the load reached 192 kN. Then, flexural failure occurred on the PRC side. Several small cracks appeared beyond 100 kN on the back side under the PRC-side loading point. The PRC girder had a low rigidity compared with the steel girder and owing to the application of the axial force (prestress) for a long duration, the junction was thus significantly influenced, and several cracks were generated. In the case of GS V, when the static loading reached 80 kN, bending cracks were confirmed at the lower edge and they propagated upward by 300 mm until the load reached 190 kN. Then, flexural failure was observed on the PRC side. Figure 5.20 provides photographs of all specimens at failure loads. All the specimens failed on the PRC side, which is in accordance with the specimen design objective.

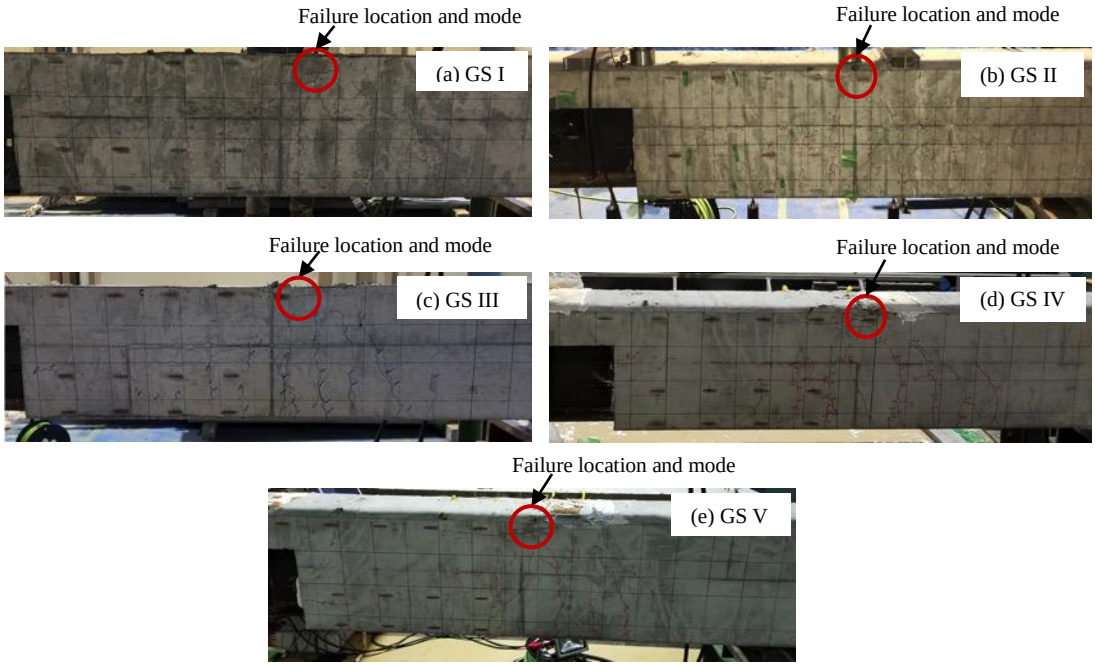

Figure 5. 20: Photographs of specimens at failure loads: (a) GS I, (b) GS II, (c) GS III, (d) GS IV, (e) GS V.

5.9 Long-term stud shear forces at junction: an FE evaluation

The time dependent deformation behaviour of the hybrid girder specimens (GS I to V; as presented in preceeding section) distinctively indicated that interms of deformation, the junction part has been influnced mostly under sustained loading [(Haque MN, 2019)]. Since, the time dependent deformation is obivous for headed stud connections used for that girders, that definitely would have influence on shear force behaviour of connections; therefore, a clear understanding of this behaviour can lead to design those structures more rationaly for practical applications. To elucidate the long-term shear behavior of studs inside the junction, it is necessary to clarify the magnitude and direction of the shear force acting on the studs. As there is no rational method is available to directly measure the time dependent shear force of connections, an approximate evaluation through a finite element (FE) approach is applied for the girder specimens and presented in this section.

5.9.1 Conceptual forces on junction of hybrid girder

As per the conceptual design idea of the junction part [(Shinozaki H, 2014)], it is assumed that the headed studs installed on the upper and lower flanges of the steel girders together with flanges combinedly resist the shearing force caused by bending and axial force, and the headed studs those placed on the girder web resist the shearing force due to the applied load and applied prestress. As the shear force is assumed to be borne by half by the headed studs placed on the upper and lower flanges and half by the flanges, these studs will not experience much level of shear forces. Therefore; the headed studs placed on web part are likely to experience higher level of shear forces; so an investigation is needed to evaluate their time-dependent shear behavior. Figure 5.21 shows the relationship between the sectional force and external force (prestress) acting on the junction part and the shear force acting on the headed studs. In addition, for the rotation of the steel girder, as shown in Figure 5.21 (b), for the bending moment M and the shear force generated in the studs P_n, the following equation is assumed to be established.

$$M = \sum_{i=1}^{n} P_n \cdot x \qquad (5.1)$$

$$P_n \leq V_n \times N \quad (5.2)$$

where, V_n is the shear strength of each stud, P_n is the shear force fixed in the vertical direction in each row of studs, the number of positions is determined by the shear force acting on the column which is the most distant from the center of rotation and x represents that distance.

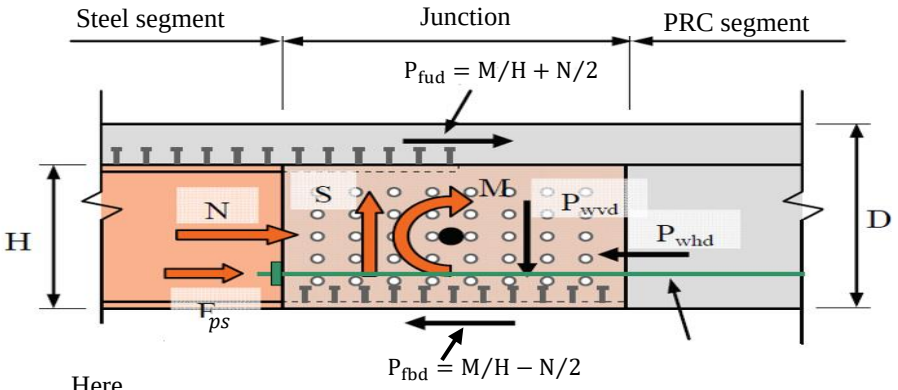

Here, M : Moment, S : Shear force, N : Axial force

F_{ps} : Prestress force

P_{fud} : Shear force acting for displacement on upper flange

P_{fld} : Shear force acting for displacement on lower flange

P_{whd} : Horizontal shear force acting on web

P_{wvd} : Vertical shear force acting on web

(a) X-sectional forces on junction

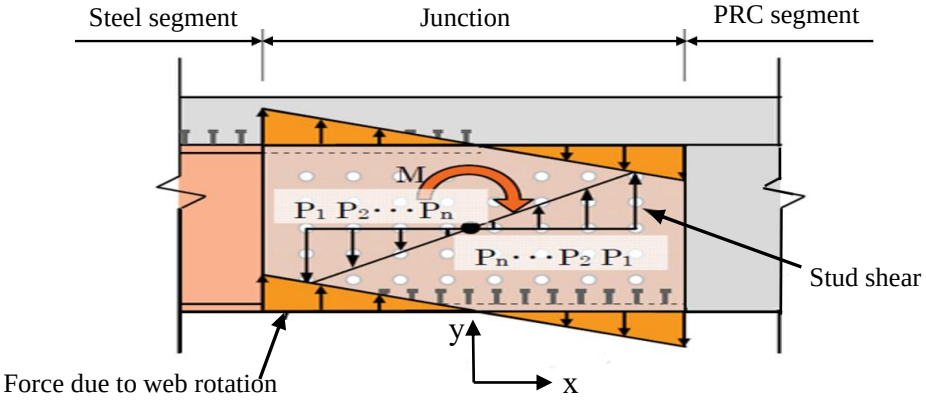

Here, P_1, P_2, ….P_n: Shear forces due to bending moment acting on each stud row on web at a distance x_1, x_2, ... x_n from center of rotation

(b) Conceptaul forces acting on studs.

Figure 5. 21: Conceptual diagram on X-sectional and shear forces on headed studs

5.9.2 Calculation of shear forces on stud connections: FE approach

During the experimental measurement, strain gauges were installed in between the studs in web part of the junction as shown in Figure 5.22. The positions of the studs and strain gauges in web of that junction are shown in Figure 5.23 (a) and a closed-up view of that is further illustrated in Figure 5.23 (b). Based on the experimentally measured data, to evaluate the time dependent shear behavior of headed stud connections at the girder web of the junction part, a finite element (FE) approach as mentioned in earlier research [(JIME, 2014), (Ueda N, 2014)] was used. Each stud position marked alphabetically was considered as a nodal point and 4 nodal studs constituted an element from 1 to 8 as shown. The nodal stud A was placed in origin assuming the influence of local deformation and

crack as small as comparing to others. For FE calculations, force and displacement arrangement followed as, u_{ij} = x directional axial displacement; v_{ij} = y directional axial displacement; f_{xij} = x directional axial shear force; f_{yij} = y directional axial shear force. The arrangement of force and displacement vectors at nodal points of element 1 is illustrated in Figure 5.24. For calculation of

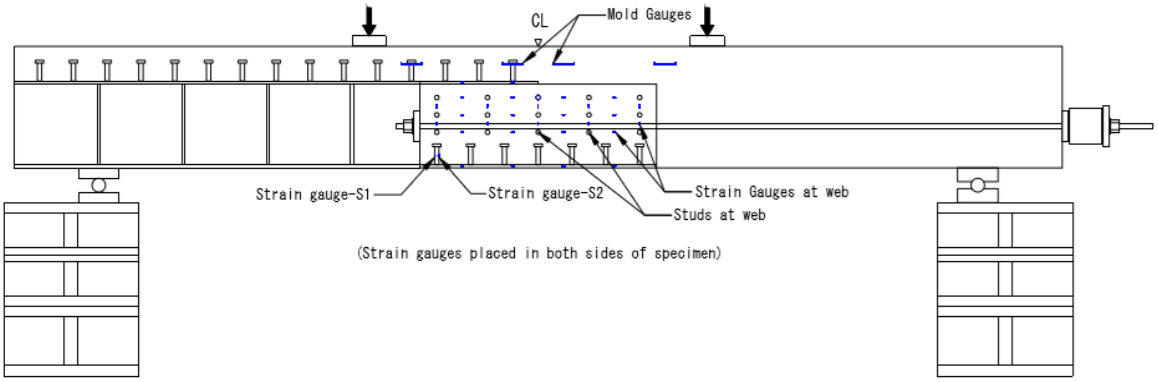

Figure 5. 22: Sensor layout at the girder web at the junction

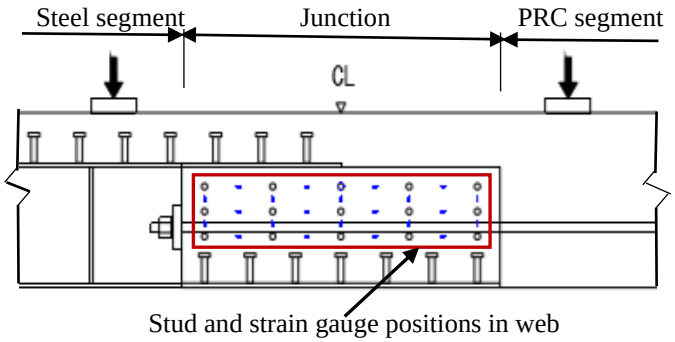

(a) Stud and strain gauges positions in web

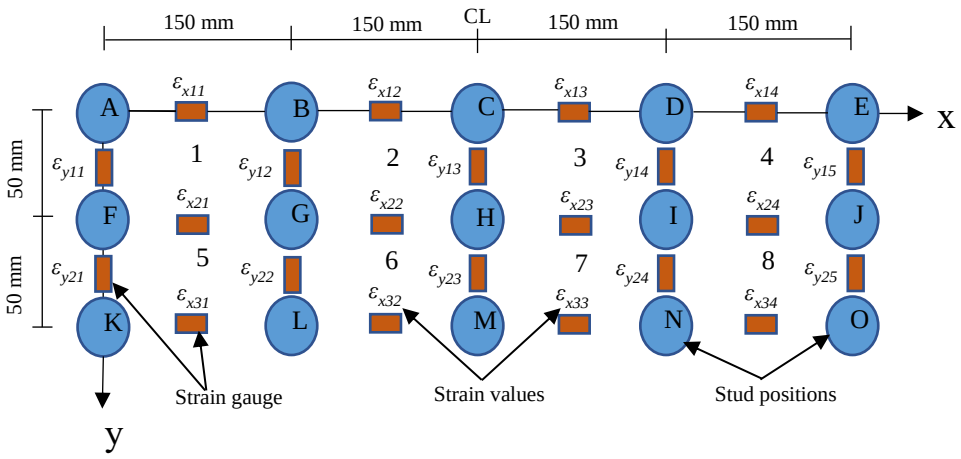

(b) Detailing of element and nodal studs

Figure 5. 23: Junction details in (a) and (b)

the time dependent shear force acting on each stud due to sustained loading, equation (5.3) was considered as element stiffness equation.

$$[k]^e\{u\}^e = \{f\}^e \qquad (5.3)$$

where, $[k]^e$ = stiffness matrix; $\{u\}^e = d$ isplacement vector; $\{f\}^e$ = force vector. For the calculation of force vector $\{f\}^e$ at the node as shown in Figure 5.24, the stiffness matrix $[k]^e$ and the displacement vector $\{u\}^e$ were needed to be determined. The displacement vector $\{u\}^e$, the relative nodal displacement was calculated by multiplying the strain obtained experimentally from the strain gauge placed between two nodes by the length between them, assuming the uniform strain distribution between the two adjacent nodes. Stiffness matrix $[k]^e$ was determined as per equation (5.4).

$$[k]^e = \int_{-1}^{1}\int_{-1}^{1}[B]^T[D][B]|J|dsdt \qquad (5.4)$$

where, $[B]$ and $[D]$ were matrixes and $|J|$ was the Jecobian matrix. For calculation of the matrixes, the following equation (5.5) governing the Hook's is considered.

$$\sigma = E\varepsilon\,,\ \ \tau = G\gamma \qquad (5.5)$$

where, σ = vertical stress, E = Young's modulus, ε = vertical strain, τ: shear stress, G = lateral elasticity coefficient and γ = shear strain. Since the plate thickness was small relative to the x and

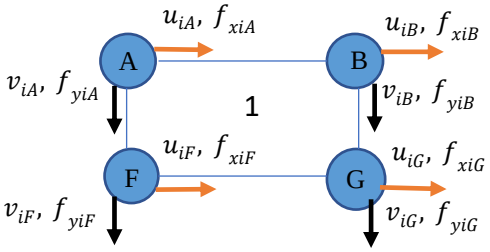

Figure 5. 24: Forces and displacement vectors at nodal points of element 1

y axis, the plane stress formulae were adopted. If the stress vector is defined as $\{\sigma\}$ and the strain vector as $\{\varepsilon\}$ then, the following expression was considered as shown in equation (5.6). Therefore, the $[D]$ matrix, a symmetric matrix that relates the stress vector and strain vector and expressed as shown in equation (5.7).

$$\{\sigma\} = [D]\{\varepsilon\} \qquad (5.6)$$

$$[D] = \frac{E}{1-\nu^2}\begin{bmatrix} 1 & \nu & 0 \\ \nu & 1 & 0 \\ 0 & 0 & \frac{1-\nu}{2} \end{bmatrix} \qquad (5.7)$$

Regarding matrix $[B]$, relational expression of strain and displacement (u, v) in plane stress is expressed in equation (5.8) and accordingly $[B]$, is expressed in (5.9). Here, Ni known as shape function which was defined with a local coordinate system (s, t) of -1 to +1 for an element other than a triangle, that represented the displacement and coordinate of an arbitrary point in the element. Concept of a shape function is illustrated in Figure 5.25 and a 4-node quadrilateral element was used in this study as expressed in equation (5.10). The partial differential of (5.10) with respect to (s, t) led to an expression as shown in equation (5.11).

$$\{\varepsilon\} = \begin{Bmatrix} \varepsilon_x \\ \varepsilon_y \\ \gamma_{xy} \end{Bmatrix} = \begin{bmatrix} \frac{\partial N_i}{\partial x} & 0 \\ 0 & \frac{\partial N_i}{\partial y} \\ \frac{\partial N_i}{\partial y} & \frac{\partial N_i}{\partial x} \end{bmatrix} \begin{Bmatrix} u_1 \\ u_2 \\ u_3 \\ u_4 \\ v_1 \\ v_2 \\ v_3 \\ v_4 \end{Bmatrix} = [B] \begin{Bmatrix} u_i \\ v_i \end{Bmatrix} \tag{5.8}$$

$$[B] = \begin{bmatrix} \frac{\partial N_i}{\partial x} & 0 \\ 0 & \frac{\partial N_i}{\partial y} \\ \frac{\partial N_i}{\partial y} & \frac{\partial N_i}{\partial x} \end{bmatrix} = \begin{bmatrix} \frac{\partial N_1}{\partial x} & \frac{\partial N_2}{\partial x} & \frac{\partial N_3}{\partial x} & \frac{\partial N_4}{\partial x} & & 0 & & \\ & 0 & & & \frac{\partial N_1}{\partial y} & \frac{\partial N_2}{\partial y} & \frac{\partial N_3}{\partial y} & \frac{\partial N_4}{\partial y} \\ \frac{\partial N_1}{\partial y} & \frac{\partial N_2}{\partial y} & \frac{\partial N_3}{\partial y} & \frac{\partial N_4}{\partial y} & \frac{\partial N_1}{\partial x} & \frac{\partial N_2}{\partial x} & \frac{\partial N_3}{\partial x} & \frac{\partial N_4}{\partial x} \end{bmatrix} \tag{5.9}$$

$$\begin{cases} N_1(s,t) = \frac{1}{4}(1-s)(1-t) \\ N_2(s,t) = \frac{1}{4}(1+s)(1-t) \\ N_3(s,t) = \frac{1}{4}(1+s)(1+t) \\ N_4(s,t) = \frac{1}{4}(1-s)(1+t) \end{cases} \tag{5.10}$$

$$\begin{cases} \frac{\partial N_1}{\partial s} = -\frac{1}{4}(1-t), \ \frac{\partial N_2}{\partial s} = \frac{1}{4}(1-t) \\ \frac{\partial N_3}{\partial s} = \frac{1}{4}(1+t), \ \frac{\partial N_4}{\partial s} = -\frac{1}{4}(1+t) \\ \frac{\partial N_1}{\partial t} = -\frac{1}{4}(1-s), \ \frac{\partial N_2}{\partial t} = -\frac{1}{4}(1+s) \\ \frac{\partial N_3}{\partial t} = \frac{1}{4}(1+s), \ \frac{\partial N_4}{\partial t} = \frac{1}{4}(1-s) \end{cases} \tag{5.11}$$

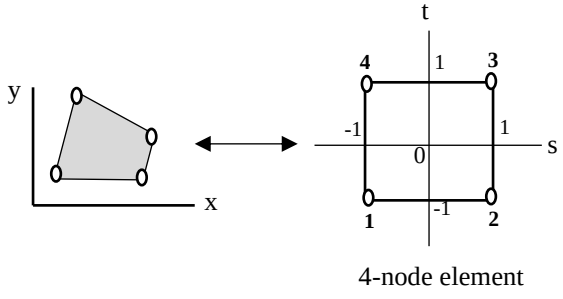

Figure 5. 25: Shape function

The matrix $[B]$ in equation (7.9) contained $\partial Ni/\partial x$ and $\partial Ni/\partial y$ of (x, y) coordinate system, whereas the shape function contained Ni in (s, t) coordinate system which cannot be partially differentiated with respect to (x, y). Therefore, a Jacobian [J] matrix was introduced as shown in (5.12) where, $x_1 \sim x_4$ and $y_1 \sim y_4$ are the nodal coordinate of an element. The relationship between $\partial Ni/\partial x$, $\partial Ni/\partial y$ and $\partial Ni/\partial s$, $\partial Ni/\partial t$ is expressed in equation (5.12). Using equations (5.12) and (5.13) and assigning the expressions in (5.9), the matrix $[B]$ was obtained.

$$[J] = \begin{bmatrix} \frac{\partial x}{\partial s} & \frac{\partial y}{\partial s} \\ \frac{\partial x}{\partial t} & \frac{\partial y}{\partial t} \end{bmatrix} = \begin{bmatrix} \frac{\partial N_1}{\partial s} & \frac{\partial N_2}{\partial s} & \frac{\partial N_3}{\partial s} & \frac{\partial N_4}{\partial s} \\ \frac{\partial N_1}{\partial t} & \frac{\partial N_2}{\partial t} & \frac{\partial N_3}{\partial t} & \frac{\partial N_4}{\partial t} \end{bmatrix} \begin{bmatrix} x_1 & y_1 \\ x_2 & y_2 \\ x_3 & y_3 \\ x_4 & y_4 \end{bmatrix} \quad (5.12)$$

$$\begin{Bmatrix} \frac{\partial N_i}{\partial x} \\ \frac{\partial N_i}{\partial y} \end{Bmatrix} = [J] \begin{Bmatrix} \frac{\partial N_i}{\partial s} \\ \frac{\partial N_i}{\partial t} \end{Bmatrix} = \frac{1}{|J|} \begin{bmatrix} \frac{\partial y}{\partial t} & -\frac{\partial y}{\partial s} \\ -\frac{\partial x}{\partial t} & \frac{\partial x}{\partial s} \end{bmatrix} \begin{Bmatrix} \frac{\partial N_i}{\partial s} \\ \frac{\partial N_i}{\partial t} \end{Bmatrix} \quad (5.13)$$

In order to obtain the rigidity matrix of equation (5.4), the Gaussian integration was introduced to calculate the integral value in the coordinates called Gauss points with the integral ranged from –1 to +1. Since, two-point integration and three-point integration are widely used in the FE calculation, here three-point integration was used as illustrated in equation (5.14) with values of $c_1 = 5/9$, $c_2 = 8/9$, $c_3 = 5/9$, $s_1 = -\sqrt{3/5}$, $s_2 = 0$ and $s_3 = \sqrt{3/5}$.

$$\int_{-1}^{1} f(s)ds \approx c_1 f(s_1) + c_2 f(s_2) + c_3 f(s_3) \quad (5.14)$$

As per the previous Gaussian integral, assuming $f(s, t) = [B]^T[D][B]|J|$, the following expression was achieved as shown in equation (5.15) where, subscripts i, j refer to the value calculated at each Gaussian point.

$$[k]^e = \sum_{i=1}^{3} \sum_{j=1}^{3} c_i c_j [B]_{ij}^T [D][B]_{ij} |J|_{ij} \quad (5.15)$$

Each element in this analysis consisted of 150 mm arm length in horizontal direction and 50 mm in vertical direction with same material, hence same stiffness matrix was obtained for element 1 to 8. By substituting the value of element stiffness matrix in equation (5.3), the forces acted on studs (nodes) of each element were obtained. Therefore,

$$[8 \times 8]^e \begin{Bmatrix} u_{iA} \\ u_{iB} \\ u_{iG} \\ u_{iF} \\ v_{iA} \\ v_{iB} \\ v_{iG} \\ v_{iF} \end{Bmatrix} = \begin{Bmatrix} fx_{iA} \\ f_{xiB} \\ f_{xiG} \\ f_{xiF} \\ f_{yiA} \\ f_{yiB} \\ f_{yiG} \\ f_{yiF} \end{Bmatrix}$$

As, equation (5.3) applicable for stiffness matrix for each element, the overall stiffness matrix for 15 nodal studs was required to determine the shear force acted on each stud. Overall stiffness matrix $[K]$ (the number of nodes x degrees of freedom) of 15 studs with two degrees of freedom led to a 30 x 30 stiffness matrix as shown herein.

$$[30 \times 30] \begin{Bmatrix} u_A \\ u_B \\ \vdots \\ u_N \\ u_o \\ v_A \\ v_B \\ \vdots \\ v_N \\ v_o \end{Bmatrix} = \begin{Bmatrix} f_{xA} \\ f_{xB} \\ \vdots \\ f_{xN} \\ f_{xo} \\ f_{yA} \\ f_{yB} \\ \vdots \\ f_{yN} \\ f_{yo} \end{Bmatrix}$$

Hence, the shear force (f_x and f_y) at each stud (nodal point) was obtained using stiffness matrix and nodal displacement values as calculated by the method already mentioned above.

5.10 Evaluated long-term stud shear forces at junction under sustained loading

The girder specimens were subjected to different loading histories as presented in Table 5.4 Based on the experimental data, an FE calculation, as already mentioned in the preceding section was conducted and results thus obtained on time dependent shear behavior of connections are presented for discussions. The shear force behaviour for headed studs in web part of the junction for static loading specimen is presented in Figure 5.26. This figure demonstrated the evaluated shear forces for different studs due to the introduction of prestress force and decompressive design loads of 60 kN and 80 kN for the control specimen GS I. The three other girder specimens GS II, GS III and GS V were subjected to sustained loading of different durations and the headed stud shear forces under those loading conditions are shown in Figures 5.27-5.29. For GS III, sustained loading of 30 kN, 40 kN, and 50 kN were below the design load that did not produce whole composite action through connections, hence shear behavior only under sustained design load (60 kN and 80 kN) discussed here. For sustained loading specimens, it was observed that due to the introduction of prestress force, three stud layers (upper, middle and lower) were mostly under compressive shear force which was the likely case as they were below the neutral axis. Few studs showed tensile shear force because of flange position that covered half of the web area as well as that the positions of neighboring studs or reinforcement that influenced the stud concrete interaction resulted with such shear force direction. Just after introduction of 60 kN load, due to flexure induced tensile stress below the neutral axis, the instantaneous shear force increased in magnitude in both directions and

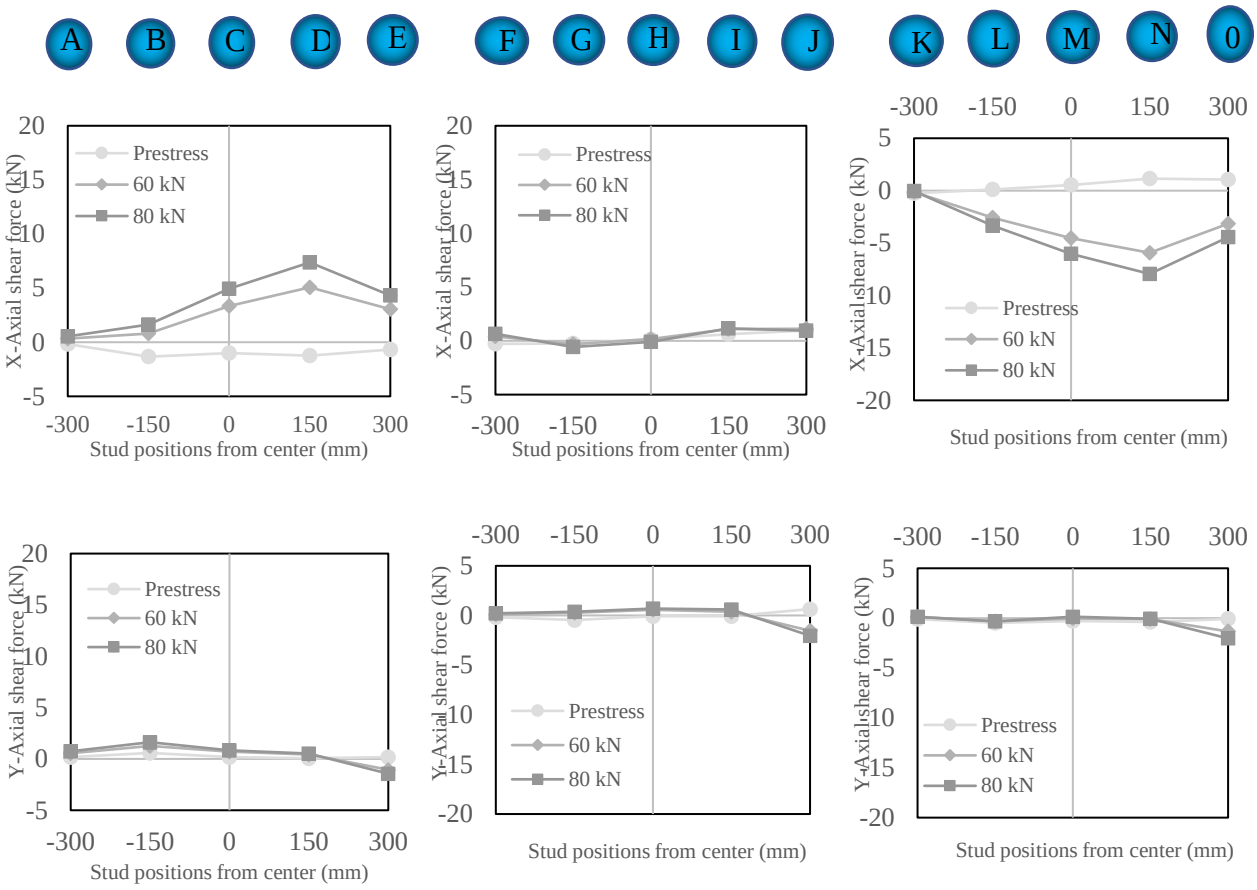

Figure 5. 26: Headed stud shear forces under static loading for GS I

when the same load sustained for 14 days, then shear force showed further increment in magnitude with a sign of sustained loading effects. The upper and lower layer of studs mostly experienced the tensile shear force whereas the lower layer experienced the compressive shear force. As the lower layer was very close to both prestressing bar and studs at lower flange, due to which this layer faced restraining force from them resulting in compressive shear force. When the load level reached to 80 kN, the instantaneous shear force increased in magnitude in both directions, comparatively with small incremental value that happened in 60 kN load. Some shear force values were almost closer to that of 60 kN load, the reason of that may be the existence of flanges in upper and lower part which could carry the instantaneous bending effects as bearing force. But when the 80 kN load sustained for 14 days, shear force magnitude showed mostly incremental behavior with a clear effect of sustained loading. Few studs in different layers did not show consistent shear variations due to the reason of nearby studs, position of prestress bar, anchor plate and reinforcing bar which have influenced the behavior. Comparing the specimen GS II and GS III, under the same sustained loading, shear forces differed slightly to each other with a very possible reason of earlier loading history, as G III was subjected to prestress force for 2 days, then 3 steps intermediate sustained loading (30 kN, 40 kN and 50 kN) for 42 days before 60 kN load level and specimen G-II was not subjected to such prior loading. That earlier loading history also have influenced the shear force

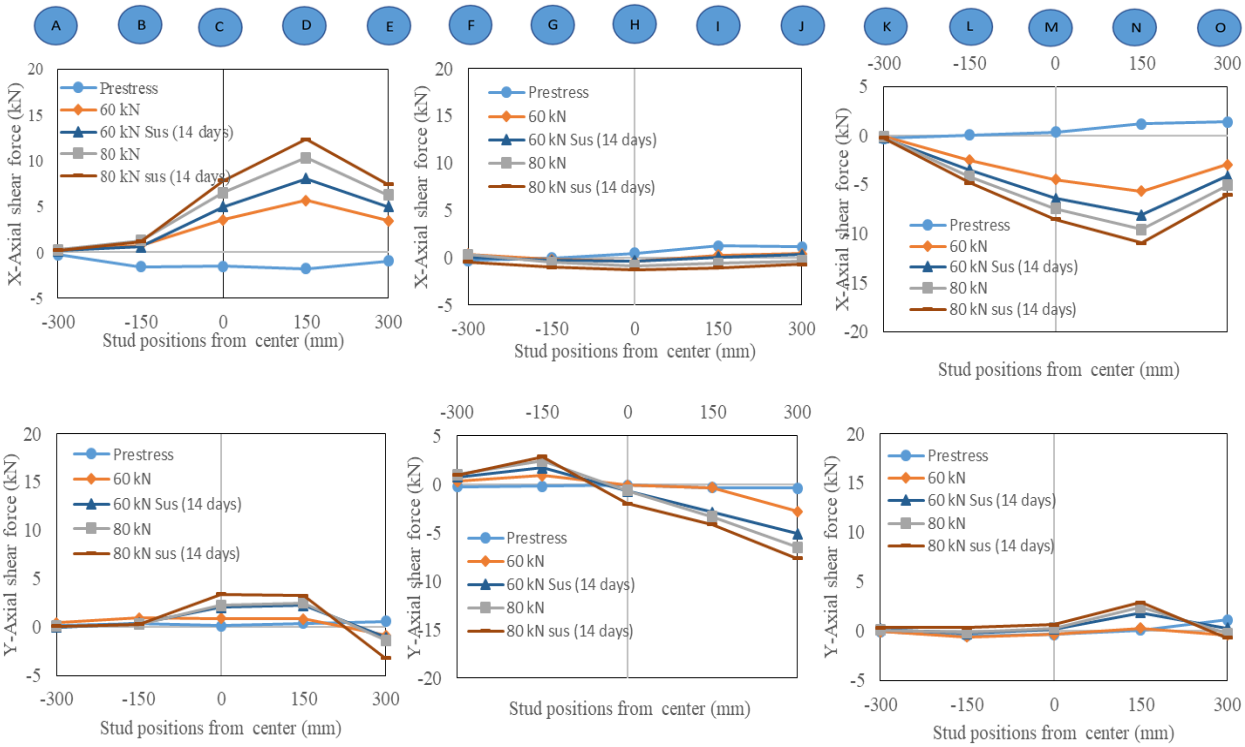

Figure 5. 27: Headed stud shear forces under sustained loading for GS II

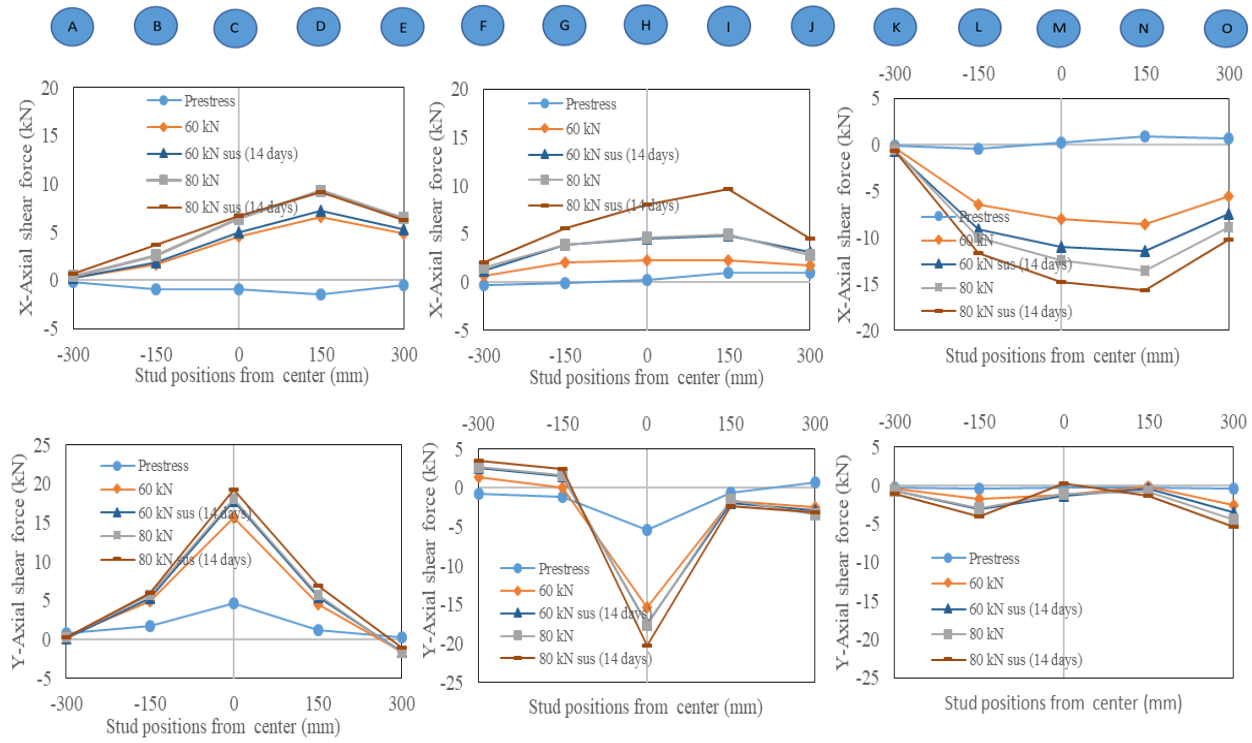

Figure 5. 28: Headed stud shear forces under sustained loading for GS III

at 80 kN load. To determine whether the stud shear forces changes with more exposure time, specimen GS V was maintained under prestress for 14 days before the 60 kN load was applied, and then it was maintained 60 kN load for a longer period than GS II. For GS V, at 60 kN load, the stud

shear forces were higher than those for GS II. This was mainly because of the previous loading history and exposure time of GS V. Despite identical load levels, GS V was maintained under prestress for 14 days before the 60 kN load was applied, whereas GS II was maintained under prestress for only 2 days before reaching the same load level. In GS V, the long-term prestress coupled with the low compressive strength influenced the interfacial local deformation in the stud–concrete vicinity, which was further increased when a vertical load was applied opposite to the prestressing force. This resulted in a higher shear force at the 60 kN load level.

As concrete creep and shrinkage are considered as causes of time-dependent behaviour [(Okui Y, 2007)], the specimen GS IV was maintained only under prestress for 39 days to differentiate the behaviour to those other sustained loading specimens and shown in Figure 5.30. The recorded deflection for GS IV was assumed represent shrinkage caused by environmental effects which therefore demonstrated how the behavior can be influenced over variations of environmental conditions. However, comparing the shear force behavior due to prestress force for GS IV with that of other sustained loading specimens GS II, GS III and GS V, it was clarified that shear due to creep (other than shrinkage) significantly dominated than that caused by shrinkage. It is thus necessary to clarify why sustained loading has significant impact on increasing shear force on stud connections. When external load sustained on girder, it was flexure that induced deflection at girder and mostly

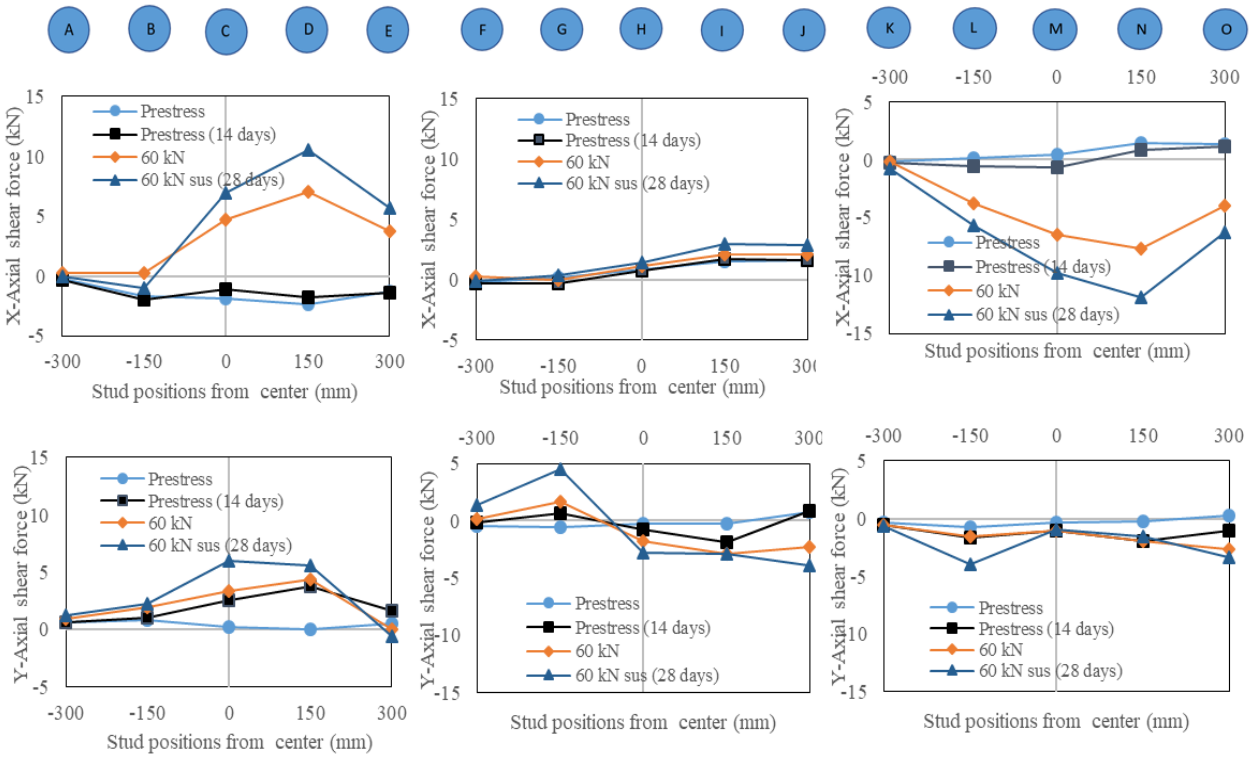

Figure 5. 29: Headed stud shear forces under sustained loading for GS V

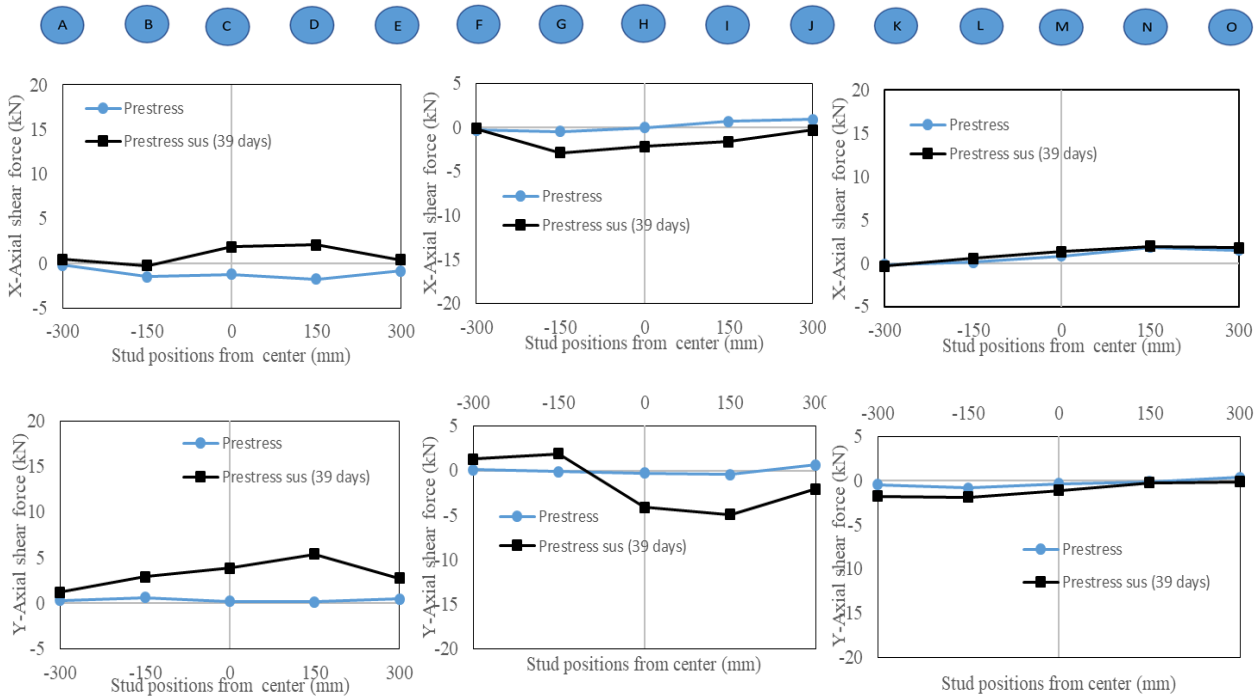

Figure 5. 30: Headed stud shear forces under sustained prestress for GS IV

influenced part was junction. Owing to this deflection, local deformations have taken place at stud-concrete vicinity as well as slip deformations also taken place at steel-concrete interface. These deformations phenomena were continued throughout the loading time which have directly influenced the shear forces acting on stud connections. The shear force behavior of any stud also could change depending on how the neighboring studs behaved due to any deflection or deformation by external forces. In most cases of sustained loading specimens, middle layer studs have been influenced less in terms of magnitude and variations of shear force comparing to upper and lower layer, which was due to the position of prestressing bar with active involvement of prestress force near to that layer. It was observed that studs in three layers who remain in the area from center line to rightward region where the upper flange was terminated showed higher magnitude of shear force, whereas the region from centerline to leftward side which contain upper flange showed shear force magnitude with relatively lesser value. This clearly indicated the influence of upper flange in shear force behavior. Thus, the area where upper flange did not exist has behaved as a shear influence area as shown in Figure 5.31, where change of shear magnitude over time significantly noticed. The axial shear force parallel to girder's longitudinal axis was mostly dominating. In contrary, it seemed that upper flange actively influenced shear force magnitude normal to the girder's axis as it took a portion of flexural force as bearing force. As sustained loading influences the shear force behaviour; this phenomenon clearly put a concern that if shear force magnitude changes increasingly over the sustained loading period at connections, then due to local deformations and slippage, overall

deformations of girder would be influenced/aggravated with immediate effects of appearing cracks earlier than expected. Also, the shear force for which the connections were designed will experience that level of force at an earlier time than predicted. This will affect the service life of the structures.

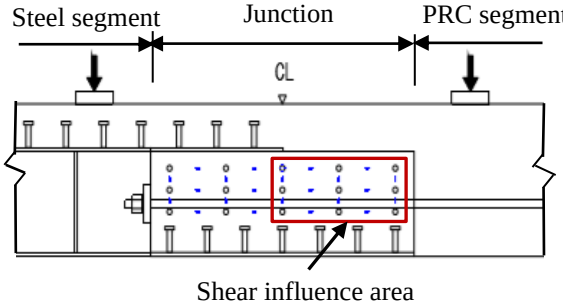

Figure 5. 31: Shear influence area

5.11 Confirmation of shear strength of stud connections

To confirm the strength of headed stud, three pushout specimen were prepared keeping consistent with the size of the girder specimen; they were of different ages and compressive strength as mentioned in Tables 5.8-5.9, The specimens were tested under cyclic loading and the shear force–slip relationship obtained for such are illustrated in Figure 5.32. The vertical axis indicated the shear force per-stud obtained by dividing the applied load by the number of studs. The shear force was maximized when the slip displacement was 4.49 mm for P I, 6.24 mm for P II, and 14.34 mm for P III. The degree of change in slip at maximum shear force varied with somewhat a higher value. As all the specimens have same material characteristics except age and compressive strength of concrete, it seemed a bit complex to differentiate the factors which were dominant in that case but most importantly it seemed compressive strength of concrete reasonably substantiated it. The slip displacement at maximum shear force for P III reached to a higher value compared with the other two as the compressive strength was relatively higher and the stud failure was observed which

Table 5. 8: Concrete mix proportions and strength

Specimen	Concrete mix proportions (kg/m3)						Concrete compressive strength		Type of cement
-	W/C Ratio (%)	Cement	Water	Coarse aggregate	Fine aggregate	Air entraining agent	Strength (Mpa)	Age from casting (days)	-
P I	44.5	394	175	990	767	3.94	36.0	14	Early strength Portland cement
P II							39.92	28	
P III							41.62	42	

Table 5. 9: Summary of material properties

Specimen	Yield strength *fy* (Mpa)			Tensile strength *fu* (Mpa)		
-	Steel web	Steel flange	Stud	Steel web	Steel flange	Stud
P I	396	347	440	536	446	487
P II						
P III						

accumulated and sustained with such higher shear force-slip displacement. The shear strength ratio as presented in Table 5.10, revealed that fact as the days passed, concrete gained much compressive strength and progressed to the strength as closer to the specifications value and beyond as reflected in P III. However, in real structures, girder specimen will be matured enough in terms of age to gain

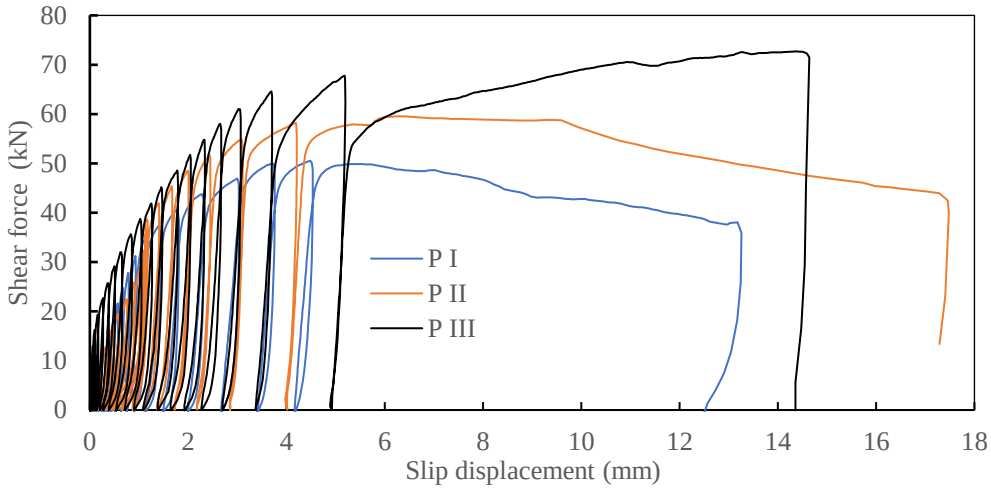

Figure 5. 32: Shear force and slip displacement in pushout test.

Table 5. 10: Summary of stud strength and failure Mode

Specimen	Shear strength (kN)		Ratio (experimental. /specifications.)	Failure mode
-	Experimental	As per JSCE specification		-
P I	50.50	63.04	0.80	Concrete failure
P II	59.53	64.68	0.93	Concrete failure
P III	72.68	64.68	1.12	Stud failure

necessary strength before subjected to field loading. Hence, it could be expected that desired strength would be achieved. In this study, sustained maximum shear force that the stud connections have experienced under 60 kN loading were approximately 12 kN in GS V and 18 kN in GS III. Considering the age of those girder specimens and with the pushout specimens these shear forces are almost 16 % and 25 % of experimentally confirmed same aged strength of stud specimens. At 80 kN sustained load, the maximum stud shear force was approximately 22 kN in GS III, which is almost 30 % of experimentally confirmed strength of stud. Although maximum sustained shear force remained below 50 % of stud capacity, it warrants detailed study with longer duration on how much stud capacity can be considered in design realizing the time dependent sustained loading effects on shear behavior of connections which associated with local deformations at stud-concrete vicinity as well as deformations at steel-concrete interface.

5.12 Comparative sensitivity analysis for hybrid girder

To clarify the deformation behaviour of hybrid girder for the sustained loading under the present scope of this study, a distinctive behaviour is presented under the instantaneous and long-term loading distinguishing how the time dependent deformation differ from that of instantaneous one. Firstly, the stud connections which were used in designing the girder; they were examined experimentally and consequent FEA analysis was done to reproduce and comprehend the experimental behaviour. Experimental and FEA both confirmed the time dependent deformation behaviour for studs is inevitable under sustained loading. Then, five scaled down hybrid girder specimens that were devised with same stud shear connections were subjected to different long-term loading histories. Since, the junction part of the girder was mostly influenced in terms of deformation as presented in preceding sections , the headed studs at the web of that junction were likely to experience time dependent shear forces that can lead local deformations with reduction of stiffness and considered to having an influence on the deformation of the whole girder. To evaluate the shear forces on that stud connections, a finite element calculation (an FE approach) was used and presented in earlier part of this chapter. To obtain a clear understanding about the time dependent effect in shear connections and how they can influence the deformation behaviour of the whole girder, a comparative sensitivity analysis is conducted that focused on the necessity of stud existence in junction part as well as on the impact of reduction stud stiffness (due to instantaneous and time dependent deformation) on the deflection of hybrid girder.

5.12.1 Analysis approach and results

For the sensitivity analysis, an FEA model (half of the specimen) of the hybrid girder is prepared as presented in Figure 5.33. As part of the analysis, bond between PC bar and concrete is neglected in prestressing phase and perfect bond is assumed in loading phase. Internal reinforcements (deformed bars) at hybrid girder are not modeled since concrete is modeled as a linear material. Stud connections are modeled as spring elements (stiffness is reduced as needed) and steel-concrete interface is modeled as non-linear material. For this analysis, to assess the influence of deformations of the shear connectors to the overall deformation of the girder; two concepts could be followed. Firstly, installation of the proposed stud deformation model as s spring element and then the FEA analysis is most logical one. Secondly, for long-term loading cases; due to induced stress and consequent strain, as stiffness degrades with time and it is inevitable therefore, reducing the stud stiffness and consequent FEA analysis could be conducted. In this sensitivity analysis, considering a convenience; the second option is adopted and the analysis process is shown in a flowchart in Figure 5.34. Figure 5.35 and 5.36 show how shear forces develop at stud connections during prestressing phase (phase 1) and loading phase (phase 2). This analysis results differ with some

margin than the evaluated stud shear forces at pre-stressing and loading phase (60 kN) as presented earlier which were evaluated from the experimentally measured data. This difference might be due to the reason as in evaluated case that already explained that stud shear forces is influenced by different factors, i.e., positions of other studs, prestressing bar, flanges and reinforcement. All studs did not experience same amount of shear forces and consequently their deformation behaviour differed from each other. Hence in experimental case, studs did not experience similar stiffness reduction. This type of interference and influences are not considered in FEA model. As similar to

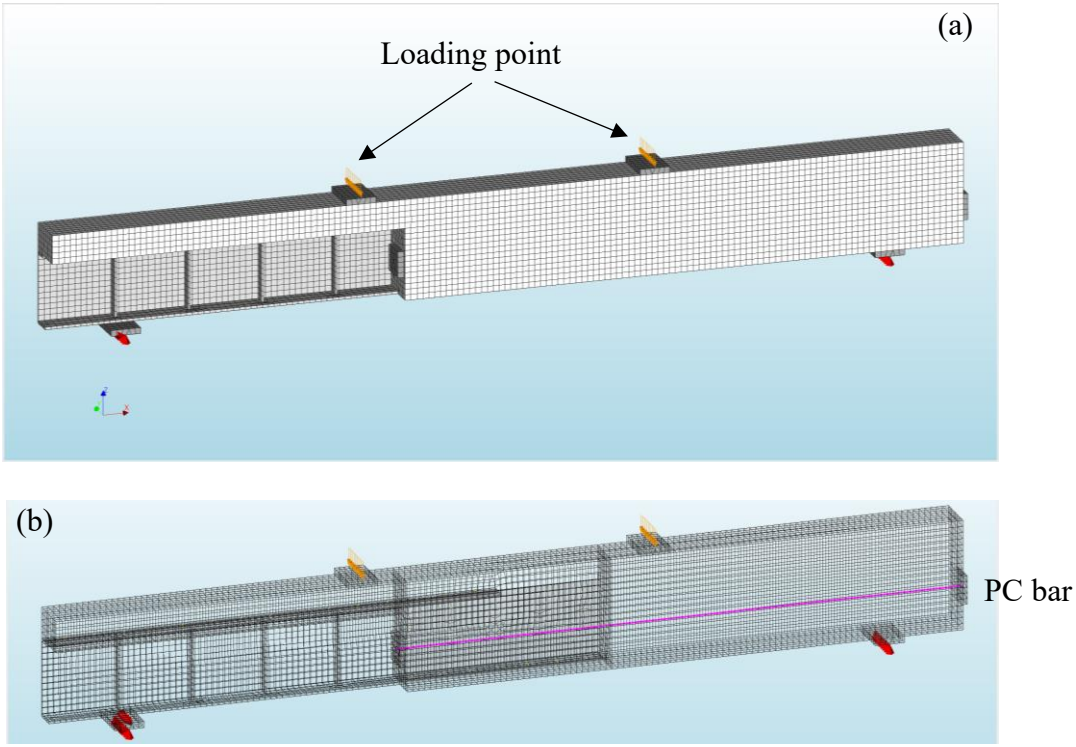

Figure 5. 33: FEA model of hybrid girder

Analysis procedure

Phase 1: Prestressing phase

-Tensile stress is internally introduced at PC bar.
- No bond is assumed between PC bar and concrete.

Phase 2: Loading phase

- Vertical load is applied.
- Stress and strain are carried over from Phase 1.
- PC bar and concrete are perfectly bonded (by grouting).
- Stud shear stiffness is degraded when needed.

Figure 5. 34: Analysis procedure

Figure 5. 35: Stud shear forces at prestressing phase; (a) horizontal and (b) vertical

Figure 5. 36: Stud shear forces at 60kN design load; (a) horizontal and (b) vertical

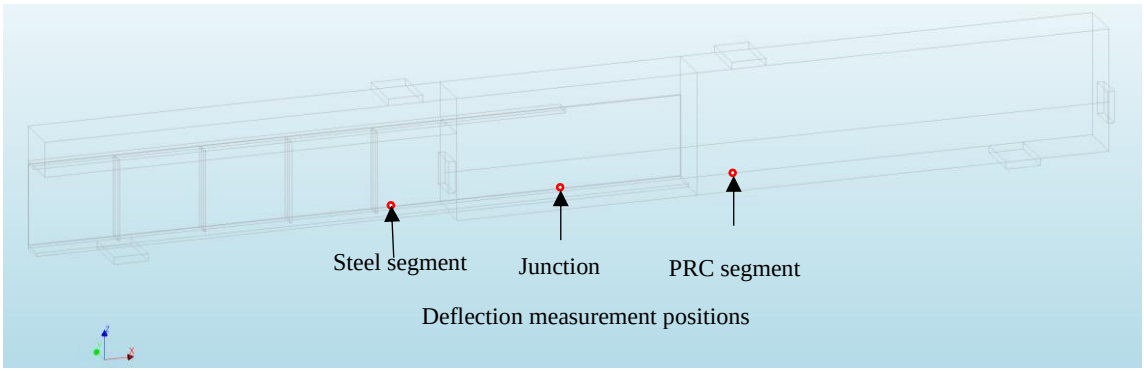

Figure 5. 37: Deflection measurement positions in FEA

Table 5. 11: A comparative sensitivity on influence of stud deformations on hybrid girder

Cases	Loading Condition	Deflection (mm)			Remarks
		Steel segment	Junction	PRC	
Cases 1	At prestress (phase 1)	-0.143	-0.255	-0.287	Control specimen case
	At 60kN load (phase 2)	1.183	1.149	0.820	
Cases 2	At prestress (phase 1)	-0.132	-0.245	-0.283	Considering no studs on web of junction
	At 60kN load (phase 2)	1.254	1.215	0.851	
	Change in deflection	(+6.0%)	(+5.7%)	(+3.8%)	
Case-2a	At prestress (phase 1)	-0.143	-0.255	-0.287	Stiffness reduced by 80% for studs on bottom flange in the loading phase
	At 60kN load (phase 2)	1.235	1.201	0.852	
	Change in deflection	(+4.4%)	(+4.5%)	(+3.9%)	
Case-2b	At prestress (phase 1)	-0.143	-0.255	-0.287	Stiffness reduced by 80% for studs on web and bottom flange in the loading phase
	At 60kN load (phase 2)	1.322	1.295	0.903	
	Change in deflection	(+11.7%)	(+12.7%)	(+10.1%)	
Case-2c	At prestress (phase 1)	-0.143	-0.255	-0.287	Stiffness reduced by 80% for studs on web, bottom and top flanges in the loading phase
	At 60kN load (phase 2)	1.542	1.472	1.012	
	Change in deflection	(+30.3%)	(+28.1%)	(+23.4%)	

hybrid girder test specimens that were experimented in laboratory, deflections are obtained at same positions as shown in Figure 5.37. A comparative statement on different combinations of degradation of stud stiffness are presented in Table 5.11 as to demonstrate the sensitivity of presence of stud connections on junction part and how their instantaneous and time dependent deformations can influence the deformations of whole girder. From this sensitivity analysis, it is observed that the stud connections in the junction part can have a noticeable level of influence on the girder deflections. The absence of studs (reductions of studs) on web part of junction can lead to approximately 6% increase in deflection than the junction with studs on web. Considering the time

dependent behaviour of stud connections, if the stiffness of all studs is reduced by 80% then it can lead to approximately 28% increase of deflection on the junction part which is relatively much higher than instantaneous deflection. Even though a reduction of stud stiffness of 80% seems excessive, still it could lead to a deflection value which is much lesser than what obtained in experimental case as presented in Table 5.7. Since, all studs will not experience the same deformation and stiffness degradation, reducing the stud stiffness only is not enough to determine the sustained loading effect on deflection of the whole girder but it is an indication regarding the long-term deformations under the sustained loading which could lead to aggravate the overall deformation of the whole girder. In this regard, for such sensitivity analysis, other factors like concrete creep induced by compressive stress at upper part of the concrete slab of junction part needs to be counted as an influential factor. Also, the effect of prestress needs to be checked as it could have little influence on it.

5.13 Summary and conclusions

Five scaled-down hybrid girder specimens with headed stud shear connections were tested to investigate their long-term deformation behaviour. Distinct time-dependent deformation behaviour was confirmed through the experimental results, and the influence of environmental effects on deformation behaviour was determined. Since, those hybrid girder specimens were subjected to different long-term loading histories; the junction part which was devised with stud connections was mostly influenced in terms of deformation. Therefore, studs at the web of that junction were likely to experience time dependent shear forces that can lead local deformations having an influence on the deformation of the whole girder. To evaluate the shear forces on that stud connections, a finite element calculation (an FE approach) was used and a distinctive instantaneous and time dependent shear behavior is clarified and to what extent, environmental effects can influence the behavior was also checked. To clarify; how the instantaneous and long-term deformations of stud connections could have influence on deformations on the girder, a sensitivity analysis with a simplified FEA is conducted for girder specimen. A distinctive illustration on the presence of stud connections as well as the influence of their time dependent deformations was checked. Based on the results, the following conclusions can be drawn.

(a) The long-term (time-dependent) deformation due to sustained loading is inevitable in a hybrid girder with headed stud connections. Such effects should be considered in the girder design to accommodate them while considering the long-term serviceability. They must be taken into consideration for other types of connections as well. The consistent deformation behaviour among different segments clearly confirmed the phenomenon of load transfer

with composite action through the headed stud connections with enhanced stud capacity, which was an objective of this study.

(b) The long-term deformation behaviour under sustained loading tended to exhibit an asymptotical nature over time. Such deformation behaviour significantly depends on previous loading history, i.e. a longer duration of sustained loading leads to greater deformation, although the rate of deformation progresses with a relatively low value. This is because the local creep deformations in the stud–concrete vicinity are aggravated with exposure time.

(c) Owing to long term sustained loading, junction part of the girder is mostly influenced in terms of deformation as it was directly under the flexural load. This long-term consistent deformation induced local slip deformations at stud-concrete vicinity and that aggravate the deformation of the whole structure.

(d) Creep deformation was dominant despite a significant amount of shrinkage deformation caused by environmental effects. However, the absolute shrinkage effects from that caused by prestressing were not evaluated. Prestressing over a long duration affects deformation at the stud–concrete interface, which, when coupled with shrinkage, aggravates deformation as well as crack behaviour.

(e) A distinct crack pattern was observed, with cracks appearing at an earlier load level under sustained loading than under static loading, which reduced the ultimate load capacity of girder specimens. The effective prestress force and concrete compressive strength also influenced these phenomena. The distinctive flexural cracks clarified the active influence of bending in the junction.

(f) In case of long-term shear forces on headed stud connections; owing to sustained load, local slip deformations at stud-concrete vicinity & steel-concrete interface continued with time that influenced the shear forces on stud connections. That also influenced by earlier loading history, i.e., magnitude increases with time, the position of neighboring studs, reinforcement bars, anchor plates, and by concrete strength.

(a) The axial shear force parallel to girder’s longitudinal axis was mostly dominating than normal to the girder axis. Since flanges took a portion of flexural force as bearing force and the area where upper flange did not exist has behaved as a mostly influenced area (shear influence area) over time, this clearly indicated the influence of upper flange in shear force behavior.

(a) For the hybrid girder presented under this study, stud connections in the junction part plays a sensitive role in influencing the deformations behaviour of hybrid girder.

(b) Reductions of stud connections can lead to an increased deflection and owing to time dependent sustained loads, those stud connections undergone deformations which is very localized at stud concrete vicinity and aggravate with time. For these local deformations, stud stiffness degraded and influence the deformations of the whole girder upto a remarkable level than instantaneous deformation as presented in sensitivity analysis in this chapter.

(c) For sensitivity analysis, even though a reduction of stud stiffness of 80% seems excessive, still it could lead to a deflection value which is much lesser than what obtained in experimental cases. Hence, reducing the stud stiffness only is not enough to determine the sustained loading effect on deflection of the whole girder. Therefore, other factors like concrete creep induced by compressive stress at upper part of the concrete slab and the effect of prestress need to be checked as they could have influence on it.

(d) These matters were not studied earlier, and these specific phenomena need to be considered with due attention in designing of such girder for practical applications.

5.14 References

Japan Society of Civil Engineers, Standard Specifications for Hybrid Structures. Tokyo:2014.

Nilson AH, Darwin D, Dolan CW. Design of Concrete Structures. New York: Mac-Graw Hill; 2010.

Japan Society of Civil Engineers. Standard specifications for steel and composite structures. Tokyo: 2009.

Kwak HG, Seo YJ. Long-term behavior of composite girder bridges. Computers and Structures 2000; 74:583-599.

Al-Deen S, Ranzi G, Vrcelj Z. Long-term experiments of composite steel-concrete beams. The Twelfth East Asia-Pacific Conference on Structural Engineering and Construction. Procedia Engineering 2011;14:2807–2814.

Okui Y, Nagai M. Block FEM for time-dependent shear-lag behaviour in two-I girder composite bridges. Journal of Bridge Engineering ASCE 2007; 12(1): 72–79.

Haigen C. Analysis of stress and deflection about steel-concrete composite girders considering slippage and shrink & creep under bending. The Open Civil Engineering Journal 2015; 9:171-176.

Bradford MA, Gilbert RI. Experiments on composite T-Beams at service load. Civil Engineering Transactions 1991; CE33 No. 4:285-291.

Al-Deen S, Ranzi G, Vrcelj Z. Long-term experiments of composite steel-concrete beams. The Twelfth East Asia-Pacific Conference on Structural Engineering and Construction. Procedia Engineering 2011;14:2807–2814.

Ban H, Uy B, Pathirana SW, Henderson I, Mirza O, Zhu X. Time dependent behaviour of composite beams with blind bolts under sustained loads. Journal of Constructional Steel Research 2015; 112:196–207.

Haque MN, Maki, T. Experimental study on time-dependent deformation of hybrid steel- PRC girder with headed stud shear connections under sustained loading, Structures, No.22, p.327-340, 2019.9.

Shinozaki H, Asai H, Kaminaga Y, Maki T, Mutsuyoshi H. A study on joint of composite steel girder and PC girder using shear connecting method. Journal of Structural Engineering JSCE 2014;60A(2014/3):861–871.

Introductory course on finite element method for marine engineers, Journal of the JIME, Vol. 49, No. 2, 2014.

Ueda N, Phamavanh K, Sano R, Nakamura H, Kunieda M, Study on Evaluation Method on Damage Region and Failure Criterion on RC Member Failed in Shear Compression by Means of Strain Index, Journal of JSCE (Material. Concrete Structures), Vol. 70, No. 1, 2014, pp. 1-18.

.

CHAPTER 6
6 CONCLUSIONS AND RECOMMENDATIONS

6.1 Conclusions

Under the present scope of this research, five scaled-down hybrid girder specimens with headed stud shear connections were tested to investigate their long-term deformation behaviour. It is considered that; since these girders are devised with stud connections especially the junction part, they will play a sensitive role in determining the long-term deformations of the girder. As part of determining the long-term deformation of those hybrid girder; time dependent deformations of stud connections were clarified and quantified both experimentally and with consequent FE analysis. Then, those hybrid girder specimens were experimented with different long-term loading histories and distinct time-dependent deformation behaviour was confirmed through the experimental results, and the influence of environmental effects on deformation behaviour was determined. It was observed that the junction part which was devised with stud connections was mostly influenced in terms of deformation. Therefore, studs at the web of that junction were likely to experience time dependent shear forces that can lead local deformations having an influence on the deformation of the whole girder. To evaluate the shear forces on that stud connections, a finite element calculation (an FE approach) was used and a distinctive instantaneous and time dependent shear behavior is clarified and to what extent, environmental effects can influence the behavior was also checked. To clarify; how the instantaneous and long-term deformations of stud connections could have influence on deformations on the girder, a sensitivity analysis with a simplified FEA is conducted for girder specimen. A distinctive illustration on the presence of stud connections as well as the influence of their instantaneous and time dependent deformations was checked. Based on the results, the following conclusions can be drawn.

(a) For headed stud connections subjected to sustained shear forces, immediately after the application of force, the displacement increases rapidly at initial stages and continued time with an asymptotical nature. The higher the shear force level, the increase in displacement is also remarkable. Increase of long-term displacement indicates a reduction of stiffness that accounted almost 50%. The increase is due to creep deformation of concrete around the stud which is very much localized at stud-concrete vicinity.

(b) The residual displacement after unloading with that of slip displacement at peak force of each cycle for static specimen exhibit a unique relationship regardless of the maximum slip displacement that holds the previous relational expression proposed by Shima et al. However; in contrary to that, the increase in displacement due to sustained loading causes

an increase in residual displacement because of creep deformation in concrete near the stud that does not recover even after unloading.

(c) The sustained loading specimens showed a lower level of ultimate failure load than the control specimen; which exhibited that sustained loading histories have influenced the failure load. The failure mode for the sustained loading specimen clearly exhibited that failure behaviour is very much localized beneath and around the headed stud locations and with the increase of shear force, residual strain increases with every further step of repeated load that leads to much localized deformation.

(d) For shear force-slip displacement envelop curve of FEA shows a transition towards increasing displacement under sustained loading as observed in experimental result although long-term deformation values are lesser than what obtained in experimental cases. Since FEA could not account the variations of the environmental conditions that always exist in laboratory.

(e) The cumulative slip displacement over time progresses with a slower incremental rate in both experimental and FEA cases that resembles the nature of asymptotical curve. Long-term slip displacement accounts a reduction of stiffness of shear stud as observed in both the cases.

(f) The internal stress-strain contour distribution in FEA shows that shear stud generated large tensile strain after the sustained load, and due to this tensile strain, the concrete around shear stud have more cracks that can comprehend accelerating the creep deformation of concrete around the shear stud. This also an indication that concrete non-linearity exist in that state.

(g) Using FEA, parametric study has been conducted and a simplified prediction model is proposed that can nearly model the actual stud deformation behaviour. Even though this model has some limitations, this model could be applied to quantify the long-term deformation of headed studs in hybrid girder for practical applications. The simplified model has the following formulae.

$$\frac{\delta(t)-\delta(t_o)}{\delta(t_o)} = R_{final}\,[(1\text{-}\exp\{\beta(t-t_0)^{\alpha}\}]$$

Where, $R_{final} = 2.9 * \frac{50}{f_c'} * (\frac{3h}{40d}) * (\frac{f_y}{400}) * (\frac{49p}{25})$ and

$$\delta(t_0) = 3.5 * \frac{250}{f_c'} * (\frac{3h}{200d}) * (\frac{3f_y}{2500}) * \left(\frac{7p}{10}\right)$$

$$\beta = -0.45 \; and \; \alpha = 0.35$$

(h) For hybrid girder with stud connections, time-dependent deformation is inevitable. Such effects should be considered in the girder design to accommodate them while considering the long-term serviceability. The consistent deformation behaviour among different segments clearly confirmed the phenomenon of load transfer with composite action through the headed stud connections with enhanced stud capacity, which was an objective of this study.

(i) The long-term deformation behaviour under sustained loading tended to exhibit an asymptotical nature over time. Such deformation behaviour significantly depends on previous loading history, i.e. a longer duration of sustained loading leads to greater deformation, although the rate of deformation progresses with a relatively low value. This is because the local creep deformations in the stud–concrete vicinity are aggravated with exposure time.

(j) Owing to long term sustained loading, junction part of the girder is mostly influenced in terms of deformation as it was directly under the flexural load. This long-term consistent deformation induced local slip deformations at stud-concrete vicinity and that aggravate the deformation of the whole structure.

(k) Creep deformation was dominant despite a significant amount of shrinkage deformation caused by environmental effects. A distinct crack pattern was observed, with cracks appearing at an earlier load level under sustained loading than under static loading, which reduced the ultimate load capacity of girder specimens. The effective prestress force and concrete compressive strength also influenced these phenomena. The distinctive flexural cracks clarified the active influence of bending in the junction.

(l) In case of long-term shear forces on headed stud connections; owing to sustained load, local slip deformations at stud-concrete vicinity & steel-concrete interface continued with time. That also influenced by earlier loading history, i.e., magnitude increases with time, the position of neighboring studs, reinforcement bars, anchor plates, and by concrete strength.

(m) For the hybrid girder presented under this study, stud connections in the junction part plays a sensitive role in influencing the deformations behaviour.

(n) Reductions of stud connections can lead to an increased deflection and owing to time dependent sustained loads, those stud connections undergone deformations which is very localized at stud concrete vicinity and aggravate with time. For these local deformations,

stud stiffness degraded and influence the deformations of the whole girder upto a remarkable level than instantaneous deformation as presented in sensitivity analysis.

(o) For sensitivity analysis, even though a reduction of stud stiffness of 80% seems excessive, still it could lead to a deflection value which is much lesser than what obtained in experimental cases. Hence, reducing the stud stiffness only is not enough to determine the sustained loading effect on deflection of the whole girder. Therefore, other factors like concrete creep induced by compressive stress at upper part of the concrete slab and the effect of prestress need to be counted as they could have influence on it.

6.2 Suggestions and recommendations for future investigations

(a) As in reality, girders are subjected to both flexure and shear force; to assessing the long-term deformation behaviour, the influence of shear force needs to be considered that could be emphasized in future research.

(b) Since, this study focused on the long-term deformation (deflection) behaviour as a very fundamental study; reductions of stud stiffness (as spring) is considered as time dependent phenomena in a simplified way. Hence time dependent proposed deformation model of stud is to be considered in detailed FEA study in future.

(c) From serviceability point of view which includes not only the deflection but also fatigue and vibration and those also require a due investigation. So, investigating the remaining factors shall have importance and could be investigated in the future, in order to realize the reduction of the number of shear connectors in junction part of the hybrid girder.